Giant vesicles – An ideal tool to study lateral phospholipid distribution and domain dependent protein membrane interactions

Dissertation

zur Erlangung des akademischen Grades
doctor rerum naturalium
(Dr. rer. nat.)
im Fach Biophysik

eingereicht an der
Mathematisch-Naturwissenschaftlichen Fakultät I
der Humboldt-Universität zu Berlin

von
Diplom-Biochemiker
Martin Thomas Stöckl
geb. 23.02.1980 in Ingolstadt

Präsident der Humboldt-Universität zu Berlin
Prof. Dr. Dr. h.c. Christoph Markschies

Dekan der Mathematisch-Naturwissenschaftlichen Fakultät I
Prof. Dr. Lutz-Helmut Schön

Gutachter:
1. Prof. Dr. Andreas Herrmann
2. Prof. Dr. Thomas Pomorski
3. Prof. Dr. Daniel Huster

Tag der mündlichen Prüfung: 12.12.2008

The most exciting phrase to hear in science,
the one that heralds the most discoveries,
is not "Eureka!" but "That's funny..."

Isaac Asimov

Zusammenfassung

In der vorliegenden Arbeit wird ein neuer Ansatz vorgestellt, um Lipiddomänen, die Bindungsorte peripherer und integraler Membranproteine darstellen können, zu charakterisieren. Insbesondere wurde die Analyse der Fluoreszenzlebenszeiten von NBD-markierten Lipidanaloga benutzt, um Lipiddomänen in *Giant unilamellar vesicles* (GUV) und darauf aufbauend, in der Plasmamembran von Säugerzellen zu untersuchen. Das typische Zeitfenster von Fluoreszenzlebenszeiten im Bereich von Nanosekunden ermöglicht es, auch sehr kurzlebige Lipiddomänen nachzuweisen.

Mit Hilfe des *Fluorescence lifetime imaging* (FLIM) wurden für die *liquid disordered* (ld) und *liquid ordered* (lo) Domänen in GUV jeweils spezifische Werte für das Abklingen der Fluoreszenz gemessen. Sogar die Existenz von submikroskopischen Domänen in GUV konnte nachgewiesen werden. Die Fluoreszenzlebenszeit des Lipidanalogs C6-NBD-PC zeigte in der Plasmamembran von Säugerzellen eine breite Verteilung. Dies legt in Übereinstimmung mit FLIM-Experimenten an aus der Plasmamembran von HeLa-Zellen gewonnenen *Giant vesicles* nahe, dass in der Plasmamembran von Zellen eine Vielzahl verschiedener submikroskopischer Lipiddomänen existiert.

Darauf aufbauend wurde die Fluoreszenzmikroskopie an GUV angewendet, um die Bindung von fluoreszenzmarkiertem alpha-Synuclein an mittels FLIM charakterisierte Lipiddomänen zu untersuchen. Die Experimente zeigten, dass das Protein mit hoher Affinität an negativ geladene Phospholipide unter der Vorraussetzung bindet, dass diese sich in ld Domänen befinden. Im Gegensatz dazu erfolgt keine Bindung wenn diese Lipide in lo Domänen lokalisiert sind. Im Vergleich zum wildtypischen alpha-Synuclein zeigte die Variante A30P eine geringere Affinität zur Membran, während die E46K-Variante eine stärkere Bindung zeigte. Dies deutet darauf hin, dass bei den erblichen Formen des *Morbus Parkinson* eine veränderte Assoziation des alpha-Synucleins mit der Membran eine Rolle spielen kann.

Schlagwörter:

GUV

FLIM

Mikroskopie

Lipiddomänen

Synuclein

Abstract

In the present study a novel approach to characterize lipid domains, which may provide binding sites for peripheral or integral membrane proteins, is demonstrated. In particular, analysis of fluorescence lifetimes of NBD-labeled lipid analogues was used to study lipid domains in Giant unilamellar vesicles (GUV) and – based on the GUV results – in the plasma membrane of mammalian cells. As fluorescence decays in a few nanoseconds it is possible to to detect also very short-lived lipid domains.

Fluorescence Lifetime Imaging (FLIM) revealed that the fluorescence decay of NBD-lipid analogues showed domain dependent decay times in the liquid disordered (ld) and the liquid ordered (lo) phase of GUV. Even the existence of submicroscopic domains in lipid membranes could be detected by FLIM. A broad distribution of the fluorescence lifetime was found for C6-NBD-PC inserted in the plasma membrane of mammalian cells. In agreement with FLIM studies on lipid domain forming Giant vesicles derived from the plasma membrane of HeLa-cells this may suggest that a variety of submicroscopic lipid domains exists in the plasma membrane of intact mammalian cells.

Based on that, fluorescence microscopy was used on GUV to study the binding of fluorescently labeled alpha-synuclein at lipid domains previously characterized by FLIM. The experiments suggested that alpha-synuclein binds with high affinity to negatively charged phospholipids, when they are embedded in a ld as opposed to a lo environment. When compared with wildtype alpha-synuclein, the disease-causing alpha-synuclein variant A30P bound less efficiently to anionic phospholipids, while the variant E46K showed enhanced binding. This suggests that an altered association of alpha-synuclein with membranes may play a role in the inherited forms of Parkinson's disease.

Keywords:

Giant unilamellar vesicles

fluorescence lifetime imaging

microscopy

lipid domain

synuclein

Abbreviations

aa	amino acid
APS	Ammonium persulfate
C-	Carboxy-
C_6-NBD-Chol	1-Palmitoyl-2-[6-[(7-nitro-2-1,3-benzoxadiazol-4-yl)amino]hexanoyl]-sn-Glycero-3-cholesterol
Cm	Chloramphenicol
DMSO	Dimethylsulfoxide
dNTPs	Desoxyribonucleotides
DTT	Dithiothreitol
FBS	fetal bovine serum
FLIM	Fluorescence lifetime imaging microscopy
GF	gelfiltration
GPMV	Giant plasma membrane vesicles
GUV	Giant unilamellar vesicles
Hepes	4-(2-hydroxyethyl)-1-piperazineethanesulfonic acid
IEX	ion exchange chromatography
IgG	Immunoglobulin G
IPTG	Isopropyl-β-D-Thiogalactopyranosid
Kan	Kanamycin
ld	liquid disordered
lo	liquid ordered
N-	Amino-
NBD-	6-[(7-nitro-2-1,3-benzoxadiazol-4-yl)amino-
o.n.	over night
PAGE	polyacrylamide gelelectrophoresis
PBS	phosphate buffered saline
PI(4,5)P_2	Phosphatidylinositol-4,5-bisphosphate
PMSF	Phenylmethylsulfonylfluorid
PSM	N-palmitoyl-D-sphingomyelin
RT	room temperature
SDS	Sodium dodecylsulfate
SEM	standard error of the mean
SSM	N-stearoyl-D-sphingomyelin
TEMED	N,N,N',N'-tetramethyl-ethane-1,2-diamine
TMR	Tetramethyl-6-rhodamine
Tris	2-Amino-2-hydroxymethyl-propane-1,3-diol
TRITC	Tetramethylrhodamine-isothiocyanate
WT	wildtype

Glycerolipids were abbreviated using the following scheme:

DO	Di-oleoyl-	PC	phosphatidylcholine
DP	Di-palmitoyl-	PS	phosphatidylserine
DS	Di-stearoyl-	PA	phosphatidylglycerol
PO	Palmitoyl-oleoyl-	PG	phosphatidic acid

Amino acid exchanges were abbreviated using the following scheme: OXXZ

O	amino acid in the wildtype protein
XX	position of amino acid
Z	introduced amino acid

Amino acids were abbreviated according to the common one-letter code.

Table of content

1 Introduction

1.1 The plasma membrane

One of the major prerequisites for life is the ability to keep up chemical gradients against the environment. Hence one of the earliest steps in the evolution of life was the invention of selective permeable barriers [1]. As the most important nutrients like sugars, amino acids or ions are very hydrophilic such a barrier has to be hydrophobic to prevent diffusion across the barrier. Normally hydrophobic components are insoluble in an aqueous medium. This challenge is ideally solved by amphiphilic phospholipids, whose acyl chains are able to form a very tight hydrophobic core within a bilayer, while the hydrophilic headgroups provide at least poor solubility in aqueous medium and shield the core from noxious interactions. Furthermore these amphiphilic properties are a prerequisite for the self-assembly of bilayered structures (Fig. 1).

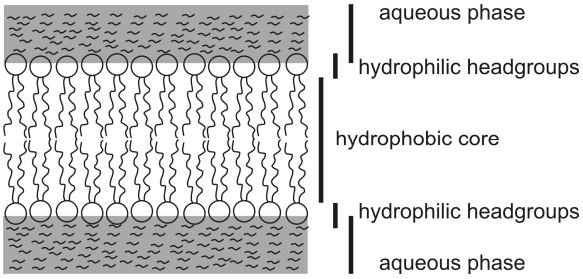

Fig. 1: Structure of a simple phospholipid bilayer. The apolar acyl chains of the lipids form a hydrophobic core from which polar substances are mainly excluded, thus providing an excellent barrier against diffusion of such compounds. The polar headgroups of the lipids shield the hydrophobic core and by that permit the formation of stable phospholipid bilayers.

Although a huge variety of different phospholipids with specific functions and properties exist in biological membranes, this basic building scheme is conserved. Two major types of lipids are found: On the one hand the glycerol based phospholipids which consist of a glycerol backbone which bears two acyl chains at position 1 and 2 linked via ester-bonds and at least a phosphate-ester at position 3. Different lipid types are discerned by different moieties linked to that phosphate yielding phosphate-diesters. The most prominent compounds are choline, ethanolamine and serine yielding phosphatidylcholine (PC), phosphatidylethanolamine (PE) and phosphatidylserine (PS) respectively. Also phosphatidylinositoles (PI) are found which are phosphorylated to a variable extent. On the other hand, for the sphingolipids sphingosine serves as the lipid backbone. The linkage to a fatty acid via an amide-bond yields a ceramide molecule. The addition of a phosphocholine headgroup to the ceramide leads to

sphingomyelin (SM) which is also a common component of plasma membrane of mammalian cells. For glycosphingolipids the phosphocholine moiety is replaced by carbohydrates or their acid derivatives. Apart from these lipids bearing long hydrocarbon chains also the sterols (especially cholesterol) belong to the lipids forming lipid membranes. Figure 2 gives an overview over the above mentioned types of lipids.

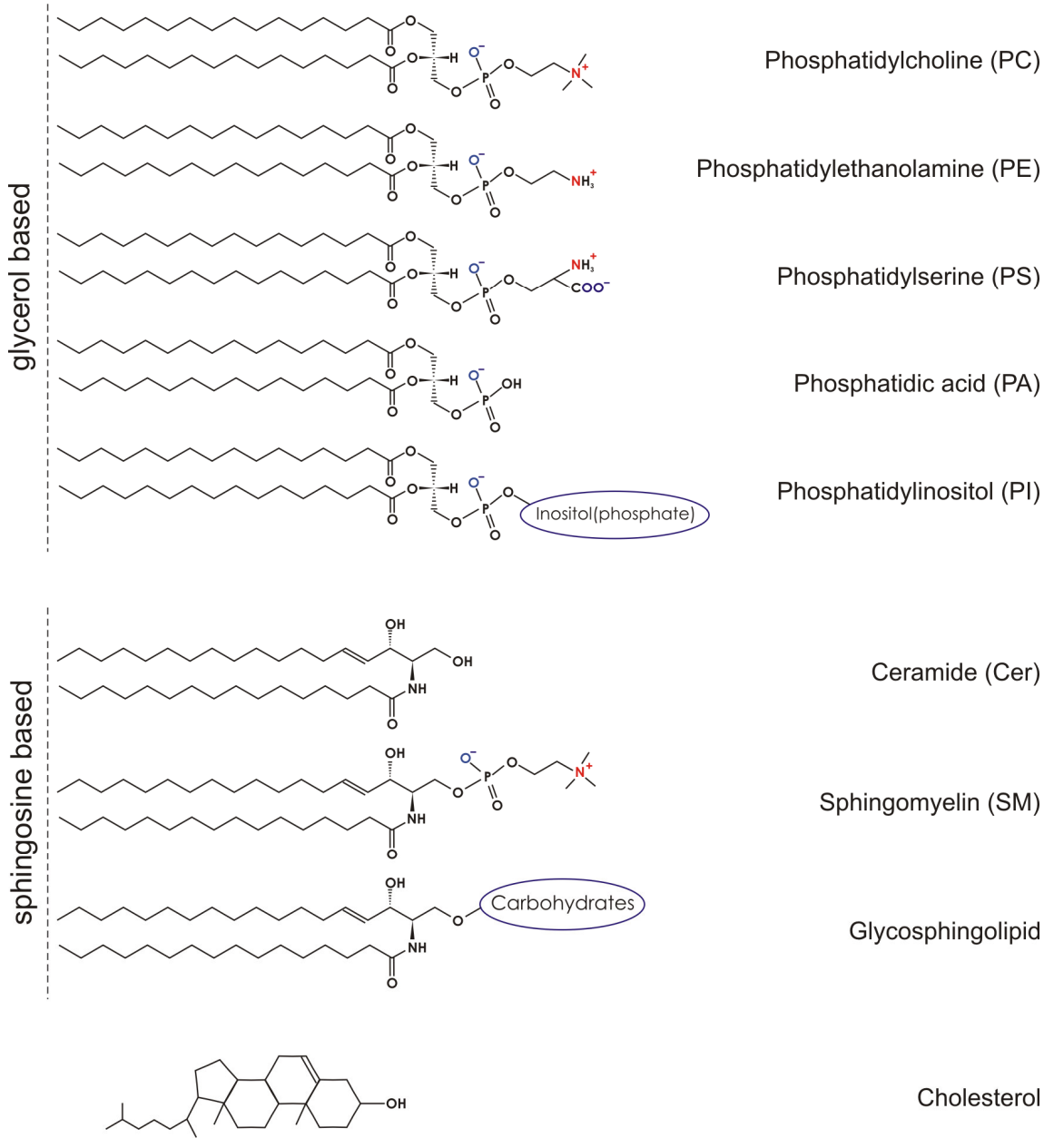

Fig. 2: Molecular structures of common lipids in biological membranes. Charged moieties bearing negative (blue) or positive (red) charges are highlighted.

Bilayers formed of phospholipids resemble such a successful structural development that they can be found encasing each living cell ranging from bacteria to mammalian cells. While the basic layout is strongly conserved during the evolution, the lipid and protein composition is adjusted to fit the particular needs imposed e.g. by the environment. For example archaea which often populate extremophilic habitats, possess membranes of phospholipids in which the glycerol of the headgroup is linked to isoprenoid side chains via ether-bonds instead of acyl chains via ester-bonds. This feature renders these membranes more stable against distortion by high temperatures and also prevents headgroup hydrolysis. Although lipid membranes can keep concentration gradients that span over several orders of magnitude, they are quite vulnerable to mechanical stress, for instance exerted by osmotic pressure. While animals strictly regulate the osmolarity in their bodies, plants and single cellular organisms have developed supporting reinforced cell walls in order to cope with this challenge. Different chemical compounds are used for this purpose, ranging from peptidoglycan in bacteria to cellulose in higher plants or chitin in true fungi.

Only in the last few decades it has become evident that the barrier function of the membrane is only one of many. Apart from keeping the cell interior of the cell separated from the environment the plasma membrane is now thought to provide also a specialized compartment within the cell where particular processes like metabolism (e.g. uptake of nutrients) and cell signaling take place. The mere restriction of the diffusion of membrane associated enzymes and signaling molecules to the two dimensional plane of the plasma membrane increases the local concentration of the interaction partners and facilitates – or initially makes possible – the tight and effective regulation of the involved processes. Apart from only providing a passive scaffold for receptors and other proteins the membrane lipids may also play an active role, contributing to signal transduction. For example, diacylglycerol formed after cleavage of the lipid headgroup of PIP2 by phospholipase C is a prominent second messenger [2]. Another very well studied feature is the loss of membrane asymmetry characterized by the appearance of phosphatidylserine at the extracellular leaflet of the plasma membrane as a signal of apoptosis. But not only single lipid species are involved in signaling, moreover the physical properties of the membrane like bilayer thickness or lateral pressure may also affect and therefore regulate the function of membrane proteins (for a review see Marsh (2008) [3]).

Additionally, new studies reveal that a complex regulation network controls signaling and traffic at the plasma membrane [4,5,6,7,8,9]. Presumably these interactions are also mediated

by the presence of lipid heterogeneities in the plasma membrane [10,11,12]. The so called "Rafts", which are supposed to be enriched in phospholipids and (glyco)sphingolipids with long saturated fatty acids, are segregated from non-Raft domains which are mainly formed by phospholipids with unsaturated acyl chains. Despite their first description dating from over three decades ago their exact nature is still elusive [13,14,15]. Initially, rafts were defined on the basis of their resistance to extraction by Triton X-100 at 4°C [16,17], while meanwhile these methods are thought to artificially induce rafts in the membrane [18,19,20]. As in normal cells these domains seem to be very small and their detection is often difficult, the driving force for the formation of rafts still discussed. On the one hand lipid-lipid interactions which are capable to cause large scale lipid domains in model membrane systems (see 1.3) can induce such lipid domains and enrich certain proteins in such preformed lipid domains due to preferential protein-lipid interactions [3]. On the other hand membrane heterogeneities could also be triggered by the enrichment of certain lipid species around the transmembrane domains or membrane anchors of proteins or protein clusters triggered by direct protein-protein interactions [21]. What is cause and what is effect remains yet elusive and is refered to in recent research (for reviews see Hancock, (2006) [22] and Jacobson *et al.* (2007) [23]). Furthermore compensative effects are present as in the plasma membrane naturally these domains are very small due to interactions of membrane proteins with the scaffolding cytoskeleton what creates obstacles to lipid diffusion and prevents the demixing of phospholipids. This has been corroborated by simulations and direct experiments [24]. Large scale lipid separation is observed, if the plasma membrane becomes detached from the cortical cytoskeleton and forms so called "membrane blebs", although no separation in domains is found when looking at intact cells [25]. In contrast to that, segregated lipid domains large enough to be seen in an optical microscope can be found in certain cell types like activated platelets or T-cells [26,27,28,29,30,31]. A cooperative action of the mechanisms described above comprehensively explains how lipid rafts are able to regulate the activity of membrane proteins and steer the formation of such large scale signaling platforms. In fact, by the exertion of a tight control of the local concentration of signaling proteins and their downstream effectors, membrane signaling can be effectively regulated. The other way round, also the activity of some proteins like phospholipases or sphingomyelinases can influence the properties of the plasma membrane and also lipid domains by altering the tightly controlled lipid composition [29].

These findings clearly show that the "fluid mosaic model" proposed by Singer and Nicholson (1972) [32] is not valid when portions of the plasma membrane at the µm-scale are concerned. While on a very small scale (approx. 10 nm) lipids and proteins are able to diffuse freely, their diffusion may be hampered by raft boundaries and proteins anchored to the cytoskeleton [33,34,35]. This is in good agreement with a model in which proteins embedded in a tightly packed cellular membrane with all different sorts of lipid domains and membrane proteins communicate not only by inter-protein interactions but also via their specific distribution into lipid domains (see Fig. 3 and a review by Kusumi and Suzuki (2005) [36]).

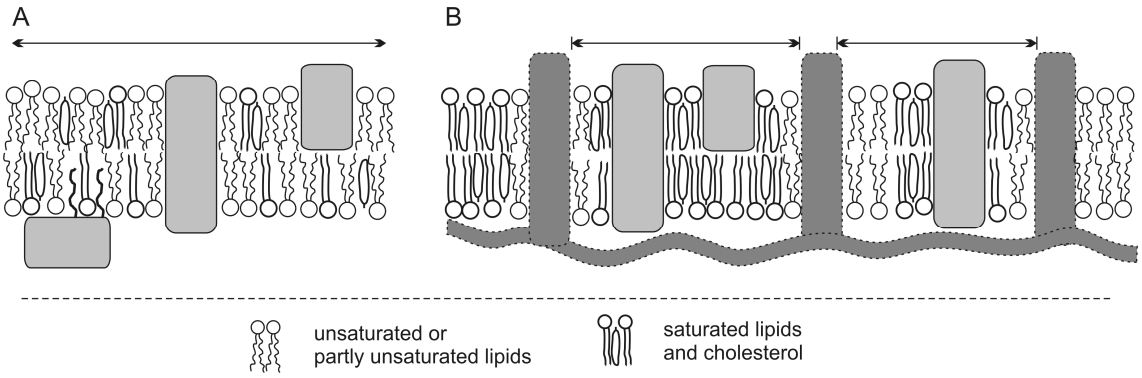

Fig. 3: Proposed models for the organization of the plasma membrane. Membrane proteins (light grey) can span both leaflets of the membrane or be peripherally associated. (A) Fluid mosaic model proposed by Singer and Nicholson (1972) [32]. Membrane proteins can diffuse freely within the membrane plane. (B) Recent models include obstacles to diffusion caused by lipid domains (rich in saturated lipids and cholesterol) and "fences" formed by the cytoskeleton and the associated membrane proteins (dark grey). Free diffusion is possible only on a nm-scale (for a review see Kusumi and Suzuki (2005) [36]).

Hence, to understand the role of lipid domains in protein-protein interactions it is challenging to unravel the mechanisms underlying the lateral sorting and organization of integral and peripheral membrane proteins. As native plasma membranes are a very complex system and lipid domain separation often is very hard to detect in live cells, model membrane systems offer a simple and versatile tool to study protein-lipid interactions and the properties of phospholipid membranes. In this work for instance the domain dependent membrane interaction of α-synuclein is studied by using Giant unilamellar vesicles (GUV) which show lipid domains on a µm-scale.

1.2 Model membrane systems

In order to study phospholipid membrane properties and in particular lipid-lipid and protein-lipid interactions several model systems have been developed which all have specific advantages and drawbacks. In general these systems can be grouped into two different classes, depending on the topology of the membrane. In the first type of systems the membrane forms planar structures, while in the second type it gives rise to vesicular structures.

The simplest system originates from phospholipids on the air-water interface which form a single monolayer (Fig. 4 A). Lipid domain formation can be studied by fluorescence microscopy and fluorescence correlation spectroscopy (FCS), which can be used to measure particle diffusion. The incorporation of substances from the aqueous buffer into the lipid monolayer can be followed by the change of the surface tension using a Wilhelmy plate. Combining two monolayers gives rise to a bilayer which can exist freestanding covering an orifice, and that makes this system perfectly suited to measure membrane conductivity, channel- or pore-formation. It is also possible to deposit these symmetric or asymmetric bilayers on solid matrices. In order to maintain the fluidity in both leaflets of the deposited bilayer, the bottom layer can be anchored to the surface using certain lipids which are connected to a polymer cushion. If only a single bilayer is formed, domain formation can be studied by fluorescence microscopy or atomic force microscopy (AFM) (Fig. 4 B and C).

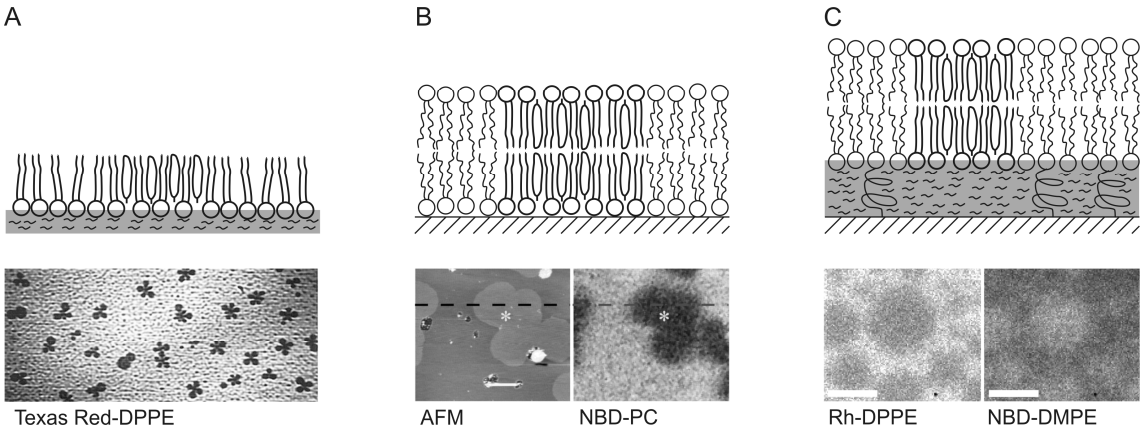

Fig. 4: Sketches of different planar lipid model systems. Domain formation in these bilayers can be easily visualized by using fluorescence microscopy or AFM. For each image the used fluorescent lipid analogue is indicated. (A) Floating lipid monolayer (DPPC/dihydrocholesterol = 84/15; 1 % Texas Red-DPPE) showing distinct DPPC domains in which the dye is enriched (Perkovic and McConnel (1997) [37]). (B) Symmetric bilayer (DOPC/SSM/Chol/GM1 = 34/34/30/2; 0.2 % C_6-NBD-PC) on a solid matrix showing identical non circular fluid domains in the AFM and fluorescence image. C_6-NBD-PC is enriched in liquid disordered (ld) domains. Domains can also be distinguished by their different bilayer thickness using AFM (Shaw *et al.* (2006) [38]). (C) Asymmetric tethered bilayer (bottom leaflet: PC/SM/Chol/tether = 39/39/19/3; 0.02 % Rh-DPPE; top leaflet: PC/PE/PS/Chol ≈ 27/27/27/20; 0.5 % NBD-DMPE) showing circular fluid domains in both leaflets. Rh-DPPE enriches in ld domains, while NBD-DMPE is excluded from these. Complete overlap of domains shows transbilayer coupling (Kiessling *et al.* (2006) [39]).

In addition, the binding of proteins to such membranes can be assessed by the surface plasmon resonance (SPR) assay. It is even possible to study structural changes of proteins bound to the phospholipid membrane by using attenuated field fourier transform IR-spectroscopy (ATF-FTIR). If not only one bilayer but a whole stack of membranes is used, membrane structure and lipid dynamics can be investigated by several methods like neutron or X-ray scattering or magic angle spinning solid phase NMR.

In contrast to these planar membrane arrangements, vesicular structures with a huge variance in size are common in biological systems. Typical diameters span from several nanometers in synaptic vesicles over the micrometer regime of mammalian cells to huge amoebae which can reach diameters of several hundred micrometers. It should be noted that also in these large cells there may exist regions with high membrane curvature (e.g. filopodiae, invaginations of mitochondria) which show membrane properties otherwise typical for much smaller membrane systems (Fig. 5).

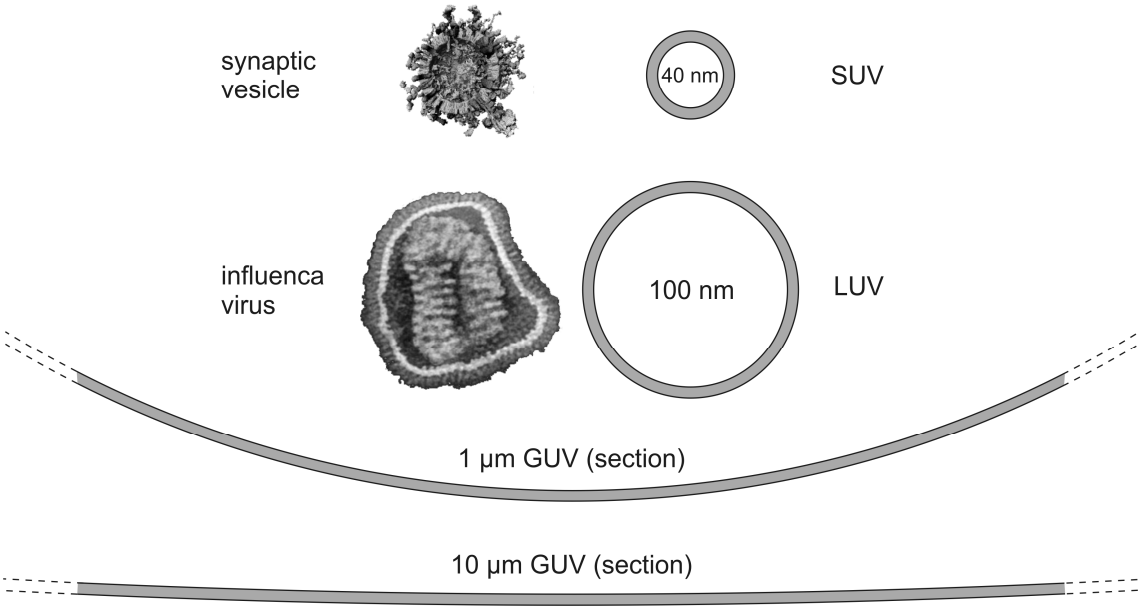

Fig. 5: Size comparison of common vesicular lipid model systems. Shown biological objects, diameter of vesicles and lipid bilayer thickness are to scale. Bilayer thickness is assumed as 5 nm.

In a homologous way also vesicles with different diameters over three orders of magnitude can be produced. Apart from multilamellar vesicles which are circumvented by more than one phospholipid bilayer, unilamellar vesicles consisting of a single bilayer are commonly used as lipid model system. The smallest of those vesicles, so called SUV (Small unilamellar vesicles), consist only of several hundred lipid molecules and have diameters of several nm. Because of their small size the ratio between the thickness of the phospholipid bilayer and the vesicle diameter is large, leading to high curvature stress. Thus these vesicles can be used to study the effects of membrane distortions. The vesicles also have a high propensity to aggregate to relieve membrane stress.

Approximately one order of magnitude larger (common diameters: 100 nm - 200 nm) are the so called LUV (Large unilamellar vesicles). So LUV may resemble intracellular vesicles like lysosomes or other trafficking vesicles. Because of their larger size this type of vesicles is much more stable and tightly sealed. This makes the LUV an ideal tool to study e.g. disturbing effects of certain proteins or lipids. In addition membrane organization or lipid flip-flop or transporter activity of reconstituted membrane proteins can be studied [40]. In general LUV are ideally suited for fluorescence or electron paramagnetic resonance experiments.

The largest vesicles which are readily available are the so called GUV (Giant unilamellar vesicles) with diameters up to several tenths of micrometers. Because of their size these vesicles can be easily visualized by optical microscopy. So, shape changes induced by the incorporation of phospholipids or their conversion can be directly traced [41,42,43]. Also direct observation of membrane permeabilization is possible [44]. GUV made from appropriate lipid mixtures show the formation of laterally segregated domains. It is possible to visualize these domains by fluorescent compounds, with distribution coefficients or physical properties like fluorescence lifetime or general polarization, dependent on the different domains [26,31,45,46,47,48,49,50]. Eventually this approach provides the opportunity to investigate the domain specific binding of fluorescently labeled proteins [51,52,53].

1.3 Lateral lipid segregation

Membranes may not only consist of a single type of phospholipid but of a complex mixture of different kinds of phospholipids. As these differ not only in their headgroups but also in the length and/or saturation grade of the fatty acid chains, lipids show different chemical and physical properties like charge of the headgroup, lipid shape or melting temperature. Especially differences in the melting temperatures of lipids can drive their lateral separation into distinct lipid domains. Below their phase transition temperature lipids are in the gel phase exhibiting an ordered arrangement into a two-dimensional lattice with their acyl chains mainly in the all-trans configuration [54]. At temperatures higher than the transition temperature this lattice “melts” and the lipids are free to show a fluid behavior, what means that single lipids are able to diffuse freely with their acyl chains being mostly disordered. In that case the lipids form the so called liquid disordered (ld) phase. The addition of cholesterol to lipids can induce another lipid phase, the so called liquid ordered (lo) phase which shows characteristics of both phases described above. While the lipids are still able to diffuse freely in the lo phase a greater degree of ordering is present caused by the intercalation of the cholesterol between the acyl chains of the lipids, leading to more stretched configurations. Again, this phase can melt to form a ld phase above a certain transition temperature. In Figure 6 different lipid phases of bilayers are sketched.

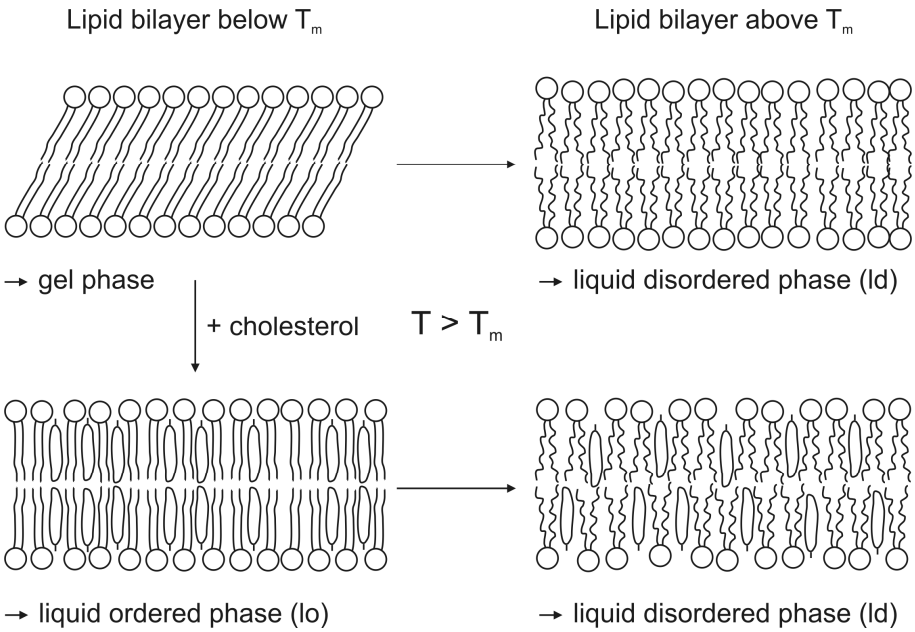

Fig. 6: Common phases of lipid bilayers. Lipid bilayers are in different phases depending on temperature and composition. Below a lipid specific melting temperature (T_m) lipids form a two-dimensional crystal phase (gel phase). The presence of a certain amount of cholesterol leads to an increased fluidity (lo phase). With the transition above T_m the degree of ordering decreases and another phase (ld phase) is formed.

A well studied lipid system showing complex phase behavior consists of a mixture of an unsaturated phosphatidylcholine like POPC or DOPC in combination with a saturated phosphatidylcholine or sphingomyelin and cholesterol. For example at 30 °C lipid mixtures made from saturated (DPPC) and unsaturated (DOPC) phosphatidylcholine will separate into a ld phase consisting mainly of DOPC and a gel phase consisting of DPPC, because of the different states of order of the lipids. With a melting temperature (T_m) of about -19 °C [55] DOPC is in the ld phase at 30 °C, where the phospholipids are in a fluid state and show a fast diffusion. This low phase transition temperature is caused by the C-C double bonds in the fatty acid chains, which increase the flexibility of the lipid and favor less condensed lipid packing. In contrast the fatty acid chains of DPPC are completely saturated and therefore quite stiff, leading to a much higher melting temperature for the liquid-gel phase transition (T_m = 42 °C) [55]. Hence at 30 °C the DPPC lipids form a gel phase in which the fatty acid chains are tightly packed and lateral diffusion is reduced.

The presence of cholesterol significantly changes the behavior of the then ternary lipid system. Due to the small hydrophilic portion of the molecule which is not large enough to cover the hydrophobic sterol rings and shield them from the aqueous environment, pure cholesterol is not able to form a bilayer by itself but will form crystals in solution instead.

In the presence of phospholipids cholesterol will mix with these, as the large lipid headgroups are able to cover also the hydrophobic part of the cholesterol molecule. This explanation is often referred to as the "umbrella model". This model was corroborated by the finding that a sphingomyelin lacking the three methyl groups at the choline nitrogen is incapable to support the incorporation of cholesterol [56], while the length of the fatty acid chains is not of great importance [57]. Interaction of cholesterol with the fatty acid chains of phospho- or sphingolipids leads to an increased degree of order and thus to a more stretched configuration of the fatty acid chains, responsible for an increased bilayer thickness. This condensation of phospholipids is much more favorable in the case of stretched fatty acid chains of saturated phospholipids compared to the kinked chains of unsaturated lipids, leading to the enrichment of cholesterol in such lipid phases [58]. These interactions are the cause of the formation of a liquid ordered instead of a solid gel phase above a certain cholesterol threshold. Additionally also the type of headgroup, length of the acyl chain and other factors can lead to preferential interactions between lipids, so certain lipids tend not to mix ideally with each other but form distinct laterally segregated lipid domains in which one lipid or the other is enriched.

The coexistence of these different domains does not only depend on the lipid composition but also on the temperature. As separated lipid domains formed by lipids being in different phases are entropically unfavorable, increasing the temperature above a certain level leads to a phase transition of the gel or lo phase and the formation of a single homogeneous ld phase in which the lipids are ideally mixed.

As the formation and the disintegration of laterally segregated lipid domains is thought to play a role in signaling at the plasma membrane of cells many studies have been undertaken to investigate the underlying factors driving phase separation in phospholipid bilayers. Especially the before mentioned model system (GUV) has been excessively studied by using different techniques. The formation of laterally segregated lipid domains larger than a few hundred nanometers can be easily studied by fluorescence microscopy. The addition of fluorescent probes which specifically enrich in ld or lo lipid phases allows the facile identification of the respective lipid domains. Additional information on the actual condition of a certain lipid phase can be gained for example out of the domain shape. Domains in the gel phase often show elongated forms which do not change over time while fluid phases (ld and lo) show a round shape and tend to coalesce as the lipids try to minimize the energy associated with the line tension between different domains (Fig. 7).

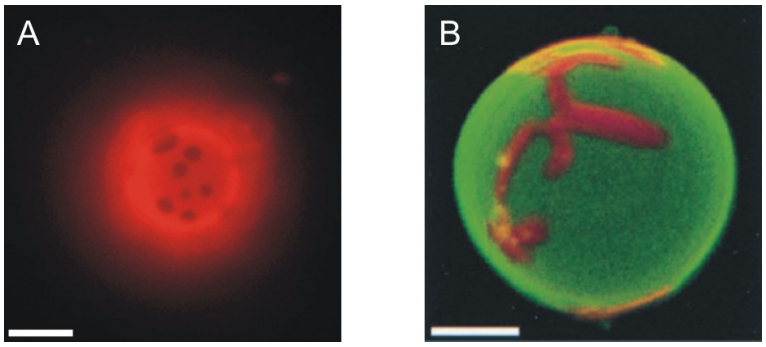

Fig. 7: Lipid domains show phase dependent morphology. (A) Image of the top hemisphere of a GUV (DOPC/SSM/Chol = 1/1/1) taken by epifluorescence microscopy. This lipid mixture shows a ld-lo-phase coexistence. The red fluorescent N-Rho-EYPE is enriched in the ld domain. The dark liquid lo domains show nearly circular shapes. (B) Image of the top hemisphere of a GUV (DLPC/DPPC = 60/40) reconstructed from z-stacked confocal images (Korlach *et al.* (1999) [45]). Solid gel-phase DPPC domains (labeled by DiI-C_{20}; red) are clearly separated from liquid disordered DLPC domains (Bodipy-PC; green) and show irregular shapes. White bars correspond to 2 µm (A) and 10 µm (B), respectively.

In addition the domain dependent diffusion of lipids or proteins can be studied by using methods like FCS, recovery after photobleaching (FRAP) or single particle tracking (SPT) [45,59,60,61]. By these means it is also possible to study asymmetric phospholipid bilayers which are more similar to biological membranes, assessing issues like the question if a strongly segregated leaflet can induce domains in its opposing counterpart [39,62]. This is of special interest, as in the asymmetric plasma membrane of mammalian cells presumably only the extracellular leaflet which is enriched in sphingomyelin is able to form lipid domains, while the cytoplasmic leaflet, rich in unsaturated phosphatidylethanolamine and phosphatidylserine, should not show such a propensity [63]. Therefore the mechanism is still in question by which information generated by the formation of rafts in the outer leaflet is transmitted to the cell interior, where downstream signaling proteins are peripherally associated. A discussed model for example is the induction of lipid domains opposite to those formed in the outer leaflet [39,62]. In general such studies based on fluorescence microscopy are performed on supported or freestanding bilayers or GUV.

The drawback of all microscopic approaches is the limited resolution of the optical microscope. Hence the visualization of lipid domains which are smaller than the resolution limit of about two hundred nanometers stays elusive. However techniques based on fluorescence lifetime analysis are able to breach this limit, as they do not rely on the localization of the fluorescent probe and its distribution between different lipid domains. Instead it is possible to measure certain physical parameters like the stability of the excited

state which is dependent on the incorporation of the probe in a certain membrane domain. Yet different domains which are localized in the same focal spot can be identified as the fluorescence lifetime decay will show the characteristic components typical for the lipid environment surrounding the respective probe [64]. Other fluorescence based methods for the detection of domain formation rely on the Förster resonance energy transfer (FRET) between two different lipid membrane probes (for reviews see Heberle *et al.* (2005) [65] and Silvius and Nabi (2006) [66]). In short, this approach is based on the change of the local concentration of the probes which occurs when laterally separated lipid domains are formed. If both fluorescent probes reside in the same phase an increase in the FRET-signal will be detected as the local concentration of the probes increases causing a decreased average donor-acceptor distance. If the probes preferentially distribute to different domains the FRET-signal will be weaker due to the separation of donors and acceptors [67,68,69,70,71]. The size resolution of this approach is on the scale of tenths of nanometers, as the detection of smaller domains is hampered by the fact that probes in neighboring domains can exchange energy when their distance comes into the range of the Förster radius. Smaller domains can be resolved only by methods which detect changes of physical parameters of the membrane probes caused by the state of the surrounding lipids. Beside the before mentioned fluorescence lifetime approach additional techniques can be used which directly measure the degree of order in the lipids. For instance the hyper-fine splitting of spin-labeled probes determined with electron paramagnetic resonance (EPR) spectroscopy depends on the interactions with neighboring lipids. Direct measurement of the order parameters of lipids is also possible by ^{2}H-NMR [72] or small angle X-ray scattering techniques [73]. Indeed, these approaches are not limited by the size of the lipid domains but depend only on the domains to persist for the duration of the measurement. Furthermore bilayers deposited on a solid matrix can also be investigated by using AFM or ion beam mass spectrometry [38,74]. The visualization of lipid domains below the optical resolution in this case relies on the differences of height of the different domains or their different lipid composition. A drawback of these techniques is that most of them require specifically prepared model systems which are often quite artificial. For instance only the fluorescence lifetime and the EPR approaches are readily applicable to measurements of whole cells. Of these two only the fluorescence lifetime based method, using the fluorescence lifetime imaging microscopy (FLIM) technique, offers imaging of the sample allowing a straightforward isolation of the signal originating from the plasma membrane.

1.4 α-Synuclein and Parkinson's disease

1.4.1 Parkinson's disease

Parkinson's disease is a degenerative neuronal disease which affects about 1 - 2 % of the population at an age above 65 years [75]. The most prominent symptom of the disease is a tremor of hands and limbs with a slow frequency especially severe in the resting state. The decrease in the shaking when the affected body part is deliberately moved was already observed by James Parkinson who described the illness for the first time in his essay "An Essay on the Shaking Palsy" in 1817 [76]. Additional general motor symptoms include stiffness, caused by an increased muscle tone, slow movements and reduced reflexes. Normally the first symptom to appear is the tremor. Due to the progressive character there is no sudden starting point of the illness, instead the symptoms are very faint in the beginning, often unnoticed, normally occurring unilaterally on one side of the body. During the progression of the disease the patients are more and more severely affected and the whole body is involved. Additional symptoms which are not directly associated with motor functions amongst others include sleeping disorders, depressions and also cognitive impairments.

On the physiological level the cause of the disease is a severe loss of neuromelanin containing dopaminergic neurons especially in the *substantia nigra pars compacta*. These neurons normally are involved in the control of motor processes, thus it is clear that the impairment of this regulatory function leads to the observed symptoms (Fig. 8). As a loss of neurons is irreversible there is up to now no cure for the Parkinson's disease. In addition, since the cellular mechanisms (see 1.4.2) which lead to the neuronal loss are not understood in detail, therapies are only able to ease the symtoms, but cannot stop the progression of the disease.

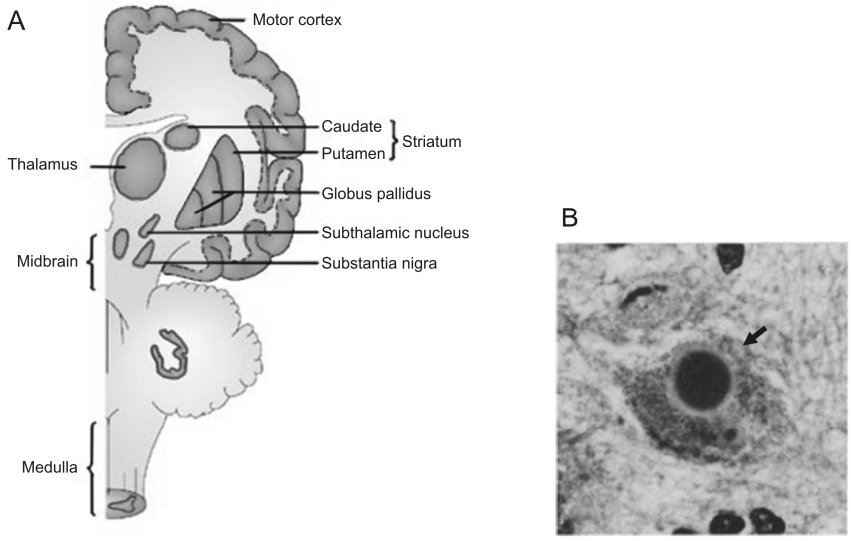

Fig. 8: Regions of the brain affected with Parkinson's disease. (A) A section of the brain is sketched (adopted from Farrer (2006) [77]). Areas with loss of neurons are shaded in grey. Affected areas are evident from microscopy by depigmentation due to neuronal loss and the presence of Lewy Bodies (see B and 1.4.4). (B) Neuronal cell with protein aggregates (Lewy body; arrow). Brain section stained with hematoxylin-eosin. Image taken from Ohama and Ikuta (1976) [78].

Since primarily dopaminergic neurons are affected in the disease, the drugs used for therapy aim to compensate the reduced dopamine levels in the brain. As dopamine itself can't be administered, not being able to cross the blood brain barrier, one way to increase the dopamine levels is to provide a progenitor molecule which is able to cross the blood brain barrier and is afterwards metabolized to dopamine. For that purpose L-DOPA (3,4-dihydroxyphenylalanine) can be used which is converted in one step into the active dopamine. To prevent the loss of the drug due to conversion into dopamine taking place in the periphery a DOPA carboxylase inhibitor is combined with the drug. Further approaches aim to stimulate the intrinsic dopamine production or reduce dopamine degradation by inhibition of monoamine oxidases. In severe cases which are not sufficiently treatable by drug therapy deep brain stimulation of brain regions affected by the disease can be used to ease symptoms.

1.4.2 Origin of the Parkinson's disease

In most cases of patients suffering from Parkinson's disease no specific cause is known. So the disease is normally considered to be idiopathic. In addition certain environmental and genetic factors have been identified which can lead to Parkinsonism and the observed symptoms. Apart from MPTP (1-Methyl-4-phenyl-1,2,3,6-tetrahydropyridine), which is

known to induce Parkinson's disease in cases of drug abusers [79], especially certain pesticides are suspected to be able to induce the disease [80]. In a rodent model of the Parkinson's disease the pesticides paraquat and rotenone are able to evoke the typical symptoms after administration [81,82]. These compounds have in common that they interact with the complex I of the respiratory chain, blocking the generation of ATP producing reactive oxygen species at the same time. Especially dopamine producing neurons are damaged, as these express the dopamine transporter which transports the toxic product of MPTP (MPP+) into these cells. This uptake pathway can also be imagined for paraquat which has a similar structure. In addition to the idiopathic and toxin caused cases, Parkinson's disease can occur cumulatively in certain families indicating genetic risk factors. Several gene loci associated with the disease have been found. While in some cases the affected genes have been identified, the cause in other cases is still unclear. Affected genes can be grouped into different classes according to their function. While two mitochondria linked proteins (PINK1 and HTRA2) and an additional kinase (LRRK2) have been identified, another group of genes is linked to the proteosomal degradation pathway. Genes from all associated processes like ubiquitin ligation (Parkin) and hydrolysation (UCH-L1) as well as a protein with chaperone and antioxidential function (DJ-1) have been found (Fig. 9). For reviews see Farrer (2006) [77], Thomas (2007) [83] and Mizuno, *et al.* (2008) [84].

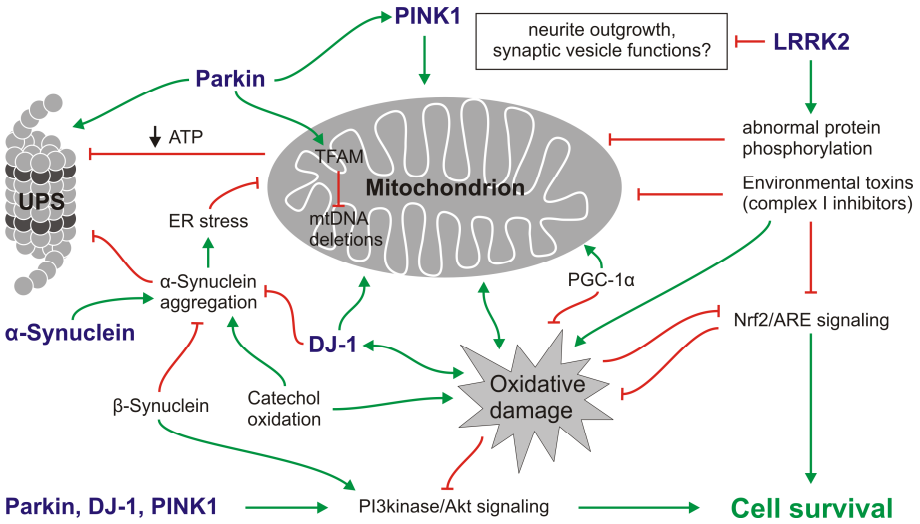

Fig. 9: Regulatory network associated with the development of Parkinson's disease. Genes which have been identified to be associated with inherited forms of Parkinson's disease are shown in blue. Processes in which these factors are involved form an intersecting regulation network. Stimulating correlations are indicated by green arrows while inhibiting correlations are indicated by red lines with blunt ends. The image is adopted from Thomas (2007) [83].

In addition, α-synuclein, a protein whose function to date is not known, seems to play a major role for the development of the disease. It has been reported that gene triplication and certain point mutation leading to single amino acid exchanges (A30P, A53T and E46K) can lead to the observed accumulation of Parkinson's disease cases in affected families [85,86,87]. Also polymorphisms of the α-synuclein gene are associated with the Parkinson's disease [88]. The link between α-synuclein and Parkinson's disease becomes especially evident, when the fact is taken into account, that intra- and extracellular deposits of α-synuclein aggregates in the form of amyloid fibrils are found in brains of patients who have died of the disease.

1.4.3 α-Synuclein

α-Synuclein is a small soluble protein. The main splicing variant consists of 140 amino acids (aa) and is preferentially expressed in the brain. Also shorter isoforms (126 aa, 112 aa, 98 aa) exist which are differentially expressed in different brain regions and non-neuronal tissues [89,90]. Beside α-synuclein two additional proteins with similar sequence named β-synuclein and γ-synuclein belong to the family of synucleins. All these proteins have in common that they lack a defined secondary and tertiary structure in solution and therefore belong to the class of intrinsically disordered proteins. The sequence of α-synuclein is highly conserved among different species [91]. Although α-synuclein is lacking a defined protein fold its hydrodynamic radius is too small for a 140 aa polypeptide being in the random coil state. Thus this compaction of the protein is a hint at residual structure in α-synuclein. Indeed long range interactions between the N-terminal part and the C-terminal part have been found by NMR-spectroscopy [92]. In the protein three "domains" with different characteristics can be identified. The N-terminal part (residues 1 to 63) of the protein consists of five imperfect amino acid repeats which contain a highly conserved hexameric sequence motif (KTKEGV). This sequence motif is also found in the lipid-binding domain of apolipoproteins [91,93]. The different "domains" of α-synuclein and their specific properties are indicated in Figure 10.

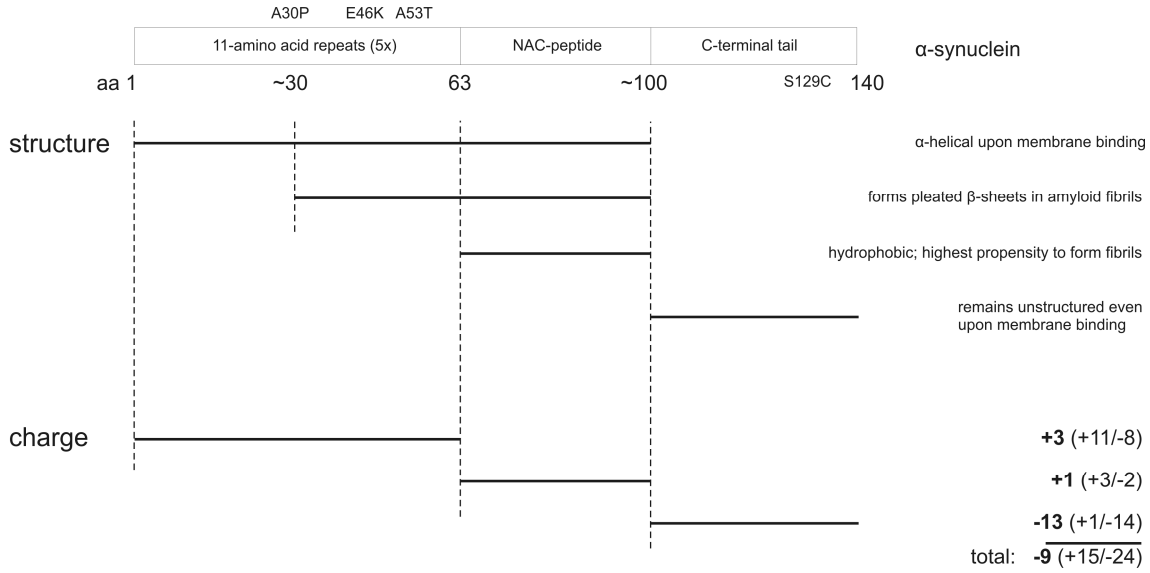

Fig. 10: "Domain"-structure of *α-synuclein.* Roughly, α-synuclein contains three regions with different properties. The N-terminal part (aa 1-63) mainly consists of five 11-amino acid repeats which share homologies with apolipoprotein-like class-A2 amphipathic α-helices. The central part (aa 63-100) is highly amyloidogenic and is responsible for the transition of α-synuclein from random coil to β-sheet structure. The first 97 aa form an α-helix upon membrane binding, while aa 30-100 form the core of α-synuclein fibrils. The C-terminal part (aa 100-140) is very acidic and remains unstructured even upon membrane binding. In addition, the mutations known to cause PD are shown above the sketched structure. Below the introduced aa-change for protein labeling is indicated.

Upon binding to phospholipid membranes or SDS-micelles, the first one hundred amino acids of α-synuclein form an amphipathic α-helix [94,95,96,97,98]. This helical region is divided in two antiparallel helices separated by an unstructured eight amino acid long loop. In the NMR-structures of α-synuclein bound to SDS-micelles such a loop can be seen (Fig. 11) [97,98,99]. Also EPR-experiments using physiologically more relevant small unilamellar vesicles report a broken helix [100,101]. The break in the helix is presumably due to the small diameter of SDS-micelles or SUV forcing the α-synuclein to form two separate helices, since wrapping one single helix around the micelle or vesicle would induce a lot of bending stress. Indeed, in molecular dynamic simulations with planar lipid bilayers harboring negatively charged phospholipids one straight single helix was observed [102]. A NMR-structure of α-synuclein bound to a SDS-micelle is shown in Figure 11.

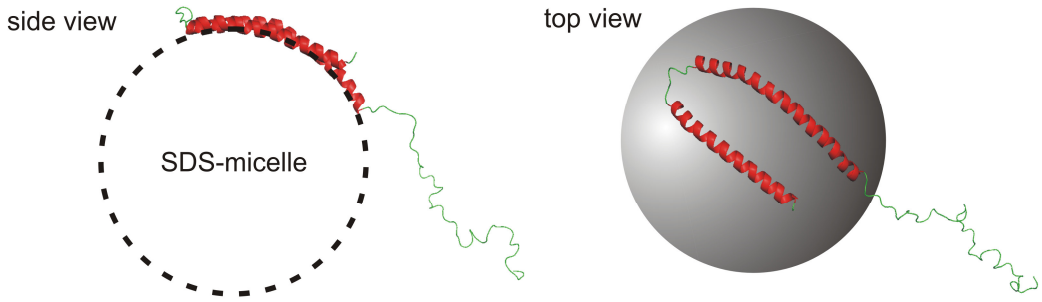

Fig. 11: Model of α-synuclein bound to a SDS-micelle. The N-terminal part of α-synuclein forms two antiparallel helices (red; aa 3-37; aa 45-92) and wraps around the SDS-micelle. The linker between the helices and the C-terminal tail (aa 97-140) are mainly unstructured (green). α-Synuclein structure was calculated from pdb entry 1XQ8 [97].

In 1993 Ueda *et al.* discovered a 35 amino acids long peptide in the amyloid deposits formed in the brain of patients who had died of Alzheimer's disease. This peptide was termed "Non-Aβ component (…)", in short NAC [103]. They were also able to identify the corresponding full length precursor protein which later was named α-synuclein after its homologue in rat. The NAC-peptide comprises residues 61 to 95 of α-synuclein and is the most hydrophobic part of the protein. The peptide shows a strong propensity to form β-amyloid structures, which is also transmitted to the full length α-synuclein. While deletion of a short amino acid sequence from the core of the NAC region (residues 71 to 82) [104,105] or the introduction of proline residues [106] strongly reduces the predisposition of α-synuclein to form aggregates, the introduction of this sequence into β-synuclein, which is naturally not prone to aggregation, is not sufficient to induce fibril formation. Rather the whole N-terminal part of α-synuclein (residues 1 to 96) is required to evoke a propensity toward amyloid fibrillization in the α-synuclein/β-synuclein chimera [107]. Studies on α-synuclein fibrils have shown that approx. the residues 30 to 100 will form the fibril core consisting of five antiparallel β-strands running perpendicular to the fibril axis [108,109,110,111,112,113,114].

In contrast to the N-terminal part of the protein the C-terminal region (residues 103 to 140) is rich in anionic amino acids and prolines. This part of the protein remains unstructured even after binding to membranes and a specifically folded structure has not been observed [94,97]. Nevertheless this part may serve as binding site for interaction partners of α-synuclein or divalent cations. E.g. the N- and C-terminal regions of α-synuclein are required for the formation of mature fibrils from protofibrils formed by the core region [113]. In addition long range contacts between the C-terminal and N-terminal part of the protein have been shown, which are supposed to exert a stabilizing effect on the native structure of α-synuclein by shielding the NAC-region and therefore protecting the protein from aggregation [115,116].

In fact interruption of these interactions by the binding of polycations, heating or the known pathogenic mutations (A30P, A53T) leads to a higher aggregation propensity of the unfolded α-synuclein [117,118,119]. This is consistent with the finding that α-synuclein is more prone to aggregation when the C-terminal part of the protein is deleted [105,120,121,122,123].

Although α-synuclein is a very abundant protein accounting for about 0.5 - 1 % of total soluble protein in neurons, the exact physiological function has not yet been identified [124]. The lack of a defined structure in solution may allow α-synuclein to bind to several different partners of interaction. Due to this large flexibility the protein seems to be involved in many different pathways. E.g. α-synuclein is found associated with synaptic vesicles [125,126,127] or terminals [128,129]. α-Synuclein also seems to play a role in the regulation of the trafficking of cytoplasmic vesicles, since the protein can inhibit the vesicular transport from endoplasmatic reticulum (ER) to the Golgi [130,131]. Genomic screens have shown that about one-third of the genes which have an influence on the toxic effect of α-synuclein are associated with pathways like lipid metabolism or vesicle transport. In addition, deletion or overexpression of α-synuclein in mouse neurons caused alterations of the lipid metabolism and changed the composition of cellular membranes [130,132,133,134]. In a mouse system α-synuclein is also able to rescue a phenotype with motor degenerations caused by deletion of cysteine string protein α (CSPα), probably by interactions with the SNARE-machinery [135,136]. α-Synuclein also seems to be involved in the regulation of the neurotransmitter release, as it is seems to control priming of synaptic vesicles [137,138,139]. Apart from these more or less specific interactions at the presynaptic terminal, α-synuclein shows a broad range of interactions with lipid structures ranging from biological vesicles [140,141,142,143] and certain parts of the plasma membrane [128] to artificial phospholipid bilayers [144,145,146,147,148,149] or detergent micelles [97,98,150] (for reviews see Uversky, (2007) [151] and Beyer (2007) [152]).

In the case of negatively charged multilamellar vesicles it has been shown that α-synuclein does not only bind laterally to the membrane but also destabilizes the vesicles and induces the formation of small vesicular structures [148]. Also in planar membranes α-synuclein is able to induce defects [153,154]. To the contrary, α-synuclein is able to change the degree of order of the lipids when bound to uncharged small unilamellar vesicles, probably “healing” lipid packing defects [146,152]. Apart from that, membrane bound α-synuclein also has a protective effect on unsaturated phospholipids by the prevention of oxidative damage [155].

To sum up, these findings propose that α-synuclein on the one hand can have a deleterious effect on membranes explaining the observed permeabilization of vesicles (see 1.4.4), but may on the other hand prevent premature vesicles fusion due to an increase in the stability of vesicles in the cells.

Apart from direct binding to phospholipid membranes α-synuclein also interacts with proteins at the membrane. For example membrane bound α-synuclein strongly inhibits the phospholipase D2 [156]. A lot of additional potential partners of interaction have been identified in direct interaction studies (for a review see Dev *et al.* (2003) [157]) or a proteomic search [158]. Whether α-synuclein is involved in metal cation homeostasis or binding of these cations influences disease progression remains to be elucidated (for reviews see Brown (2007) [159] and Wright and Brown (2008) [160]). In any way, a specific function of α-synuclein has not been identified yet. α-Synuclein rather seems to be involved in a vast network of cellular signaling pathways. Due to the complexity of this network cause and effect are difficult to assign, so the exact function of α-synuclein remains to be elucidated. The manifold interactions of the protein with phospholipid vesicles and membrane structures suggest that α-synuclein plays an important role in the regulation of vesicle transport and fusion processes.

1.4.4 The link between α-synuclein and Parkinson's disease

Although the exact physiological function of α-synuclein is still unknown, there is a clear established link that the protein is involved in the noxious events leading to the development of Parkinson's disease. A very prominent feature here is the development of extra- (Lewy bodies; Fig. 8) or intra-cellular (Lewy neurites) deposits which are mainly composed of amyloid fibrils consisting of misfolded α-synuclein, which can be found in the brains of patients who had died of the disease [161]. Mature fibrils are formed by a pathway involving the formation of partially folded monomeric intermediates, oligomers and protofibrils [162,163,164,165,166]. While early spherical oligomers still contain a significant amount of α-helical structure, along this pathway an increase in the β-sheet content occurs [167]. While stabilization of unfolded and α-helical structures can prevent fibrillization [168], partially folded structures promote formation of larger oligomers and fibrillization [169] (for a review see Uversky and Fink (2004) [170]). Also the presence of peptidyl-prolyl-isomerases which promote structural changes enhances fibrillization [171,172]. Mature fibrils are formed from pleated β-sheets as directly shown by structural investigations and the

binding of Thioflavin and β-amyloid specific antibodies. Although it is finally not exactly known which folding state – monomer, oligomer or mature fibril – of α-synuclein is the toxic agent, several studies indicate that oligomers and prefibrillar aggregates are especially noxious for neurons [173,174] (Fig. 12).

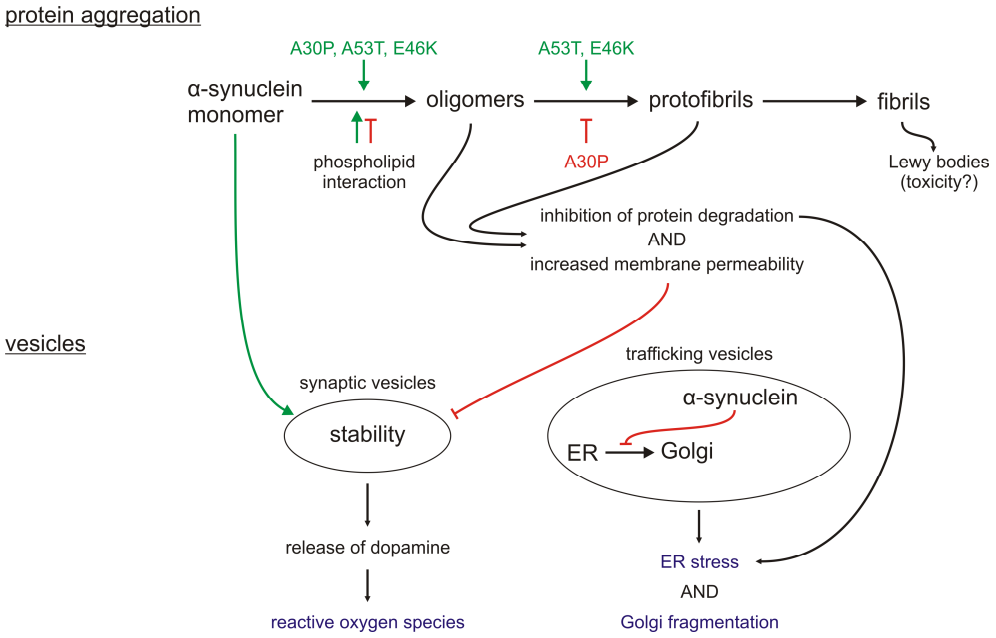

Fig. 12: Overview of proposed pathways involved in α-synuclein toxicity during development of PD. Various enhancing (green arrows) and inhibiting (red lines with blunt ends) factors contribute to the noxious effects (blue) leading to the death of dopaminergic neurons. For detailed description see 1.4.4 and accompanying references.

Hence, factors influencing the aggregation behavior of α-synuclein could give important clues to the cause of the disease. It has been shown that α-synuclein with the point mutations A30P, A53T and E46K shows an increased propensity to aggregation [175,176]. While the A53T and E46K variants exhibit faster fibrillization kinetics compared to the wildtype, the A30P variant forms amyloid fibrils at a slower rate [175,177,178,179]. Aggregation rate and morphology of oligomers and fibrils also can be influenced by the presence of heavy metal ions like iron or copper [180,181,182] or oxidized α-synuclein species [183,184]. Also the ubiquitination of α-synuclein can enhance the formation of aggregates [185,186,187]. Moreover the aggregation propensity is influenced when α-synuclein is bound to negatively charged phospholipid membranes. Here the protein to lipid ratio is of importance, as conditions where α-synuclein is in excess enhance the fibrillization while an excess of lipids has a stabilizing effect [188,189]. In biological membrane systems membrane interactions also may trigger the formation of aggregates [141]. Here also the cholesterol level can have an effect on the

aggregation [190]. Apart from that, the pathogenic mutations play a role, as the wildtype α-synuclein bound to synaptosomal membranes is more prone to aggregation, while aggregation is inhibited in the case of the A53T variant [191]. Not only is α-synuclein aggregation altered by membrane interactions, also the reverse is true, since the aggregation state of the protein is of importance for the interaction with membranes. While the monomer is quite benign, especially oligomeric forms and protofibrils of α-synuclein are able to disturb phospholipid membranes [178,182,189]. Some of these aggregates show a pore-like structure similar to that known for β-sheet pore-forming toxins [192,193,194,195] and are responsible for the observed permeabilization of membranes [196,197,198]. By a similar mechanism α-synuclein oligomers should be able to disturb biological membranes in cells, like the plasma membrane or synaptic vesicles. This hypothesis is corroborated by the finding that the plasma membrane of cells transfected with the pathogenic α-synuclein variants A30P and A53T shows a higher permeability for ions. Additionally the Ca^{2+}-homeostasis seems to be impaired in these cells [199]. This is also found for cells incubated with α-synuclein oligomers [174]. A different study shows that these α-synuclein variants lead to proton leakage from intracellular vesicles which is accompanied by a high cytoplasmic concentration of catecholamines [200], which are able to stabilize fibrils formed from A30P and A53T α-synuclein [201]. In principle these membrane perturbations don't have to be limited to these systems but may affect various cell organelles as these are all surrounded by phospholipid membranes. For example also mitochondrial functions may be impaired by the uptake of α-synuclein into this organelle [202]. Also the ER may be affected by α-synuclein which is reported by the enhanced expression of markers for ER stress [131,203] upon overexpression of α-synuclein. In addition Golgi fragmentation is observed when α-synuclein is overexpressed in COS7-cells [204]. The observed ER stress response could be induced on the one hand by the accumulation of misfolded proteins (see below), but also by impairments in the vesicular transport, by an impairment of the microtubule system [205,206] or disruption of Rab homeostasis [207]. The latter hypothesis is corroborated by studies showing that an increased expression of proteins involved in vesicular trafficking is able to reduce α-synuclein toxicity [131,208]. Last, but not least, the presence of protein aggregates could be a hint that α-synuclein interferes with cellular systems dealing with the removal of misfolded protein species. In principle this task is accomplished by different systems, namely the proteasome, the lysosomal degradation and autophagy. *In vitro* studies have shown that α-synuclein is able to bind to and inhibit the proteasome [209,210,211]. Also *in vivo* experiments have found an

inhibition of the proteasomal degradation under conditions where α-synuclein is overexpressed, however a direct link has not been demonstrated, as additional causes like ATP depletion could play a certain role [212,213]. Also lysosomal protein degradation and chaperone mediated autophagy, which depend on functional lysosomes, have been found to be of importance for α-synuclein turnover [212]. These pathways seem to be affected by the protein and its pathogenic mutants, though it is not clear if the impaired lysosomal function caused by the A53T α-synuclein variant is the primary cause or if the impairments are triggered upstream by a different mechanism. Apart from these pathways which have in common that all of them involve interactions between α-synuclein and phospholipid membrane structures, some evidence exists that α-synuclein could also trigger the toxic cascade by inducing oxidative stress in the cells or inducing apoptotic pathways [214]. Already a lot of data exist which deal with the suspected effects of α-synuclein on cell metabolism leading to the death of the dopaminergic neurons (for a review see Cookson and van der Brug (2008) [215]). Because of the complexity and level of interconnectivity of the pathways involved, it is very hard to distinguish which are primary effects of α-synuclein and its pathogenic mutants and which are secondary effects caused by alterations in downstream processes. So the ultimate cause which leads to the death of dopamine neurons and thereby to the development of Parkinson's disease still remains elusive.

To summarize, interactions between α-synuclein and phospholipid membranes seem to play a major role during the development of Parkinson's disease, as such a relation is often found in such studies (Fig. 12). While α-synuclein is able to distort biological membranes and by that impairs many cellular pathways relying on their proper function, likewise the aggregation of α-synuclein is influenced by membrane interactions. To the contrary, one proposed function of α-synuclein is the stabilization of synaptic vesicles. Therefore the characterization of the membrane binding of α-synuclein in the model system can yield valuable insights which factors may regulate membrane binding of α-synuclein.

2 Aim of the study

Factors involved in cellular processes associated with phospholipid membranes are normally hard to study in the native environment as the composition of such systems is often quite complex. For example recent studies suggest that the formation of laterally segregated lipid domains is an important regulatory element in cell signaling. Lipid domain formation can be easily studied in the GUV model system using fluorescent dyes which are specifically enriched in certain domains. The drawback of such microscopy techniques relying on the partitioning of fluorescent dyes in certain lipid domains is their limitation in size by the diffraction barrier. Since lipid domains in the plasma membrane of cells possibly are only several nanometers in diameter, detection using those methods is not possible. A possible solution would be a membrane probe which changes its physical properties according to its distribution to different membrane domains. Therefore this study aimes to develop a fluorescence lifetime based approach which can be used to investigate the domain structure in the plasma membrane of living cells. In order to evaluate the feasibility of the FLIM technique, the candidate compounds have to be characterized in a well defined phospholipid model system. For that GUV are used, as lipid domains can be easily identified by optical microscopy and the formation of different lipid phases is already well characterized.

Using GUV it is also possible to identify domain specific factors which are responsible for membrane binding of peripheral proteins. In this study the determinants triggering the recruitment of α-synuclein to phospholipid membranes should be studied using GUV showing lateral lipid domains. Although the basic requirements for the membrane interactions are already known, there is still controversy in the literature whether raft associated phospholipids trigger the membrane interactions or not [128,147]. As GUV are ideally suited to study domain specific binding of proteins to membranes by fluorescence microscopy new insights into which factors are determinative can be gained by such experiments.

3 Material and Methods

3.1 Material

3.1.1 Chemical Material

Enzymes and reagents for molecular biology were purchased from Fermentas (St. Leon-Rot, Germany) unless otherwise indicated. Phospholipids were purchased from Avanti Polar Lipids (Alabaster, AL, USA), cholesterol and Annexin V-Cy3 from Sigma-Aldrich (Taufkirchen, Germany). Lipids were used without further purification. Tetramethylrhodamine-6-maleimide was purchased from Invitrogen (Karlsruhe, Germany). Solvents used for vesicle preparation were of the purest available grade. Indium tin oxide (ITO) coated glass slides were obtained from Präzisions Glas & Optik (Iserlohn, Germany). OKT3 antibody was a kind gift of C. Freund (FMP, Berlin, Germany), TRITC-labeled anti mouse-IgG (from goat) was obtained from Sigma-Aldrich. Dulbecco's modified eagle medium (DMEM), HANKS' balanced salt solution (HBSS), Dulbecco's modified phosphate buffered saline (DPBS) and penicillin/streptomycin were obtained from PAN Biotech (Aidenbach, Germany), fetal bovine serum (FBS) from Invitrogen. Collagen A was from Seromed (Biochrom, Berlin, Germany). $HBSS^+$ refers to HBSS supplemented with 1.25 mM $CaCl_2$ and 0.5 mM $MgCl_2$. Diisopropylfluorophosphate was obtained from Fluka (Neu-Ulm, Germany).

3.1.2 Biological Material

3.1.2.1 *E. coli* strains

Tab. 1: Genotypes of *E. coli* strains used for plasmid propagation and protein expression

name	description
DH5α	F^- *endA1 recA1 hsdR17*(r_k^- m_k^+) *supE44* λ^- *thi-1 gyrA*(Na1) *relA1* *Φ*80 *lacZ*ΔM15Δ (*lacZY* A-*argF*)
XL1-Blue	*recA1 endA1 gyrA96 thi-1 hsdR17 supE44 relA1 lac* [F´ *proAB* $lacI^q$*ZΔM15* Tn*10* (Tet^r)]
Rosetta (DE3) pLysS	F^- *ompT hsdS*$_B$ (r_B^- m_B^-) *gal dcm lacY1* (DE3) pLysSRARE (Cm^r)

3.1.2.2 Plasmids

Tab. 2: Plasmids used for overexpression of α-synuclein variants

name	vector	insert
aSynWTHisN	pQE-32	aSyn NACP140
pET28 aSyn	pET 28	aSyn NACP140 (*Nco*I – *Xho*I)
pET28 aSyn S129C	pET 28	aSyn S129C (*Nco*I – *Xho*I)
pET28 aSyn A30P S129C	pET 28	aSyn A30P S129C (*Nco*I – *Xho*I)
pET28 aSyn A53T S129C	pET 28	aSyn A53T S129C (*Nco*I – *Xho*I)
pET28 aSyn E46K S129C	pET 28	aSyn E46K S129C (*Nco*I – *Xho*I)

3.1.2.3 Oligonucleotides

DNA oligonucleotides were synthesized by Invitrogen.

Tab. 3: DNA oligonucleotides used for colony PCR and PCR-based mutagenesis. Bold sequences indicate restriction sites for cloning.

name	sequence	purpose
T7-Promotor	TAA TAC GAC TCA CTA TAG G	Sequencing
T7-Terminator	GCT AGT TAT TGC TCA GCG	Sequencing
aSyn **Nco** N a	CAT G**CC ATG G**AT GTA TTC ATG AAA GGA	Cloning aSyn (1-x)
aSyn **Xho** C b	CCG **CTC GAG** TTA GGC TTC AGG TTC GTA	Cloning aSyn (x-140)
aSyn S129C a	GGC TTA TGA AAT GCC TTG TGA GGA AGG GTA TC	Mutagenesis aSyn S129C
aSyn S129C b	GAT ACC CTT CCT CAC AAG GCA TTT CAT AAG CC	Mutagenesis aSyn S129C
aSyn A30P a	GGT GTG GCA GAA GCA CCA GGA AAG ACA AAA G	Mutagenesis aSyn A30P
aSyn A30P b	CTT TTG TCT TTC CTG GTG CTT CTG CCA CAC C	Mutagenesis aSyn A30P
aSyn A53T a	GGT GCA TGG TGT GAC AAC AGT GGC TGA GAA G	Mutagenesis aSyn A53T
aSyn A53T b	CTT CTC AGC CAC TGT TGT CAC ACC ATG CAC C	Mutagenesis aSyn A53T
aSyn E46K a	CCA AAA CCA AGA AGG GAG TGG TGC ATG GTG TG	Mutagenesis aSyn E46K
aSyn E46K b	CAC ACC ATG CAC CAC TCC CTT CTT GGT TTT GG	Mutagenesis aSyn E46K

3.1.2.4 Common media and buffers

Tab. 4: Buffers used for GUV preparation and microscopy

Sucrose buffer	Glucose buffer	NaCl buffer
250 mM Sucrose	280 mM Glucose	140 mM NaCl
15 mM Sodium azide	11.6 mM Potassium phosphate	11.6 mM Potassium phosphate
	pH 7.2	pH 7.2
Approx. 280 mOsm/kg	Approx. 300 mOsm/kg	Approx. 300 mOsm/kg

Tab. 5: Media and buffers used for *E. coli* propagation and protein purification

LB medium	LB Agar
10 g/l Bacto™ Tryptone (BD Biosciences, Heidelberg, Germany)	Add 15 g Agar per l LB medium
5 g/l Bacto™ Yeast extract (BD Biosciences)	**Antibiotic stocks**
5 g/l NaCl	50 mg/ml Kanamycin in H_2O
0.1 % 1M NaOH (v/v)	34 mg/ml Chloramphenicol in EtOH

Lysis buffer	IEX start buffer	GF buffer
500 mM NaCl	20 mM Tris/HCl	50 mM Potassium phosphate
100 mM Tris/HCl	1 mM EDTA	100 mM KCl
1 mM EDTA	1 mM DTT*	pH 7.0
1 mM PMSF	pH 8.0	
pH 8.0	* DTT added freshly and only for cysteine containing α-synuclein	

Tab. 6: Buffers used for SDS-PAGE

SDS-PAGE gel composition (for two gels)	Stacking gel (5%)	Separating gel (15 %)
30 % Acrylamide/Bisacrylamide ("Rotiphorese Gel 30 (37.5:1)" Carl Roth, Karlsruhe, Germany)	0.5 ml	5.0 ml
0.5 M Tris/HCl; pH 6.8	0.75 ml	
1.5 M Tris/HCl; pH 8.8		2.5 ml
10 % SDS (w/v)	30 µl	100 µl
dH_2O	1.7 ml	2.3 ml
10 % APS	30 µl	100 µl
TEMED	3 µl	4 µl

SDS sample buffer		Coomassie staining solution		Destaining solution	
50 g/l	SDS	2.5 g/l	Coomassie brilliant blue R-250 (Carl Roth)	40 %	Ethanol (v/v)
0.5 g/l	Bromophenol blue			7.5 %	Acetic acid (v/v)
25 %	Glycerol (v/v)	45 %	Ethanol (v/v)		
25 %	β-Mercaptoethanol (v/v)	10 %	Acetic acid (v/v)		
25 %	1 M Tris/HCl; pH 6.8 (v/v)				

3.2 Methods

3.2.1 Preparation of lipid membrane vesicles

3.2.1.1 Preparation of Giant unilamellar vesicles (GUV)

GUV were produced from lipid films dried on indium tin oxide (ITO) coated glass slides by electroswelling as originally described by Angelova and Dimitrov [216,217,218]. To achieve a more homogeneous distribution of the lipids slight modifications were made. In short, lipid mixtures were made from stock solutions in chloroform kept at -20 °C. For one preparation 100 nmol of lipids (including cholesterol) were mixed to 30 µl of chloroform. Single drops of the lipid mixture were pipetted onto two ITO or titanium slides and allowed to spread. To obtain homogeneously distributed lipid films the solvent was evaporated on a heater plate at 50 - 60 °C. To remove traces of the solvent the glass slides were put under a vacuum

(< 10 mbar) for 1 h. The electroswelling chamber was assembled from both lipid ITO coated slides using 1 mm Teflon spacers (Fig. 13).

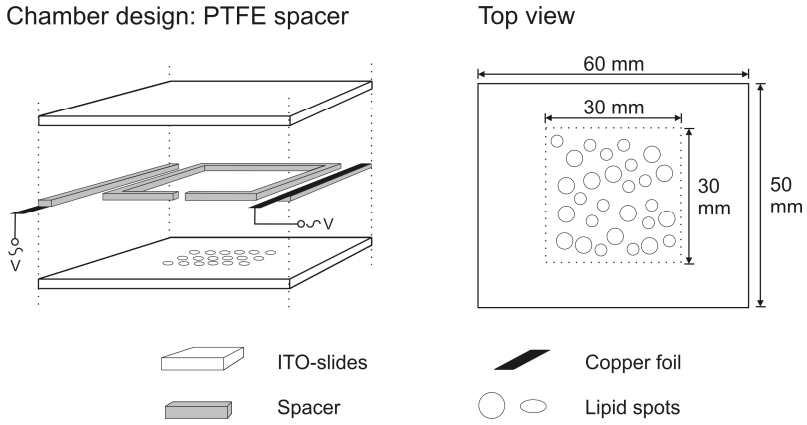

Fig. 13: Electroswelling chamber made from ITO-coated glass slides.

Alternatively, instead of ITO-coated glass slides chambers formed from two hollowed titanium sheets were used, since Ayuyan and Cohen (2006) reported that the ITO-coating may catalyse the formation of peroxides from unsaturated lipids [219]. One layer of Parafilm (Pechiney Plastic Packaging, Chicago, IL, USA) was used as insulation (Fig. 14).

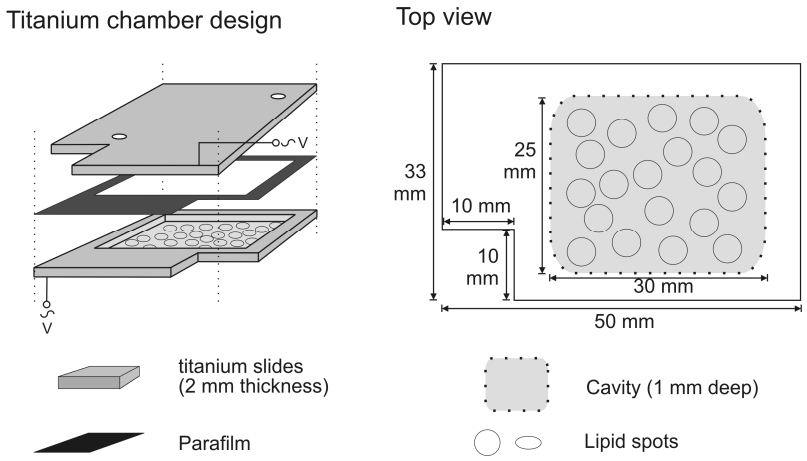

Fig. 14: Electroswelling chamber made from titanium sheets.

Both methods were used for GUV production; however no differences between GUV prepared by either method could be detected. In each case the chamber was filled with 1 ml of prewarmed (50 - 60 °C) sucrose buffer (see 3.1.2.4; Tab. 4) with an osmolality of 280 mOsm/kg. Immediately an alternating voltage (rising from 0.02 V to 1.1 V over 30 min) with a frequency of 10 Hz was applied. GUV formed during 2 h incubation at 50 - 60 °C. To detach the vesicles a voltage of 1.3 V (4 Hz) was applied for 30 min. The vesicles were stored in the dark at ambient temperature for up to 4 days until use.

3.2.1.2 Preparation of Giant Plasma Membrane Vesicles (GPMV)

GPMV were prepared from NBD-labeled HeLa-cells (see 3.2.2.3) as described by Baumgart *et al.* (2007) [25] who used a modified method described by Scott *et al.* (1976,1979) [220,221] and Holowka *et al.* (1983) [222]. In short, cells were grown to confluency in a 25 cm^2 plastic culture flask, then cells were washed twice with GPMV buffer (2 mM $CaCl_2$, 150 mM NaCl, 10 mM Hepes, pH 7.4), subsequently 1.5 ml of freshly prepared GPMV reagent (25 mM formaldehyde and 2 mM DTT in GPMV buffer) was added. The flasks were then incubated for 1 h at 37 °C while slowly shaking (60 - 80 cycles per minute). After incubation, GPMV that had detached from the cells were gently decanted into a conical tube. For the present experiments, GPMV were allowed to settle on ice for 10 - 45 min and collected by removing 20 % of the total volume from the bottom of the tube. GPMV were prepared by Anna P. Plazzo.

3.2.2 Cell culture and microscopy

3.2.2.1 Preparation of cells

HeLa- and HepG2-cells were grown in DMEM containing 4.5 g/l glucose, supplemented with 10 % heat-inactivated FBS and penicillin/streptomycin and routinely passaged in 25 cm^2 plastic culture flasks (in case of HepG2-cells coated with collagen A), medium was changed every 3 - 4 days. Jurkat-cells were grown in suspension in RPMI1640-Medium containing 2 g/l $NaHCO_3$ and acetylated Ala-Gln with 10 % heat-inactivated FBS in 25 cm^2 plastic culture flasks. Cell density was kept below 200,000 /ml by dilution. All cells were maintained at 37 °C under 5 % CO_2. HepG2-cells were prepared by Dr. Thomas Korte. Preparation of HeLa- and Jurkat-cells was done by Anna P. Plazzo.

3.2.2.2 Treatment of Jurkat-cells

For the treatment of Jurkat-cells with antibodies or sphingomyelinase 0.5 x 10^6 cells were pelleted (5 min; 200 x g). For activation with OKT3-antibody the pellet was resuspended in 25 µl RPMI1640 and 25 µl OKT3 for different times (10 min and 20 min) at 37 °C. The cells were again pelleted to remove excess antibody and incubated with 200 µl RPMI1640

containing 4 µl TRITC-labeled anti-mouse IgG (diluted 1:100) for 20 min (10 min OKT3) or 10 min (20 min OKT3), respectively.

For sphingomyelinase treatment 0.5 x 10^6 cells were pelleted and resuspended in 200 µl RPMI1640 containing 0.1 U/ml sphingomyelinase (from *Staphylococcus aureus*; Sigma-Aldrich) and subsequently incubated for 30 min at 37 °C.

3.2.2.3 Labeling of cells

NBD-labeled phospholipids were stored at -20 °C in chloroform or chloroform/methanol (1/1). Aliquots were transferred into a glass tube and dried under nitrogen-flow before being resuspended in PBS at the desired concentration. HeLa-cells (5 x 10^4) were seeded on 35 mm culture dishes with glass bottom (MatTek, Ashland, MA, USA) and grown for 1 day. After washing with cold PBS, cell labeling with C_6-NBD-PC was performed for 20 min on ice (final lipid concentration: 0.25 µM in PBS). Cells were then extensively washed with PBS (25 °C) and immediately analyzed by FLIM to ensure that NBD-lipids localized essentially in the outer leaflet of the plasma membrane. HepG2-cells were prepared according to the same protocol with minor changes: Cells were seeded on poly-D-lysine coated dishes, grown for at least 3 - 4 days, the final concentration of labeled lipids was 0.5 - 1 µM and all washing steps were done with $HBSS^+$. For labeling of treated and untreated Jurkat-cells (0.5 x 10^6), the cells were pelleted (5 min; 200 x g), resuspended with 200 µl 2.5 µM C_6-NBD-PC (in RPMI1640) and incubated for 10 min on ice. To remove the staining solution the cells were again pelleted and resuspended in 200 µl PBS. Experiments with HeLa- and HepG2-cells were done by Anna P. Plazzo and Dr. Thomas Korte, respectively.

3.2.3 Fluorescence lifetime imaging microscopy and data analysis

3.2.3.1 Fluorescence lifetime imaging microscopy (FLIM)

Confocal images were taken with an inverted IX81 fluorescence microscope equipped with a Fluoview 1000 scanhead (Olympus, Hamburg, Germany) and a 60x (N.A. 1.35) oil-immersion objective at 25 °C. FLIM images (512 x 512 pixels) were acquired by a commercial FLIM upgrade kit (PicoQuant, Berlin, Germany). The fluorophores were excited with a pulsed diode laser (pulse width: 60 ps; pulse frequency: 10 MHz; 4 µs/pixel) with a

wavelength of 468 nm. Emission was recorded using a 540/40 bandpass filter. Single photons were registered with a single photon avalanche photo diode (SPAD). The intensity of the laser was adjusted that the maximum photon count rate of the detector did not exceed 1 - 2 % of the pulse rate, thus 10^5 counts/s, to prevent a bias towards shorter lifetimes. Each photon carries a time tag saving the macroscopic "real time" and the microscopic delay time from the laser pulse. This method is called time correlated single photon counting (TCSPC) and allows for the reconstruction of the decay of the fluorescence excited state by the photon lag time. 4096 time bins are available for one excitation cycle, so that at a pulse frequency of 10 MHz the time resolution is approx. 24 ps. The real time tag is used to allocate the registered photons to the originating pixels of the FLIM image. For each image (512 x 512 pixels) 50 - 70 frames were acquired. The images were pseudocolor coded according to the average lifetime (τ_{av}) of the pixels.

$$\tau_{av} = \frac{\sum_i A_i \cdot \tau_i^2}{\sum_i A_i \cdot \tau_i}$$

For determination of fluorescence lifetimes (τ_i) and respective amplitudes (A_i) see below.

3.2.3.2 Determination of fluorescence lifetimes

For the analysis of the fluorescence lifetime parameters of the NBD-analogues in the phospholipid membranes in GUV and living cells membrane compartments were selected by applying an intensity threshold to exclude fluorescence from background or cytoplasm. If necessary the selection was refined manually to exclude regions not associated with the membrane. For the selected regions of interest (ROI) one overall fluorescence decay curve was generated by summing up the photons registered for that region. From the decay curve only the part not affected by the instrument response function (IRF) was used ("tail-fit"; approx. from 3 ns after beginning of the pulse). Using a non-linear least squares iterative fitting procedure fluorescence decay curves were fitted as a sum of exponential terms to obtain the fluorescence lifetimes of the NBD-group:

$$F(t) = \sum_i A_i \exp(-t/\tau_i)$$

where F(t) is the fluorescence intensity at time t and A_i is a pre-exponential factor representing the intensity of the time-resolved decay of the component with lifetime τ_i. Typically, appropriate fitting of a NBD fluorescence decay in GUV required three lifetime components. However, for GUV with lipid mixtures which are known to be in a single membrane phase state two lifetime components already provided adequate fitting (see 4.2.3; Tab. 11 and 12). For fitting of fluorescence decay in living cells in general three different lifetimes were applied. However, for decays originating from analogues in the plasma membrane, two lifetime components obtained a sufficient quality of the fit. Due to the tail fitting method it is likely that the short component τ_1 detected for NBD (see Results) might be underestimated. Quality of fits was judged by the distribution of the residuals and the χ^2 value.

For the calculation of lifetime histograms 2 x 2 pixels in the selected regions of interest were binned and the fitting procedure described above was repeated for each (binned) pixel using the lifetime parameters obtained from the overall decay curve as starting parameters. In the histograms the intensity weighted frequency (A_i x τ_i) of the lifetime component is summed up.

3.2.4 Molecular biology and protein purification

3.2.4.1 Cloning of the plasmid for α-synuclein expression

A plasmid (aSynWTHisN) coding for the 140 aa variant of α-synuclein was a generous gift by Erich Wanker (MDC, Berlin, Germany). To allow expression of untagged α-synuclein the open reading frame was amplified by polymerase chain reaction (PCR) (Phusion DNA-Polymerase; manufacturer's protocol; Finnzymes, Espoo, Finland) using primers which coded for *Nco*I and *Xho*I restriction sites. The amplified DNA-Fragment was subsequently digested in *Tango*-Buffer (2x) by *Nco*I and *Xho*I (5 U/50 µl each; o.n.; 37 °C). The digested DNA was purified following the protocol of the QIAquick Gel Extraction Kit (Qiagen, Hilden, Germany). The pET28 vector was as well double digested by *Nco*I and *Xho*I (same conditions), additionally dephosphorylated by incubation (1 U/50 µl; 1 h; 37 °C) with calf intestine alkaline phosphatase (New England Biolabs, Frankfurt am Main, Germany), purified by agarose gelelectrophoresis and again recovered from the gel by the Gel Extraction Kit. 9 µl of this DNA-Fragment and 5 µl linearized pET28 vector were mixed with 4 µl dH_2O

and 2 µl 10x Ligation buffer and ligated (4 h; RT) by means of T4 DNA-Ligase (1 U; New England Biolabs). For plasmid production 100 µl of calcium-competent *E. coli* XL1-Blue cells were transformed with 4 µl of the ligation sample (see below).

3.2.4.2 Site directed mutagenesis

For specific fluorescence labeling the S129C amino acid exchange was introduced using PCR-based mutagenesis. This position was chosen to assure that the dye does not interfere with structure formation and membrane binding of the N-terminal part of α-synuclein. Additional mutations (A30P, A53T and E46K) were generated using the same technique. The mutations were introduced into α-synuclein containing plasmids by means of PCR with a complementary primer pair carrying the desired mutation. In that way the amplified plasmids all carry this mutation. For a PCR-sample 0.5 µl of the template plasmid was mixed with 1 µl of each primer (Tab. 3; 20 µM), 1 µl dNTPs (10 mM), 10 µl HF-buffer (5x; Finnzymes), 36 µl dH_2O and 0.5 µl Phusion DNA-Polymerase (Finnzymes) giving a total volume of 50 µl. The sample was amplified in thermal cycler (MyCycler, Bio-Rad, München, Germany) in 20 cycles (30 s, 98 °C; 30 s, 66 °C; 3 min, 72 °C) after a first denaturation step (3 min, 98 °C). A last elongation step (10 min, 72 °C) allowed for finishing of DNA-fragments. After PCR methylated template DNA was digested by adding 1 µl of *Dpn*I (10 U/µl) and 1 h incubation at 37 °C. For plasmid production 200 µl of calcium-competent *E. coli* XL1-Blue or *E. coli* DH5α-cells were transformed with 10 µl of the digested PCR sample (see below).

3.2.4.3 Transformation of *E. coli*-cells and plasmid production

For transformation calcium-competent cells were used [223], which can be transformed by means of a heat shock. For plasmid propagation *E. coli* DH5α or XL1-Blue were transformed, while for protein expression Rosetta (DE3) pLysS-cells were used. The competent cells were mixed with the desired plasmid (for amounts see 3.2.4.1 and 3.2.4.2) and incubated on ice for 10 min. The heat shock was applied by incubation in a water bath at 42 °C for 45 s. Afterwards the cells were kept on ice for another 2 min. To allow for development of antibiotics resistance the transformed cells were mixed with 900 µl of LB medium (see 3.1.2.4; Tab. 5) and incubated for 1 h at 37 °C. For selection of transformed cells the sample was pelleted (6 min; 1,000 x g), the supernatant almost completely decanted and the

resuspended pellet spread on LB-agar dishes (see 3.1.2.4; Tab. 5) containing the appropriate antibiotic (50 µg/ml Kanamycin for XL1-Blue and DH5α; Rosetta (DE3) pLysS additionally required 34 µg/ml Chloramphenicol to maintain the pLysS plasmid). Colonies grown o.n. at 37 °C were used as inoculates for over night cultures for glycerol stocks [223], plasmid purification (XL1-Blue and DH5α) or expression tests (Rosetta (DE3) pLysS). Plasmids were purified using the QIAprep Spin Miniprep Kit (Qiagen) according to the manufacturer's protocol. The integrity of the coding region was tested by means of PCR-amplification of the T7-region of the plasmid checking the correct length and subsequent DNA sequencing (SMB, Berlin, Germany).

3.2.4.4 Expression and purification of α-synuclein variants

Before starting large scale protein expression the transformed Rosetta (DE3) pLysS clones were tested for their expression level. To do so, 5 ml of LB medium containing 50 µg/ml Kanamycin (Kan) and 34 µg/ml Chloramphenicol (Cm) were inoculated from glycerol stock or a single colony from LB-Agar plate. Identical incubation conditions (see below) as during the preparative fermentation were used. To check for protein yield, before and after induction with 1 mM IPTG an aliquot of cells equal to 1 OD_{600} was removed, pelleted by centrifugation and analyzed by SDS-PAGE. For preparative α-synuclein production 1 l of LB medium (see 3.1.2.4; Tab. 5; with 50 µg/ml Kan and 34 µg/ml Cm) was inoculated from a well grown over night culture (same medium composition) of the respective α-synuclein expressing Rosetta (DE3) pLysS clone to an approx. OD_{600} of 0.1 - 0.2. The cells were cultivated at 37 °C until an OD_{600} of 0.6 - 0.7 was reached. At that point protein expression was induced for 4 h at 37 °C using 1 mM IPTG. For purification of α-synuclein a protocol similar to the one described by Der-Sarkissian *et al.* (2003) was used [112]. In brief, the cells were harvested by centrifugation (10 min; 4,000 x g; 4 °C) and the pellet was resuspended in 10 ml of lysis buffer (see 3.1.2.4; Tab. 5) per liter LB-medium. After one freeze-thaw-cycle the sample was diluted with 10 ml of lysis buffer and the cells were lysed by ultrasonication (Branson, Danbury, CT). Endogeneous *E. coli* proteins were precipitated by boiling (10 min), subsequent centrifugation (10 min; 10,000 x g; 4 °C) and adjusting the pH to 3.5. After a second removal of precipitates (30 min; 10,000 x g; 4 °C) the supernatant was dialyzed twice (3 h and o.n.; 4 °C) against 1.5 l of IEX start buffer (DTT added freshly) in each case (see 3.1.2.4; Tab. 5). Before purification by means of fast protein liquid

chromatography (FPLC) particles were removed by filtration (0.45 µm pore size; PVDF; Carl-Roth). The first purification step was ion exchange chromatography (IEX) on Q-Sepharose FastFlow (25 ml packed in a XK 16/70 column; GE Healthcare, St. Gilles, UK). The column was perfused with the whole cell lysate at a flow rate of 6 ml/min. Unbound proteins were washed out with IEX start buffer until the UV detector (280 nm) of the ÄKTAprime FPLC-system (GE Healthcare) again reached the baseline. Subsequently impurities were removed with three column volumes at 200 mM NaCl in the start buffer and α-synuclein was eluted at 400 mM NaCl. Remaining contaminations sticking to the column were removed with IEX start buffer mixed with 1 M NaCl. Further purification and buffer exchange was achieved in a second purification step by gel filtration (16/60 Superdex 200 prepgrade, GE Healthcare). On the column, which was preequilibrated with GF buffer (see 3.1.2.4; Tab. 5), 5 ml of the pooled α-synuclein containing fractions from the IEX chromatography were injected. The proteins were eluted at a flow rate of 1.6 ml/min using gelfiltration buffer. α-Synuclein containing fractions eluting at about 90ml were identified by the specific molecular weight of the protein using SDS-PAGE and the characteristic shape of the UV-absorption spectrum. The α-synuclein containing fractions were pooled and the protein concentration was determined by UV-absorption. Molar extinction coefficients ($\varepsilon_{280} = 5960\ M^{-1}\ cm^{-1}$) were calculated using the ProtParam tool provided on the ExPaSy-Server (http://www.expasy.org). Immediately afterwards the sample was aliquoted and frozen at -78 °C until usage.

3.2.4.5 Tetramethylrhodamine (TMR) labeling of α-synuclein

For fluorescence microscopy the α-synuclein was covalently tagged with tetramethylrhodamine-6-maleimide (Invitrogen) which readily reacted with the cysteine residue introduced at position 129. The labeling reaction was set up according to the manufacturer's protocol. In short, to 450 µl of a 111 µM α-synuclein solution a tenfold molar excess of TMR-6-maleimide dissolved in 50 µl DMSO was added drop by drop. The reaction was incubated at RT for 2 h. Unbound label was removed using a NAP^5-column (GE Healthcare). The labeling efficiency was estimated to be approx. 1:1 using absorption spectroscopy. Labeling was also confirmed by SDS-PAGE and scanning the gels for TMR-fluorescence. After aliquoting labeled α-synuclein was immediately frozen at -78 °C.

Before the measurements the sample was purified a second time using centrifugable gel filtration columns (CentriSpin[10]; Princeton Separation, Adelphia, NJ, USA).

3.2.4.6 SDS-Polyacrylamide gel electrophoresis (SDS-PAGE)

For the size specific separation of proteins SDS-PAGE adapted from the original work of Laemmli (1970) was used [224]. For casting and running the gels the Mini PROTEAN 3 system (Bio-Rad) was used. In short, gels containing 15 % Acrylamide/Bisacrylamide in the separating and 5 % Acrylamide/Bisacrylamide in the stacking gel were used. For buffer compositions see 3.1.2.4 (Tab. 6). For sample preparation three volumes of the protein solution or resuspended pellet were thoroughly mixed with one volume of SDS sample buffer (4x) and heated to 95 °C for 5 min. Residual precipitates were pelleted during a centrifugation step (5 min; 10,000 x g, 4 °C) and the supernatant applied on the gel. Electrophoresis was run with running buffer at a voltage of 100 V until the samples entered the separating gel. From that point on the voltage was increased to 200 V for about 45 min. Protein bands in the gel were stained by means of incubation of the gel in Coomassie staining solution for at least 30 min. Coomassie blue unspecifically bound to the gel was washed out the gel with destaining solution until the background was only faint blue (at least 2 h). Destaining solution was exchanged if required.

3.2.4.7 Binding assay for TMR-labeled α-synuclein

To study the interaction between α-synuclein and GUV, 75 µl of the GUV-solution (see 3.2.1.1) were mixed with TMR-labeled α-synuclein and incubated at 25 °C for 30 min. The vesicle α-synuclein suspension was mixed with 225 µl of glucose buffer or NaCl buffer (see 3.1.2.4; Tab. 4). Both buffers were adjusted to an osmolality of about 300 mOsm/kg. For microscopy the sample was placed in a drop on a coverslip. Before imaging GUV were allowed to settle for 3 min to the bottom due to their greater specific density. The lateral distribution of anionic phospholipids in GUV was characterized by binding of fluorescent Annexin V-Cy3 (Sigma-Aldrich). Experiments were done as described above with the exception that instead of α-synuclein 0.3 µl of Annexin V-Cy3 in the presence of calcium chloride (final concentration: 2.5 mM) was used. In the absence of anionic lipids no binding of Annexin V to GUV was detectable. Images of the equatorial plane of the GUV were taken

by confocal laser scanning microscopy. Again images were taken with an inverted IX81 fluorescence microscope equipped with a Fluoview 1000 scanhead (Olympus) and a 60x (N.A. 1.35) oil-immersion objective at 25 °C. The green NBD-fluorescence was excited with the 488 nm laser line of an Ar-ion laser, while the red TMR-fluorescence was excited with a 543 nm He-Ne-laser. To avoid spectral overlap the system was run in sequential scanning mode where only one laser was active at the time. The emission of NBD was recorded between 500 nm and 530 nm, while the TMR-emission was recorded from 570 nm to 670 nm.

3.2.4.8 Quantitative analysis of the α-synuclein binding

To characterize the α-synuclein binding to PS containing vesicles in a quantitative way, DOPC GUV containing different amounts of DOPS were incubated with increasing concentrations of TMR-labeled α-synuclein. For microscopy the same protocol as already indicated in 3.2.4.7 was used. To quantify the amount of α-synuclein bound to the membrane images from the equatorial plane of GUV were averaged two times using the Olympus analysis software. The amount of membrane bound α-synuclein was inferred from the peak values of intensity profiles. To obtain the binding strength (K_0) of α-synuclein and the amount of available binding sites (b) of the DOPC/DOPS vesicles, data were fitted for the obtained TMR-fluorescence (TMR) according to the scaled particle theory of Chatelier and Minton, (1996) [225]:

$$\theta = \frac{TMR}{b}$$

$$c_{synuclein} = \frac{1}{K_0} \cdot \frac{\theta}{1-\theta} \cdot \exp\left(\frac{3\theta}{1-\theta} + \left(\frac{\theta}{1-\theta} \right)^2 \right)$$

To compare the binding affinity of α-synuclein at low and high ionic conditions 75 µl of the GUV solution (DOPC/DOPS = 70/30) were mixed with 0.6 µl of TMR-labeled α-synuclein (final concentration: 0.1 µM) and incubated at 25 °C for 30 min. The vesicle α-synuclein suspension was mixed with 225 µl of glucose buffer with low or NaCl buffer (see 3.1.2.4; Tab. 4) with high ionic strength. Final concentrations of NaCl were 0 mM or 105 mM, respectively. The ratio of the TMR-fluorescence at the GUV membrane between low and high ionic strength was calculated for each α-synuclein variant (WT, A30P, A53T, E46K).

3.2.4.9 Competition assay to study the binding efficacy of α-synuclein mutants

To assess the binding affinity of the α-synuclein mutants relative to the wildtype the following competition assay was used. 225 µl of glucose buffer (see 3.1.2.4; Tab. 4) were mixed with TMR-labeled wildtype α-synuclein (S129C-TMR; final concentration: 0.5 µM) and different concentrations of unlabeled protein variants (final concentrations: 0 - 5 µM). After mixing with 75 µl of GUV suspension (DOPC/DOPS = 70/30; additional 1 mol% C_6-NBD-PC) the samples were incubated for 30 min at 25 °C and the TMR-fluorescence at the GUV membrane was measured as described.

4 Results

4.1 GUV can be reliably produced from dried lipid films by electroformation

A well established method to produce GUV is the gentle hydration of dried lipid films in the presence of an alternating electric field. This method first described by Angelova and Dimitrov was used throughout this study [216,217,218]. As matrix for drying of the lipid film different conductive materials were used. GUV were prepared using ITO-coated glass slides as originally described, but also titanium chambers were used, as Ayuyan and Cohen (2006) stated that ITO may catalyze the formation of oxidized species of unsaturated phospholipids [219]. GUV suspensions prepared from ITO-coated slides had in general a high yield of vesicles, but in some cases it was difficult to form proper lipid films from PS containing lipid mixtures. In contrast the GUV yield was slightly lower when titanium chambers were used, but usable lipid films were achieved independent of the used lipid mixtures. No differences in vesicle morphology were found for both methods. In general, the GUV preparations contained a large fraction of unilamellar vesicles showing similar fluorescence intensities of the incorporated membrane probe (usually C_6-NBD-PC). Yet, multilamellar (higher fluorescence intensity) or fused vesicles were present to a more or less large fraction but were omitted from the study. In addition GUV which enclosed smaller vesicles or lipid aggregates were common. Such vesicles were used for the studies if it was obvious that the inclusions were free floating and did not impair the membrane. In lipid mixtures which yielded GUV with lateral lipid domain separation also vesicles without domain separation were observed to a small extent which demonstrated that in some cases the lipids distributed heterogeneously between the vesicles. But in all cases the main fraction of GUV showed the expected behavior.

C_6-NBD-PC was incorporated into GUV during the vesicle preparation resulting in symmetric labeling of both leaflets of the bilayer. The distribution of the probe was tested in GUV purely made from DOPC which should show a single homogeneous membrane phase presumably being a ld phase as the measurements were done at 25 °C well above the phase transition temperature of the lipid (-19 °C) [55]. The fluorescence was homogeneously distributed which is a clear sign that the probe at least at the resolution of the fluorescence microscope mixes ideally with the lipids and does not form domains or clusters of its own. On the contrary, when incorporated into GUV made from a lipid mixture (DOPC/SSM/Chol = 1/1/1; mol/mol/mol) which forms laterally separated lipid domains at 25 °C (transition temperature: approx. 43 °C [49]) C_6-NBD-PC strongly partitions in one of the domains. This is in excellent

agreement with previously published studies showing that the probe partitions strongly into ld lipid phases [38]. It can be safely assumed that this behavior is reproduced in the investigated GUV, therefore membrane regions which show bright fluorescence can be identified as ld domains. In contrast liquid ordered (lo) domains show nearly no or only weak fluorescence (Fig. 15).

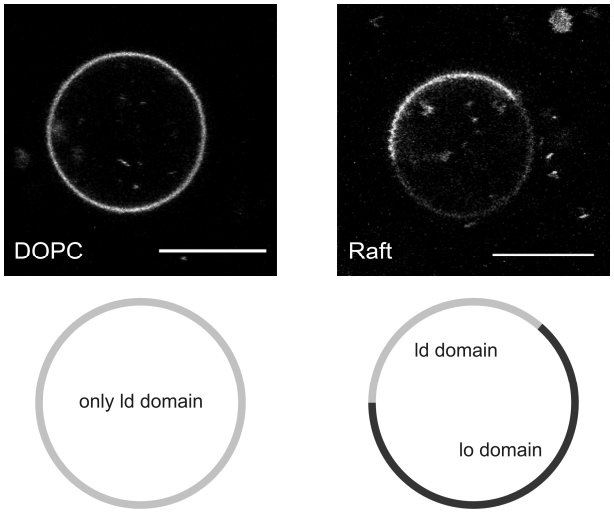

Fig. 15: C_6-NBD-PC preferentially enriches in the ld domain in GUV. Laser scanning microcopy images showing equatorial sections of GUV showing a homogeneous ld domain (DOPC: DOPC only) or lateral separation in ld and lo domains (Raft: DOPC/SSM/Chol = 1/1/1). All vesicles contained 1 mol% of C_6-NBD-PC. In vesicles with lipid domains in the µm-scale an enrichment of C_6-NBD-PC in one domain can be observed. Images were taken at 25 °C. White bars correspond to 10 µm.

4.2 Fluorescence lifetime analysis of NBD-labeled lipid analogues allows the visualization of lipid domains in model and cellular membranes

For quite a lot of research fields it is of great interest to study intrinsic properties of phospholipid membranes. One prominent topic here is the investigation of the formation of phospholipid domains in artificial or biological membranes. In the following a new method is described to investigate such issues by means of a single dye approach based on fluorescence lifetime imaging microscopy (FLIM). The described technique relies on the property of the NBD-group to show differential fluorescence lifetimes dependent on the lipid environment in which the probe is embedded. The results of the following section have been published in Stöckl *et al.* (2008a) [226].

4.2.1 Different NBD-lipid analogues show similar fluorescence lifetimes

To characterize the fluorescence lifetime parameters of the NBD-moiety of different lipid analogues the fluorescence decays of these compounds when integrated in GUV were investigated. The vesicles were prepared from pure DOPC (in the case of C_6-NBD-PS: DOPC/DOPS = 98/2) with an additional 1 mol% of the respective NBD-lipid analogue. All lipids showed a homogeneous distribution in the membrane. Lifetime analysis showed a bimodal lifetime distribution with a short (τ_1) and a long (τ_2) lifetime component of about 3 ns and 7 ns, respectively. While τ_2 represents the major component of the bimodal distribution, τ_1 only provides a minor contribution. The measured values were very similar for all investigated analogues, only C_{12}-NBD-PC showed a somewhat shorter τ_2 component. The measured values of τ_1 and τ_2 are summarized in Table 7.

Tab. 7: Fluorescence lifetimes of NBD-labeled lipid analogues in DOPC GUV (DOPC/DOPS = 98/2 in the case of C_6-NBD-PS). The concentration of NBD-labeled lipid corresponded to 1 mol% of total lipids. For estimation and explanation of τ_1 and τ_2, see 3.2.3.2 and text. Data are presented as average ± SEM. At least seven GUV were measured at 25 °C in each sample.

NBD-lipid analogue	τ_1 (ns)	τ_2 (ns)
C_6-NBD-PC	2.8 ± 0.2	7.1 ± 0.1
C_{12}-NBD-PC	2.1 ± 0.1	6.0 ± 0.1
C_6-NBD-PS	2.9 ± 0.2	7.1 ± 0.1
N-NBD-PE	2.2 ± 0.2	7.3 ± 0.1

The phospholipid analogue C_6-NBD-PC was chosen for further characterization as this compound in contrast to N-NBD-PE and C_6-NBD-PS possesses a biological headgroup without an overall charge, which could influence experiments with biological samples. These properties would also apply to C_{12}-NBD-PC, but since this probe showed fluorescence lifetimes deviant from the other NBD-analogues it was also omitted from further studies. Quantitatively similar components of C_6-NBD-PC were found in cuvette experiments with large unilamellar DOPC vesicles (Tannert and Herrmann, unpublished results).

4.2.2 Charged phospholipids and cholesterol influence the fluorescence lifetime of C_6-NBD-PC

In contrast to the above mentioned model system biological membranes consist of not only one defined lipid species but contain apart from the zwitterionic phospholipids additional lipids with negatively charged headgroups and cholesterol. In order to investigate the influence of the presence of such charges on the fluorescence lifetime components of C_6-NBD-PC GUV prepared from DOPC in combination with different amounts of DOPS were investigated. While the short lifetime component τ_1 was hardly affected, the longer component τ_2 was shifted to lower values with increasing concentration of DOPS (Tab. 8 and Fig. 16). This indicates that τ_2 is sensitive to physical properties of the membrane depending on the lipid composition. However, although the fluorescence lifetime τ_1 did not increase, an increasing contribution of this component to the overall fluorescence decay caused by DOPS was found (Fig. 16).

Tab. 8: Fluorescence lifetimes of C_6-NBD-PC in DOPC/DOPS GUV. The concentration of C_6-NBD-PC corresponded to 1 mol% of total lipids. For estimation and explanation of τ_1 and τ_2 see 3.2.3.2 and text. Data are presented as average ± SEM. At least seven GUV were measured at 25 °C in each sample.

DOPC / DOPS (mol / mol)	τ_1 (ns)	τ_2 (ns)
10 / 0	2.8 ± 0.2	7.2 ± 0.1
9 / 1	2.5 ± 0.2	6.3 ± 0.1
7 / 3	2.4 ± 0.2	5.9 ± 0.1
5 / 5	2.4 ± 0.1	5.8 ± 0.1
3 / 7	2.2 ± 0.1	5.4 ± 0.2

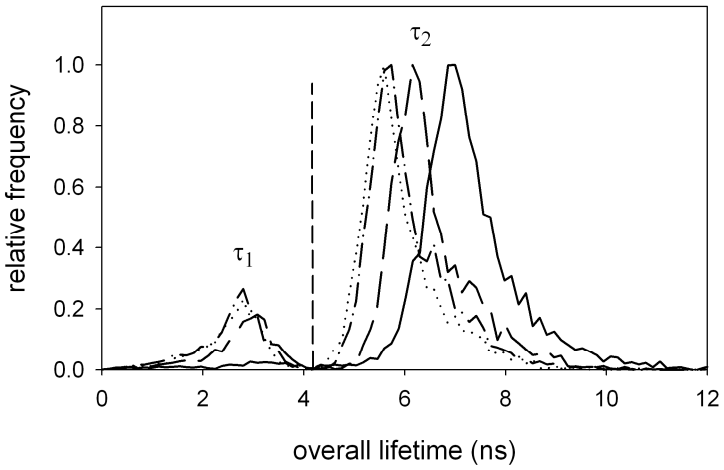

Fig. 16: Fluorescence lifetimes of C_6-NBD-PC in DOPC/DOPS GUV. Lifetime histograms of τ_1 and τ_2 of C_6-NBD-PC in GUV of different mixtures of DOPC/DOPS (mol/mol) at 25 °C: Curves are for 0 mol% (solid), 10 mol% (dashed), 30 mol% (dashed-dotted) and 50 mol% DOPS (dotted). Histograms were normalized by setting the maximum to 1.

It is known that cholesterol has an influence on the degree of order of phospholipid membranes making it an important regulator of membrane functions in cells [72]. In agreement with an increase in membrane order, the increase of the cholesterol content in DOPC vesicles from 0 mol% to 30 mol% yielded a moderate increase of τ_2. At all measured cholesterol concentrations τ_1 was almost negligible (Tab. 9 and Fig.17).

Tab. 9: Fluorescence lifetimes of C_6-NBD-PC in DOPC/Chol GUV. The concentration of C_6-NBD-PC corresponded to 1 mol% of total lipids. For estimation and explanation of τ_1 and τ_2 see 3.2.3.2 and text. Data are presented as average ± SEM. Ten GUV were measured at 25 °C in each sample.

DOPC / Chol (mol / mol)	τ_1 (ns)	τ_2 (ns)
10 / 0	1.6 ± 0.2	7.1 ± 0.1
9 / 1	2.0 ± 0.1	7.4 ± 0.1
7 / 3	2.3 ± 0.2	8.1 ± 0.1

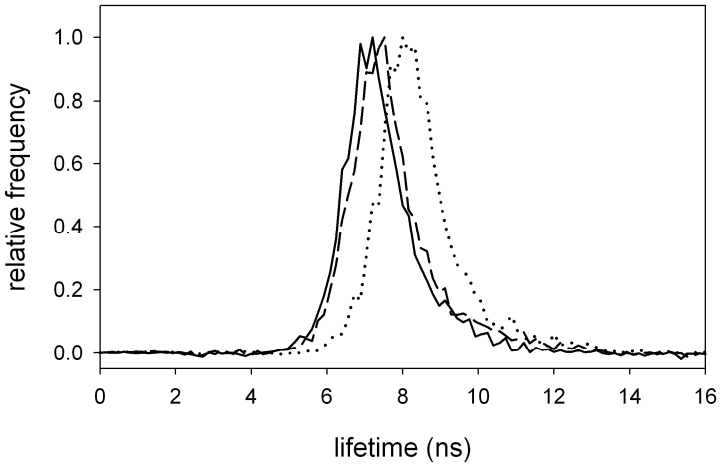

Fig. 17: Fluorescence lifetimes of C_6-NBD-PC in DOPC/Chol GUV. Lifetime histograms of τ_2 of C_6-NBD-PC in GUV of different mixtures of DOPC/Chol (mol/mol) (25 °C): Curves are for: 0 mol% (solid), 10 mol% (dashed) and 30 mol% cholesterol (dotted). Histograms were normalized by setting the maximum to 1.

4.2.3 Lifetime distribution of C_6-NBD-PC in GUV with heterogeneous lipid distribution

In contrast to the simple one- or two-component lipid mixtures described above (see 4.2.1 and 4.2.2), cellular membranes consist of different types of lipids which are not always homogeneously distributed in the phospholipid membranes but may form lipid domains enriched in certain lipid species. To assess whether lifetime of C_6-NBD-PC is sensitive to physical properties of lipid domains, GUV from mixtures of DOPC/SSM/Chol (1/1/1; mol/mol/mol) and of DOPC/DPPC/Chol (1/1/1) were prepared. GUV of those lipid mixtures are known to form lo and ld domains at 25 °C which can be visualized by lipid-like fluorophores such as C_6-NBD-PC (Fig. 15) [71,49]. Bright regions correspond to ld domains as C_6-NBD-PC recruits preferentially to these domains in this type of vesicles [38]. These GUV show a heterogeneous lateral distribution of C_6-NBD-PC documenting the domain formation. The different lipid domains are not only characterized by the preferential incorporation of the probe, but C_6-NBD-PC also shows a different fluorescence lifetime behavior in the respective domain. This can be directly seen in the different colors typical for ld and lo domain in the images pseudocolored according to the average lifetime of C_6-NBD-PC (Fig. 18 A; II). GUV prepared from DOPC and DOPC/SSM/Chol (1/1/8, excess of cholesterol) show only a pure ld or lo phase with the respective fluorescence lifetimes

(Fig. 18 A; I and III). This suggests that C_6-NBD-PC shows particular fluorescence lifetimes which are dependent on the incorporation of the probe into ld and lo domains.

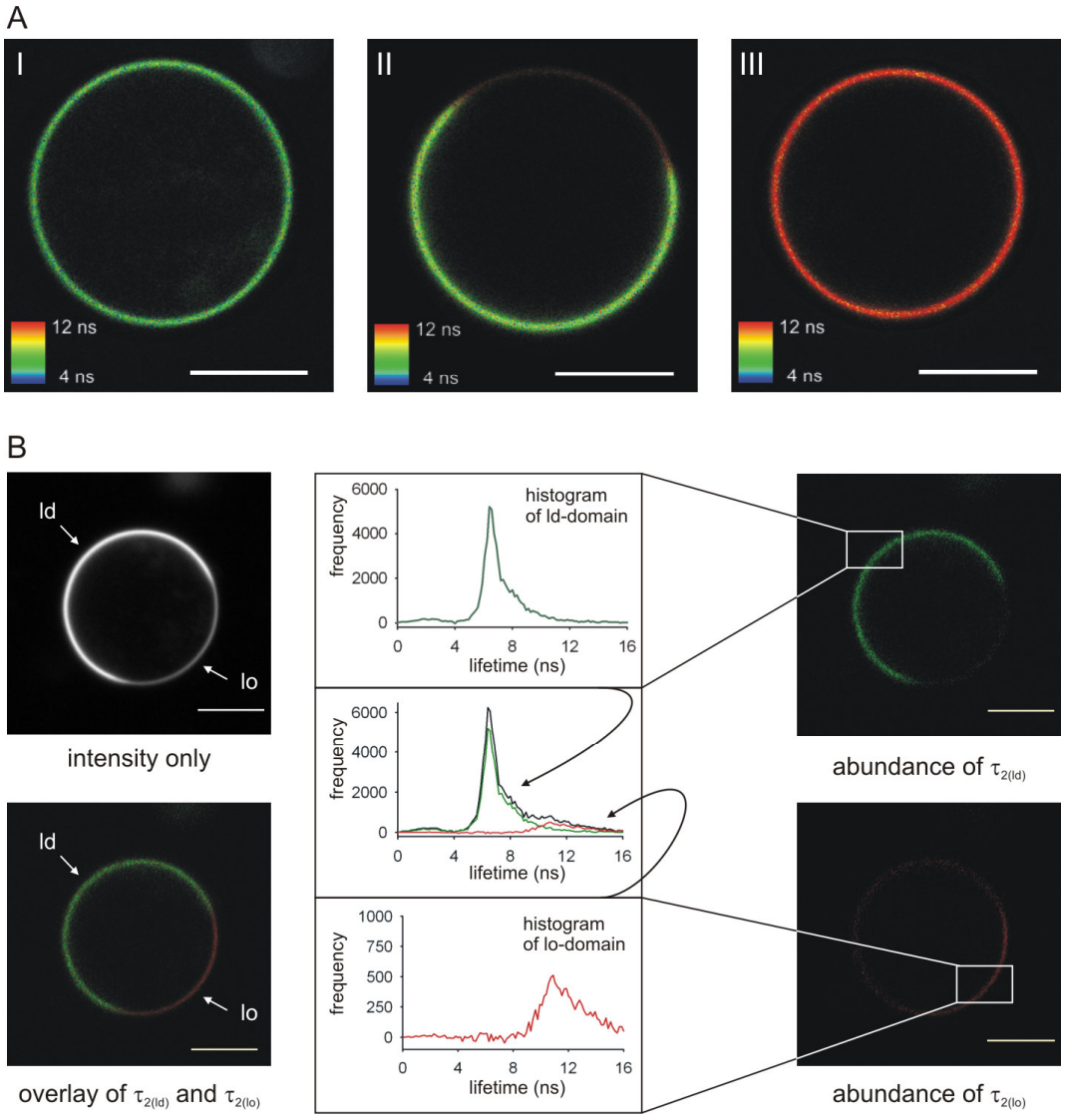

Fig. 18: Fluorescence lifetimes of C_6-NBD-PC in lipid domains of DOPC/SSM/Chol GUV. (A) Average lifetime (see scale) of C_6-NBD-PC in GUV prepared from DOPC (I, pure ld phase), DOPC/SSM/Chol = 1/1/1 (II; ld and lo phase) and DOPC/SSM/Chol = 1/1/8 (III; pure lo phase) at 25 °C. The average lifetime is longer in lo than in ld phase. (B) Lateral distribution of lifetime components $\tau_{2(lo)}$ and $\tau_{2(ld)}$ of C_6-NBD-PC in GUV prepared from DOPC/SSM/Chol = 1/1/1 (mol/mol/mol) at 25 °C. For each pixel the amplitude of the lifetime components $\tau_{2(ld)}$ (green, top image, right column) or $\tau_{2(lo)}$ (red, bottom image, right column) is presented. Comparison of the overlay of both images (bottom image, left column) with the intensity image (top image, left column) shows that $\tau_{2(ld)}$ is associated with the ld domain, while $\tau_{2(lo)}$ is associated with the lo domain. In addition for each domain the respective lifetime histogram is given (centre column). White bars correspond to 10 µm. For further details see Material and Methods and Results.

Apart from the short lifetime component τ_1 which was insensitive to the domain, for the longer lifetime τ_2 two typical components were found. The shorter component corresponds typically to the ld domain, $\tau_{2(ld)}$, while the longer corresponds to the lo domain, $\tau_{2(lo)}$. In Figure 18 B the distribution of these fluorescence lifetime components of C_6-NBD-PC in DOPC/SSM/Chol (1/1/1) GUV is presented. A similar pattern of fluorescence lifetimes was found for DOPC/DPPC/Chol (1/1/1) GUV (data not shown) providing evidence that the longer lifetime in the lo domain is not due to association of C_6-NBD-PC with sphingomyelin but only depends on the properties of the phospholipid membrane.

Since the local concentration of C_6-NBD-PC is higher in the ld domain where the probe is enriched, the shorter lifetime in comparison with the lo domain might be due to self-quenching of the probe. This could be precluded, as lifetime measurements on DOPC/SSM/Chol GUV (1/1/1) at different C_6-NBD-PC concentrations showed that τ_1 and τ_2 did not depend on NBD concentration within the range from 0.1 to 1 mol% (Tab. 10) proving that the differences between $\tau_{2(ld)}$ and $\tau_{2(lo)}$ did not ensue from self-quenching of NBD in the ld domain. As τ_1 comprises only a small contribution in each histogram it was omitted in the presentation of further results (see also 5.1.1).

Tab. 10: Concentration dependence of fluorescence lifetimes of C_6-NBD-PC in DOPC/SSM/Chol GUV (1/1/1). The concentration of C_6-NBD-PC is indicated as mol% of total lipids. For estimation and explanation of τ_1, $\tau_{2(ld)}$, and $\tau_{2(lo)}$ see 3.2.3.2 and text. Fluorescence decays for whole GUV were fitted with three components reflecting τ_1, $\tau_{2(ld)}$, and $\tau_{2(lo)}$. Data are presented as average ± SEM. Ten GUV were measured at 25 °C in each sample.

NBD-concentration (mol%)	$\tau_{1(ld)}$ (ns)	$\tau_{2(ld)}$ (ns)	$\tau_{2(lo)}$ (ns)
0.1 % C_6-NBD-PC	2.5 ± 0.2	7.1 ± 0.1	14.1 ± 0.7
0.5 % C_6-NBD-PC	3.1 ± 0.1	7.4 ± 0.1	11.8 ± 0.1
1.0 % C_6-NBD-PC	2.5 ± 0.1	7.0 ± 0.1	12.2 ± 0.1

In order to characterize the behavior of the DOPC/SSM/Chol system, lipid mixtures with different compositions were investigated. GUV composed of 10/0/0 or 4/4/2 DOPC/SSM/Chol showed a homogeneous distribution of C_6-NBD-PC. Domain formation was not detectable by fluorescence microscopy (Tab. 11). For those GUV only the shorter τ_2 component of approx. 7 - 8 ns corresponding to $\tau_{2(ld)}$ was detected. Also in 1/1/8 GUV no domain formation was observed. In this case only the long lifetime $\tau_{2(lo)}$ was found. However, both components, $\tau_{2(ld)}$ and $\tau_{2(lo)}$, were observed for lipid mixtures for which domains were visible by fluorescence microscopy (1/1/1, 3/3/4 and 2/4/4). Notably, $\tau_{2(ld)}$ and $\tau_{2(lo)}$ were

rather insensitive to the lipid mixture. $\tau_{2(ld)}$ varied between 7.0 and 7.6 ns, while $\tau_{2(lo)}$ varied between 11.4 and 12.4 ns. Figure 19 shows lifetime histograms of C_6-NBD-PC in GUV prepared from these lipid mixtures, while the representative values of fluorescence lifetimes are summarized in Table 11.

Tab. 11: Fluorescence lifetimes (τ_1 omitted) of C_6-NBD-PC in DOPC/SSM/Chol GUV. The concentration of C_6-NBD-PC corresponded to 1 mol% of total lipids. For estimation and explanation of $\tau_{2(ld)}$ and $\tau_{2(lo)}$ see 3.2.3.2 and text. If possible, fluorescence decays for whole GUV were fitted with three components reflecting τ_1 (not shown), $\tau_{2(ld)}$ and $\tau_{2(lo)}$. The presence of lipid domains visible by fluorescence microscopy is indicated in the right column. Data are presented as average ± SEM. Eight GUV were measured at 25 °C in each sample.

DOPC / SSM / Chol (mol / mol / mol)	$\tau_{2(ld)}$ (ns)	$\tau_{2(lo)}$ (ns)	**Visible Domains**
10 / 0 / 0	7.1 ± 0.1	---	no
8 / 1 / 1	7.6 ± 0.1	---	no
4 / 4 / 2	7.3 ± 0.1	---	no*
3 / 3 / 3	7.0 ± 0.1	12.2 ± 0.1	yes
3 / 3 / 4	7.1 ± 0.4	11.6 ± 0.1	yes
2 / 4 / 4	7.4 ± 0.2	11.4 ± 0.2	yes
1 / 1 / 8	---	12.4 ± 0.2	no

*Typically, GUV with a lipid composition of 4/4/2 did not show domain formation. Occasionally, small domains detectable by microscopy were observed.

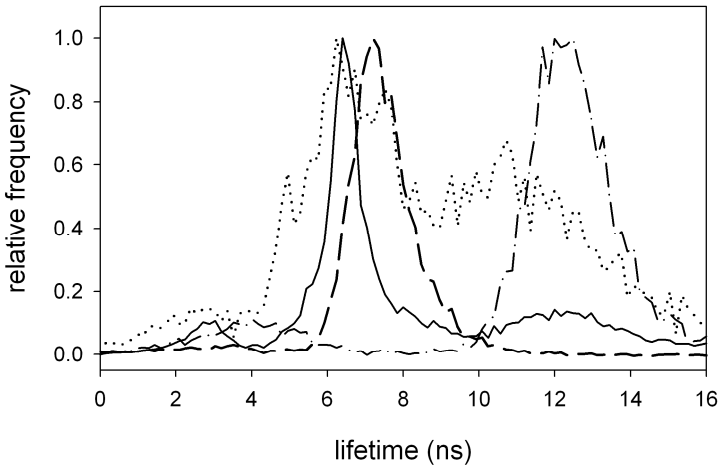

Fig. 19: Fluorescence lifetimes of C_6-NBD-PC in DOPC/SSM/Chol GUV. Lifetime histograms of C_6-NBD-PC in GUV prepared from DOPC/SSM/Chol mixtures (mol/mol/mol) at 25 °C: 4/4/2 (dashed), 3/3/3 (solid), 2/4/4 (dotted), 1/1/8 (dashed-dotted). Histograms were normalized by setting the maximum to 1. For further details see 3.2.3.2 and Table 11.

Still the question arises, whether the large increase of the lifetime component τ_2 in the ld domain with respect to the lo domain is due to the repartition of cholesterol into the DOPC-phase. This can be precluded, as during measurements of fluorescence lifetimes of C_6-NBD-PC in GUV prepared from binary DOPC/Chol mixtures the values of τ_2 only moderately increased from 7.1 ns in pure DOPC vesicles to about 8.1 ns at 30 mol% cholesterol content (Tab. 9). This is clear evidence that a NBD-lifetime of 11 to 12 ns is typical for the formation of the lo phase and not simply due to cholesterol enrichment. In addition, for DOPC/SSM/Chol (3/3/3 and 3/3/4) GUV $\tau_{2(ld)}$ is equal to τ_2 in DOPC GUV indicating that only minor amounts of cholesterol redistributed to the ld phase. In contrast, for DOPC/SSM/Chol (8/1/1, 4/4/2 and 2/4/4) GUV a higher $\tau_{2(ld)}$ is found indicating an altered composition of the ld phase.

Next, the fluorescence lifetime of C_6-NBD-PC in GUV of POPC/PSM/Chol mixtures was measured. In all lipid mixtures the content of PSM was kept constant at 20 mol%, while the cholesterol content varied between 5 and 60 mol%. In no case domains of microscopic size were detected. While at 5 mol% cholesterol apart from τ_1 only the component of τ_2 characteristic of the ld domain could be identified, for cholesterol contents in the range between 20 and 60 mol% a longer general lifetime allowed fitting of two components for τ_2, yielding the typical values $\tau_{2(ld)}$ and $\tau_{2(lo)}$ already found for the DOPC/SSM/Chol lipid mixtures. Between 20 and 40 mol% cholesterol the relative fraction of $\tau_{2(lo)}$ increased with rising amounts of cholesterol. At high cholesterol concentration (60 mol%) only minor amounts of $\tau_{2(ld)}$ could be found. As observed for DOPC/SSM/Chol lipid mixtures, $\tau_{2(ld)}$ and $\tau_{2(lo)}$ were again rather insensitive to the composition of the lipid mixture. However, $\tau_{2(ld)}$ was somewhat higher than for the DOPC-rich ld phase in DOPC/SSM/Chol GUV probably reflecting the differences in the degree of order between POPC and DOPC. Although the presence of $\tau_{2(ld)}$ and $\tau_{2(lo)}$ indicated the existence of lipid domains, neither the fluorescence intensity pattern nor fluorescence lifetime images revealed the existence of domains being of microscopic size. Hence, lipid domains are of submicroscopic size. This is in good agreement with a recent NMR-study done in a collaboration and published in Bunge *et al.* (2008) [72]. However, at 10 °C POPC/PSM/Chol mixtures may form domains in the microscopic range as observed for a (1/1/1) mixture (see Fig. 21; II). Representative values for the lifetime components are summarized in Table 12, while the corresponding lifetime histograms are presented in Figure 20.

Tab. 12: Fluorescence lifetimes (τ_1 omitted) and respective amplitudes A of C6-NBD-PC in POPC/PSM/Chol GUV. The concentration of C_6-NBD-PC corresponded to 1 mol% of total lipids. For estimation and explanation of τ and A see 3.2.3.2 and text. Amplitudes are given as a percentage of total amplitude (A_1 (not shown), $A_{2(ld)}$ and $A_{2(lo)}$). If possible, fluorescence decays for whole GUV were fitted with three components reflecting τ_1 (not shown), $\tau_{2(ld)}$, and $\tau_{2(lo)}$. Note, lipid domains were not visible by fluorescence microscopy (see 4.2.3). Data are presented as average ± SEM. Eight GUV were measured at 25 °C in each sample.

POPC / PSM / Chol (mol / mol / mol)	$\tau_{2(ld)}$ (ns)	$A_{2(ld)}$ (%)	$\tau_{2(lo)}$ (ns)	$A_{2(lo)}$ (%)
7.5 / 2 / 0.5	8.0 ± 0.1	83 ± 1	---	---
7 / 2 / 1 *	8.4 ± 0.1	85 ± 1	---	---
6 / 2 / 2 *	7.8 ± 0.1	86 ± 1	---	---
5 / 2 / 3	7.9 ± 0.4	37 ± 2	10.9 ± 0.1	52 ± 3
4 / 2 / 4	7.5 ± 0.2	25 ± 3	11.6 ± 0.1	69 ± 2
2 / 2 / 6	7.0 ± 0.4	21 ± 2	11.4 ± 0.1	73 ± 2

*Typically, GUV with a lipid composition of 7/2/1 and 6/2/2 were fitted biexponentially. In some cases a triexponential fit could be applied (not shown).

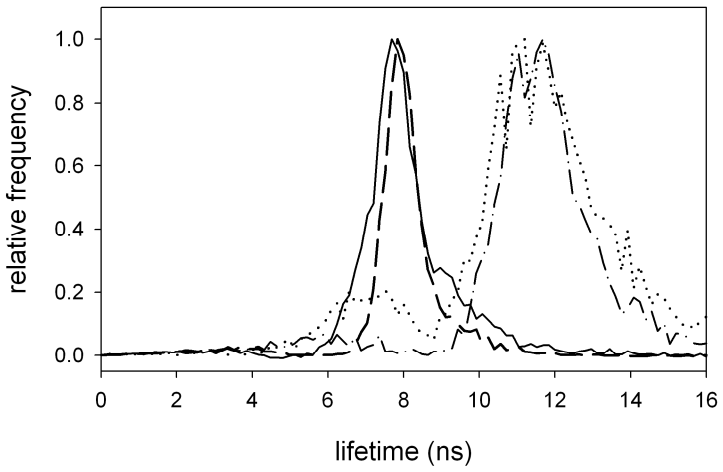

Fig. 20: Fluorescence lifetimes of C_6-NBD-PC in POPC/PSM/Chol GUV. Lifetime histograms of C_6-NBD-PC in GUV prepared from POPC/PSM/Chol mixtures (mol/mol/mol) at 25 °C: 7.5/2/0.5 (dashed), 6/2/2 (solid), 4/2/4 (dotted), 2/2/6 (dashed-dotted). Histograms were normalized by setting the maximum to 1. For further details see 3.2.3.2 and Table 12.

In summary, the characterization of the fluorescence lifetime behavior of C_6-NBD-PC in model lipid membranes showed that the longer fluorescence lifetime component τ_2 is sensitive to the lipid environment. Typically, a fluorescence lifetime of approx. 7 ns was found in pure DOPC GUV. While in the presence of DOPS shorter lifetime values for τ_2 were found, the incorporation of cholesterol led to longer values of τ_2. In GUV prepared from DOPC/SSM/Chol lipid mixtures known to form ld and lo domains on the µm-scale, domain

dependent values for τ_2 were observed. While $\tau_{2(ld)}$ was similar to the value found for DOPC GUV, the much longer fluorescence lifetime $\tau_{2(lo)}$ of approx. 12 ns was typical for the lo domain. In GUV prepared from POPC/PSM/Chol mixtures showing no lipid domains resolvable by fluorescence microscopy the typical values of $\tau_{2(ld)}$ and $\tau_{2(lo)}$ could still be recovered from the fluorescence decays demonstrating the presence of submicroscopic lipid heterogeneities.

4.2.4 Lifetime distribution of C_6-NBD-PC in Giant plasma membrane vesicles (GPMV)

In order to show that the characteristic fluorescence lifetimes of C_6-NBD-PC in the ld and lo domains are also conserved in vesicles with a biological lipid composition, GPMV produced from HeLa-cells were investigated. While at 25 °C approx. 40 % of the vesicles show phase separation, the fraction of vesicles showing distinct lipid domains increases to over 50 % at 10 °C. The investigated GUV (DOPC/SSM/Chol and POPC/PSM/Chol; both 1/1/1) also show domain separation at 10 °C. However, while for DOPC/SSM/Chol a strong partition of C_6-NBD-PC into the ld domain was observed, the ld domain specific enrichment is much weaker for the POPC/PSM/Chol mixture (Fig. 21). In contrast to these GUV, C_6-NBD-PC shows no domain dependent distribution or even a slight preference for the lo domain in the GPMV. Hence, the partition coefficient for C_6-NBD-PC between lipid domains depends on the lipid composition of domains. Identities of domains in GPMV have been determined by co-staining with N-Rho-DOPE, which is known to partition into ld domains (not shown) [25].

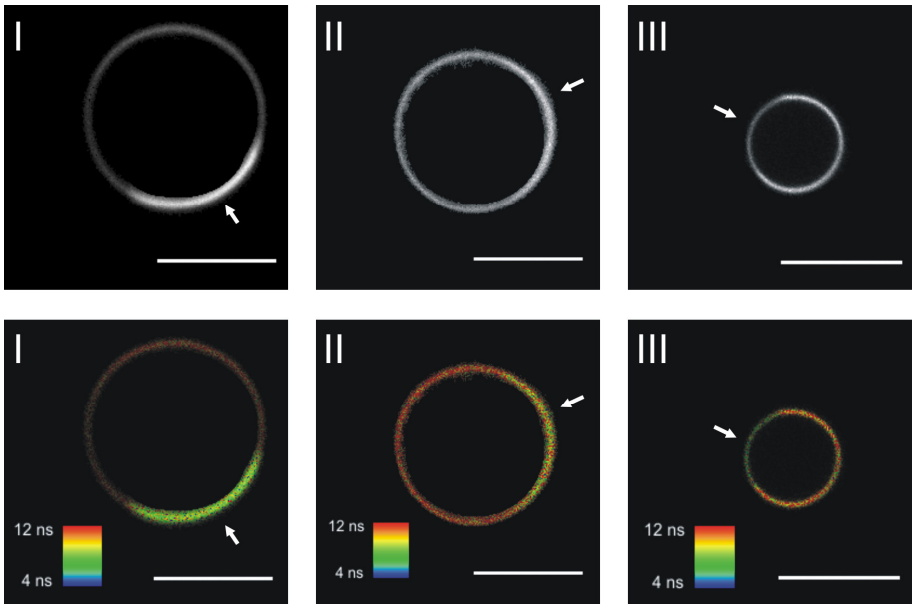

Fig. 21: Domain specific partition and fluorescence lifetime of C_6-NBD-PC in GUV and GPMV. GUV prepared from DOPC/SSM/Chol = 1/1/1 (I), POPC/PSM/Chol = 1/1/1 (II) and GPMV prepared from HeLa-cells (III; Anna P. Plazzo). Top row: Fluorescence intensity of C_6-NBD-PC. Bottom row: Average fluorescence lifetime of C_6-NBD-PC (pseudocolor, see scale). For all vesicles a longer fluorescence lifetime in the lo domain than in the ld domain independent of the partition of C_6-NBD-PC between domains was typical. ld domains are indicated by an arrow. White bars correspond to 10 µm. Images were taken at 10 °C.

The analysis of the fluorescence lifetimes of C_6-NBD-PC in the lipid domains showed that the characteristic lifetime values for τ_2 were still conserved. Independent of the domain specific distribution for the ld domains τ_2 of the fluorescence lifetime of C_6-NBD-PC was found to be in the range of 7.6 to 8.8 ns. For the lo domains values from 10.5 to 12.1 ns were measured. Notable is that the measured fluorescence lifetimes of C_6-NBD-PC increased only moderately when the temperature was lowered from 25 °C to 10 °C. Pure ld phase vesicles (DOPC and POPC) showed a similar behavior (data not shown).

However, by selection of ROIs separate analysis of domains demonstrated lipid domain characteristic values of τ_2 as observed for GUV. In Figure 22 the lifetime histograms for lo and ld domains as well as their envelope are shown (only for 25 °C). In addition some domain forming GPMV did not show a preference of C_6-NBD-PC for a specific domain. Yet, domains could be distinguished by fluorescence lifetimes (see arrow in Fig. 22 I and II). Lifetimes of GMPV were lower with respect to those found in the plasma membranes of intact HeLa-cells. Very likely, preparation of GPMV affects membrane organization, e.g. as interaction with cytoskeleton and transbilayer lipid asymmetry [25]. The analysis of fluorescence decays of C_6-NBD-PC in GPMV for which lipid domains of microscopic size

were not observed, neither by intensity nor by lifetime images, showed that the lifetime histogram of those GPMV was very similar to the envelope histogram of GPMV forming large domains (Fig. 22). Experiments with GPMV derived from HeLa-cells were performed in collaboration with Anna P. Plazzo.

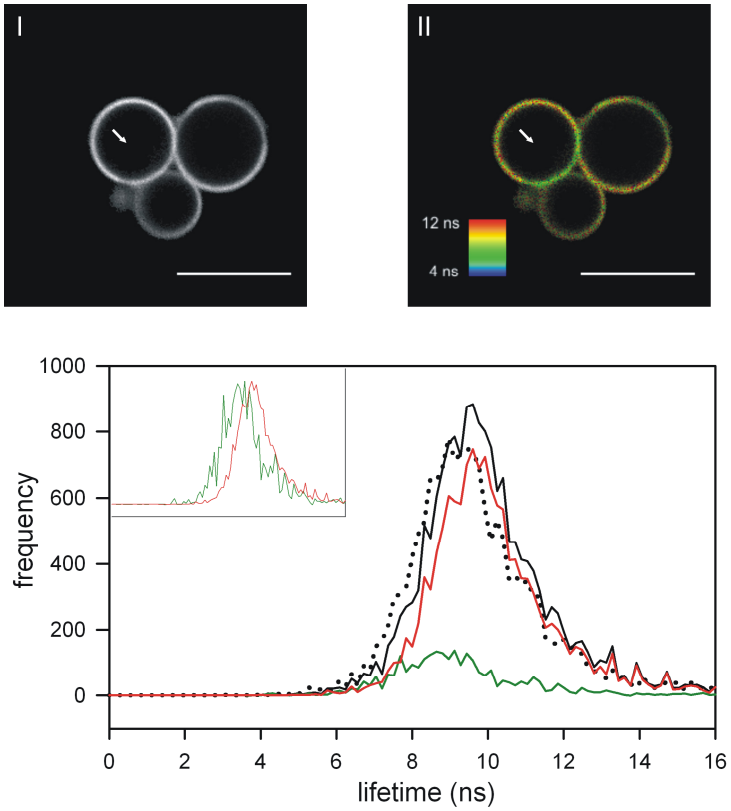

Fig. 22: Partition and fluorescence lifetime of C_6-NBD-PC in GPMV. C_6-NBD-PC shows in GPMV prepared from HeLa-cells only a very weak preference for specific domain (I; intensity image). ld (white arrow) and lo domains can be characterized by lifetime differences (II; pseudocoloring according to the average lifetime). White bars correspond to 10 µm. Below, the lifetime histograms of τ_2 for ld domains (green line) and lo domains (red line) as well as their envelope (full line, black) are shown. The histogram of GPMV showing no lipid domains (dotted line, black) is very similar to the envelope histogram of GPMV forming large domains. In the inset the normalized histograms for ld and lo domains are shown. Measurements were made at 25 °C in collaboration with Anna P. Plazzo.

In summary, the characterization of the fluorescence lifetime of C_6-NBD-PC in different vesicle systems showed that the typical values for ld and lo domains were preserved independent of the preferential enrichment of C_6-NBD-PC in a certain domain. Furthermore, independent of the presence of lipid domains on the µm-scale, similar fluorescence lifetime histograms of C_6-NBD-PC were found in the more biological GPMV originating from the plasma membrane of HeLa-cells suggesting that submicroscopic lipid domains were still present even when large scale lateral lipid segregation was not observed.

4.2.5 Lifetime distribution of C_6-NBD-analogues in cellular membranes

In order to study whether the application of the fluorescence lifetime approach based on NBD-lipid analogues is feasible also in biological systems, the fluorescence lifetime behavior of the dyes incorporated in the plasma membrane of cells was studied.

In a first experiment HepG2-cells were labeled with C_6-NBD-PC and C_6-NBD-PS. Upon incubation of HepG2-cells with C_6-NBD-PC on ice essentially the plasma membrane was labeled (Fig. 23 A). Intracellular staining was very faint if at all present. The lifetime distribution of the analogue allows distinguishing between several components (Fig. 23 A, see plot (IV) and image (III)). Whereas the amplitude of the short lifetime τ_1 around 1.8 ns was very small, two major lifetimes τ_i and τ_p with maxima centered at 6.4 ns and 10.9 ns were observed. Image analysis revealed that the longer lifetime τ_p was essentially found in the plasma membrane, while τ_i was rather associated with intracellularly localized analogues. The higher amplitude of τ_p with respect to τ_i was in agreement with the preferential localization of the analogue in the plasma membrane. Notably, if the plasma membrane was selected as ROI, beside τ_1 only the longer lifetime component τ_p was found which was similar to $\tau_{2(lo)}$ observed for lo domains of GUV. Essentially the same pattern of lifetime distribution was observed when cells were incubated for one hour at 37 °C after labeling (Fig. 23 B). The analogue remained mainly confined to the plasma membrane. Intracellular labeling was slightly enhanced probably due to transport of the analogue along endocytic pathways or some slow redistribution across the plasma membrane as also indicated by an increase of the contribution of τ_i.

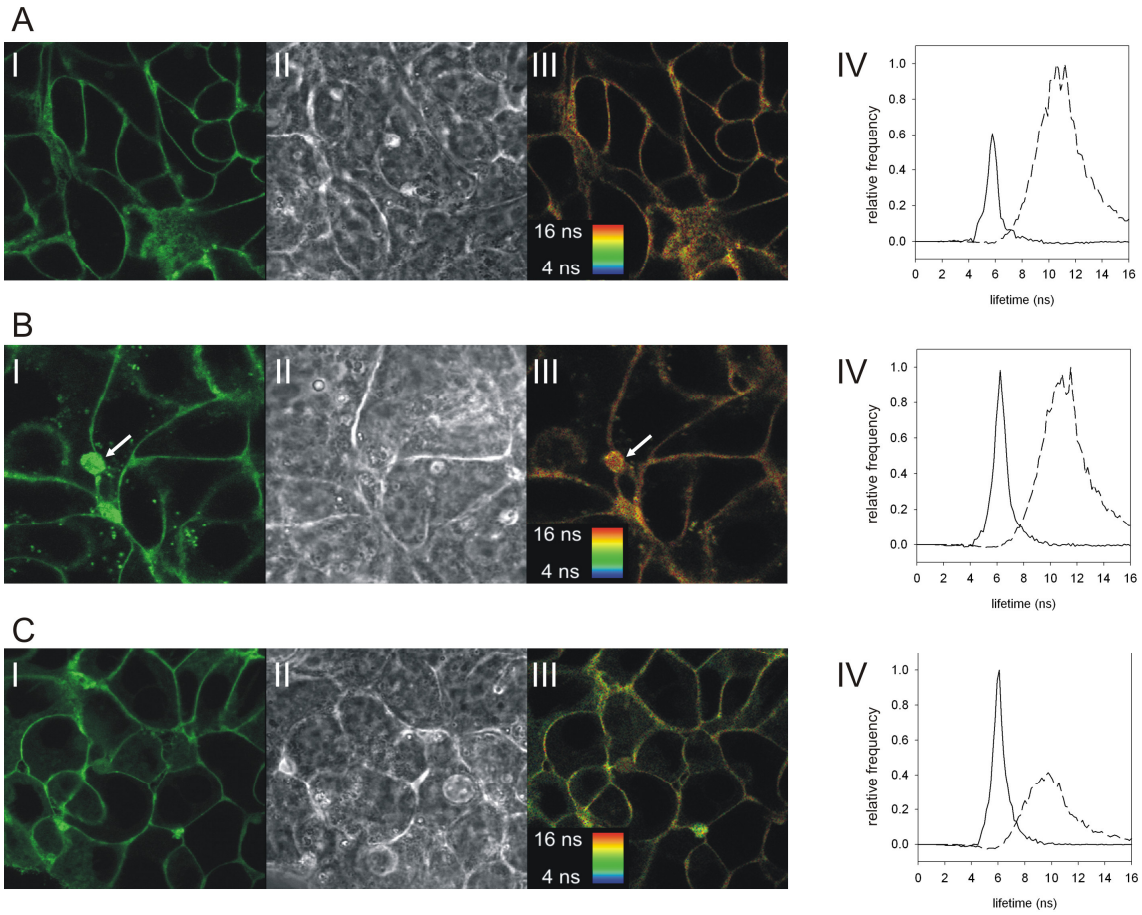

Fig. 23: Fluorescence lifetimes of C_6-NBD-PC (A, B) and C_6-NBD-PS (C) in HepG2-cells. Fluorescence lifetime of lipid analogues was measured at 25 °C immediately after labeling (A, C) and after one hour of incubation at 37 °C (B) (see 3.2.2.3). (I) – confocal fluorescence microscopy; (II) – DIC microscopy; (III) – average lifetime shown as pseudocolor image (see scale); (IV) – histogram of lifetime: τ_i (full line) and τ_p (dashed line). For explanation see 4.2.5. The larger spherical compartment in B corresponds to a canalicular vacuole (arrow). C_6-NBD-PC becomes enriched in this compartment [227]. Images were taken and analyzed in collaboration with Dr. Thomas Korte.

A similar distribution of lifetimes was observed for C_6-NBD-PS (Fig. 23 C) with a maximum at 6.5 ns and 10.9 ns for τ_i and τ_p, respectively. Again, τ_p essentially originated from molecules in the plasma membrane. However, contribution of τ_i was much higher in comparison to C_6-NBD-PC reflecting the enhanced intracellular localization of the PS analogue, as in GUV C_6-NBD-PC and C_6-NBD-PS showed similar lifetime behavior (see 4.2.1 and Tab. 7). Intracellular staining which was even stronger after one hour of incubation (not shown) is due to an aminophospholipid translocase activity which transports PS and respective analogues such as C_6-NBD-PS but not PC (analogues) to the cytoplasmic leaflet of the plasma membrane of HepG2-cells as previously shown [228,229,230]. Even at low temperature, an efficient transport is observed which leads to intracellular staining during the labeling

procedure. Upon translocation to the cytoplasmic leaflet, C_6-NBD-PS redistributes among intracellular membranes. Experiments with HepG2-cells were performed in collaboration with Dr. Thomas Korte.

The fluorescence lifetime behavior of C_6-NBD-PC was also studied in Jurkat-cells (immortalized T lymphocytes). A transition from the resting to the activated state can be induced by cross linking the CD3 receptors using an appropriate antibody (OKT3; personal communication with Marc Sylvester; FMP, Berlin, Germany). Cell activation is accompanied by rearrangements in the plasma membrane and the formation of ordered regions [27,31]. As already observed for HepG2-cells, for fitting of the fluorescence decays stemming from the plasma membrane two components were sufficient. In general, values of τ_p (10.4 ns) were similar to the values obtained for HepG2-cells. C_6-NBD-PC became enriched in some regions of the plasma membrane (Fig. 24 A, arrows). Shorter fluorescence lifetimes, presumably due to C_6-NBD-PC self-quenching, were typical for such regions. Thus, these regions were excluded from the ROIs during the fitting procedure. To study membrane rearrangements induced by the activation of these cells, Jurkat-cells were incubated with OKT3 antibodies which were cross-linked with a fluorescently labeled secondary antibody, prior to labeling with C_6-NBD-PC. Although no enrichment of the secondary antibody at the plasma membrane and no microscopic lipid domains with altered lifetimes could be detected, there was in general a pronounced decrease in the lifetime of τ_p (Fig. 24 B).

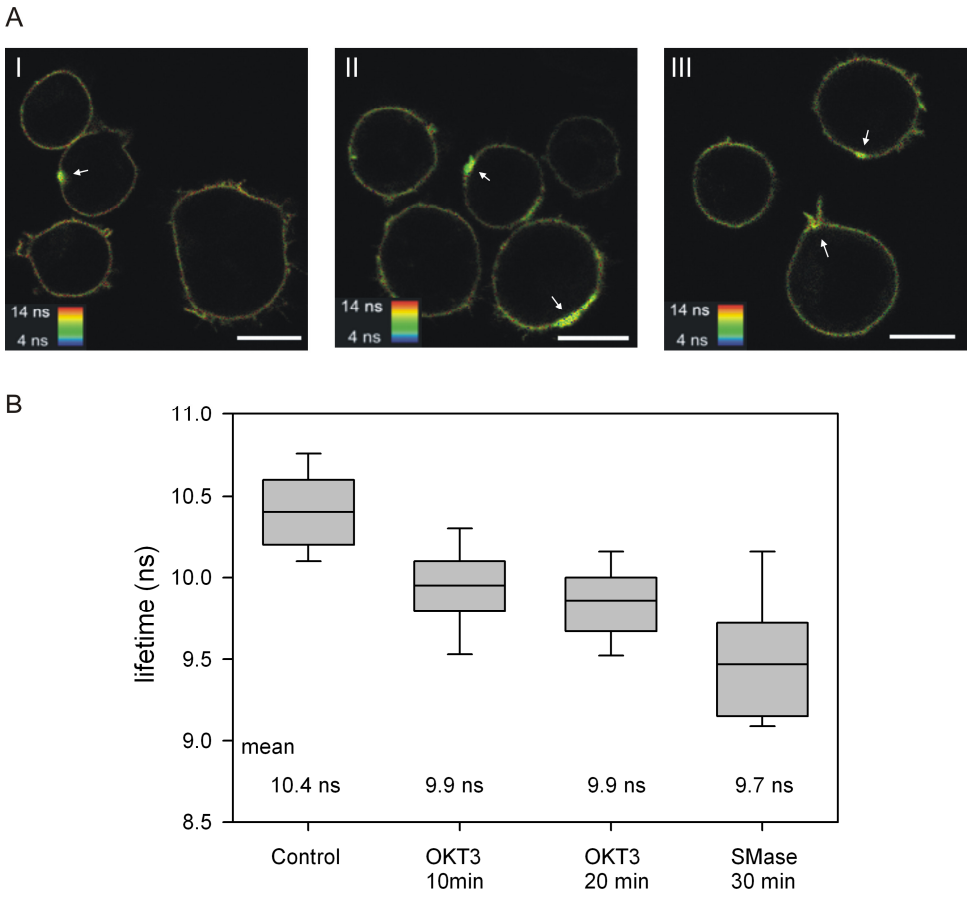

Fig. 24: Fluorescence lifetime of C_6-NBD-PC in resting and activated Jurkat-cells. Fluorescence lifetime of lipid analogues was measured at 25 °C immediately after labeling (see 3.2.2.3). (A) Fluorescence lifetime images of Jurkat-cells (2 x 2 pixels binned). Regions in which C_6-NBD-PC is highly enriched (arrows) were excluded from analysis. The average lifetime is shown as pseudocolor (see scale). (I) – not treated cells; (II) – 20 min OKT3; 10 min anti mouse IgG; (III) – 30 min sphingomyelinase. White bars correspond to 10 µm. (B) Values of τ_p in the plasma membrane of Jurkat-cells (treated as indicated). Boxes indicate median and 25th and 75th percentile, while 10th and 90th percentile are indicated by the whiskers. For each sample 23 cells were analyzed. Differences between control and treated cells are highly significant (t-test; $p<10^{-7}$ in each case).

In a second approach Jurkat-cells were incubated with sphingomyelinase which is able to cleave SM yielding ceramide. This step is also thought to be involved in the natural activation sequence of Jurkat-cells [29]. Again, shorter lifetime values of τ_p were observed (Fig. 24 B). In all samples no lipid domains on the µm-scale or morphological differences between resting and activated cells were found, although minor lifetime variations in the plasma membrane could be observed in some cells. While these may origin from lipid heterogeneities, also statistical variances in the fitting procedure may explain their existence.

In summary, the characterization of the fluorescence lifetime of C_6-NBD-PC showed no domain formation in the plasma membrane of HepG2- or Jurkat-cells. The recovered

fluorescence lifetime values were between the values of $\tau_{2(ld)}$ and $\tau_{2(lo)}$ in GUV and dependent on the membrane composition. C_6-NBD-PC incorporated in intracellular membranes e.g. showed a shorter fluorescence lifetime compared to C_6-NBD-PC localized in the plasma membrane. In addition, the altered membrane composition triggered by the activation or sphingomyelinase treatment of Jurkat-cells was sensed by the NBD-probe and reflected in an altered fluorescence lifetime.

4.3 α-Synuclein selectively binds to anionic phospholipids embedded in liquid-disordered domains

The protein α-synuclein is known to play a major role during the development of Parkinson's disease. While previous studies could clearly show that the protein associates with membranous structures like synaptic vesicles and that such interactions refer to the function of α-synuclein – which is not known up to know – the factors important for the membrane interactions are still elusive. While it is already established that negatively charged lipids are required for the recruitment of α-synuclein at the membrane, additional factors which also might play a role are still under discussion. In the following section a new approach based on GUV to study the domain specific interaction of α-synuclein with phospholipid membranes is described. These huge vesicles with diameters up to 50 µm have the advantage that membrane properties like lateral phospholipid distribution and domain formation can be visualized directly by fluorescence microscopy. For this purpose GUV were labeled with 1 mol% of the green fluorescent lipid analogue C_6-NBD-PC which is known to localize preferentially in the ld phase [38]. A characterization of the physical properties of such domains by the fluorescence lifetime is shown in 4.2.3. The results of the following section have been published in Stöckl *et al.* (2008b) [231].

4.3.1 Expression and purification of α-synuclein

For the membrane binding experiments fluorescently labeled α-synuclein variants were needed. For specific labeling of the protein a cysteine residue was generated replacing serine 129 located in the C-terminal part of the protein (Fig. 10). This position was chosen, as the C-terminal part (residues 103-140) of α-synuclein is not involved in membrane binding. In addition, serine is structurally similar to cysteine. This assured that the influence of the amino

acid exchange and the subsequent labeling with tetramethylrhodamine-6-maleimide (TMR-6-maleimide) had minimal influence on the membrane binding properties of α-synuclein. Apart from this amino acid exchange (S129C), also the α-synuclein variants known to cause hereditary Parkinson's disease (A30P, A53T and E46K), bearing a cysteine residue at the same position, were generated by means of PCR-based mutagenesis. In order to get high yields of recombinant α-synuclein the protein was expressed in the BL21 derived *E. coli* strain Rosetta (DE3) pLysS using the pET28 plasmid. During purification (see 3.2.4.4) the heat treatment precipitated most of the endogeneous *E. coli* proteins, so that mainly the heat stable α-synuclein with minor impurities remained in the supernatant (Fig. 25 C; "before IEX"). Notably, almost no α-synuclein was found in the protein pellet. In ion exchange chromatography two main protein fractions were eluted at 200 mM and 400 mM NaCl, respectively (Fig. 25 A; arrowhead and arrow). The pooled fractions eluting at 200 mM NaCl were of yellow color and showed a molecular weight of approx. 45 kDa on SDS-PAGE (not shown). Almost pure α-synuclein showing the appropriate molecular weight of 14 - 15 kDa in SDS-PAGE (not shown), eluted at 400 mM NaCl (Fig. 25 A; arrow). For buffer exchange and further purification these pooled fractions were subjected to gel filtration chromatography. Apart from minor impurities the main protein peak eluted at a retention volume of about 90 ml corresponding to an apparent molecular weight of approx. 50 kDa (Fig. 25 B; arrow). This difference is caused by the non globular extended conformation of the natively unstructured protein α-synuclein. The pooled fractions again showed a molecular weight of about 14 kDa typical for monomeric α-synuclein on SDS-PAGE (Fig. 25 C; "after GF"). An additional peak of low molecular weight compounds was detected at a volume of 120 ml (Fig. 25 B).

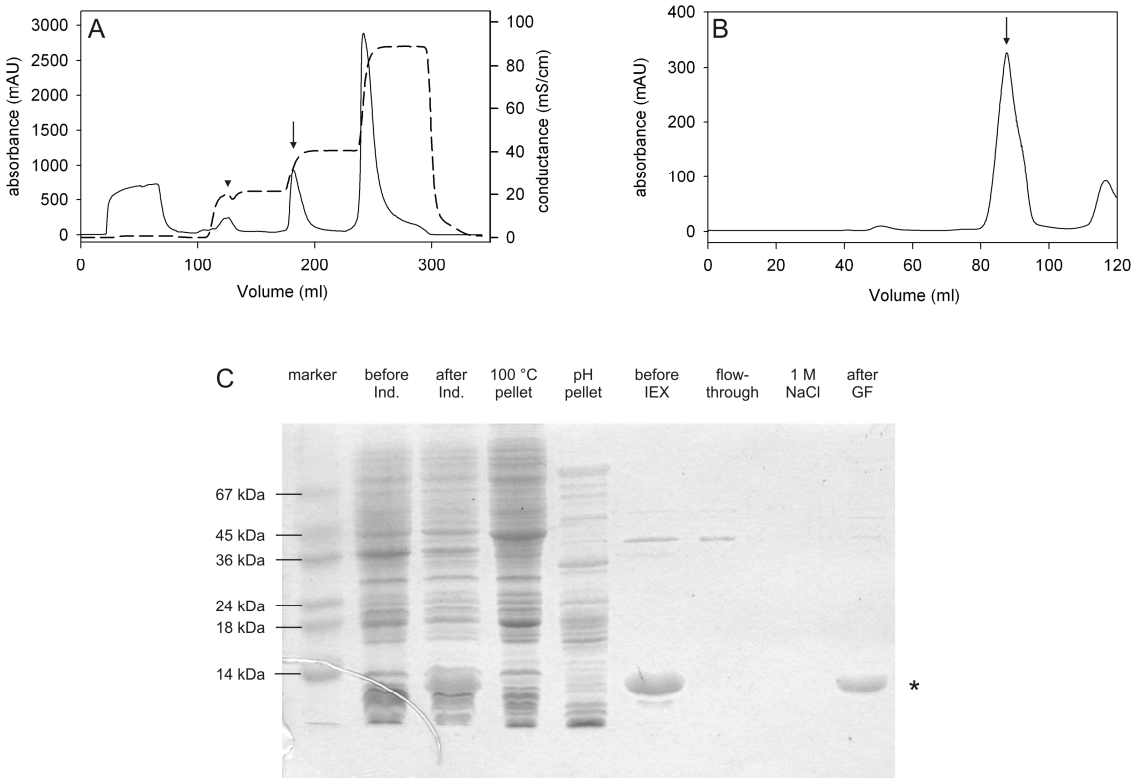

Fig. 25: Purification of recombinant α-synuclein e.g. A53T S129C. (A) IEX-chromatography after precipitation of endogeneous *E. coli* proteins by heat and pH-shift. Absorbance (full line) and conductance (dashed line) of the eluate are shown. After removement of impurities at 200 mM NaCl (arrowhead) α-synuclein containing fractions are eluted at 400 mM NaCl (arrow). (B) Gel filtration of pooled α-synuclein containing fractions from IEX. α-Synuclein eluted at a volume of 90 ml (arrow) corresponding to an apparent molecular weight of 50 kDa. (C) During purification of α-synuclein A53T S129C each step was tracked by SDS-PAGE (Coomassie staining). After induction of transformed *E. coli* by IPTG a thick band with the appropriate size for α-synuclein was visible (asterisk; lanes: "before Ind." and "after Ind."). The pellets of heat ("100 °C pellet") and pH precipitation ("pH pellet") were free of significant amounts of α-synuclein. Only minor impurities (see text) remain in the supernatant before IEX ("before IEX"). During IEX α-synuclein is absent from samples taken from the column flowthrough ("flowtrough") and the washing of the column ("1 M NaCl"). After gel filtration ("after GF") no impurities could be detected. The "marker" lane contains a molecular weight marker (Fluka, 69814).

To assure further the identity of the purified protein, UV-absorption spectra of the pooled fractions at 90 ml and 120 ml elution volumes were measured. While the fractions eluting at 90 ml showed an absorption spectrum with a maximum at 275 nm – caused by solvent exposed tyrosine – typical for an unfolded protein lacking tryptophan, the fractions at 120 ml showed a maximum of about 260 nm with only minor absorption at 280 nm. This corroborates the results of the SDS-PAGE analysis that the 90 ml fractions indeed consist of α-synuclein. The absorption at short wavelengths of the 120 ml compound suggests that negatively charged cytoplasmic substances with a low molecular weight, like nucleotides,

small RNAs or other aromatic compounds were co-purified with α-synuclein during IEX chromatography. Labeling efficiency and monomeric state of the α-synuclein variants were checked by SDS-PAGE after the labeling with TMR-6-maleimide (not shown).

4.3.2 Lipid specificity of α-synuclein binding to GUV

In a first experiment it was tested whether the known dependence of the membrane binding of α-synuclein on the presence of anionic lipids is conserved in the GUV model system. Furthermore, it was explored if specific interactions between α-synuclein and the lipid headgroup are involved or if only the negative charge is of relevance. GUV from pure DOPC or phospholipid mixtures which consisted of 70 mol% DOPC and 30 mol% of one of the following anionic lipids: DOPS, DOPA, DOPG or $PI(4,5)P_2$ were generated. In addition 1 mol% of C_6-NBD-PC was added to visualize lipid domain formation. All above mentioned lipid mixtures yielded GUV in which the fluorescence probe was homogeneously distributed, showing the absence of domain formation at least at the microscopic scale. After incubation of GUV with the TMR-labeled (S129C) α-synuclein (0.1 μM), binding of the protein to membranes was observed by a red fluorescence signal. Figure 26 shows confocal fluorescence images of equatorial sections of GUV prepared from the above mentioned lipid mixtures.

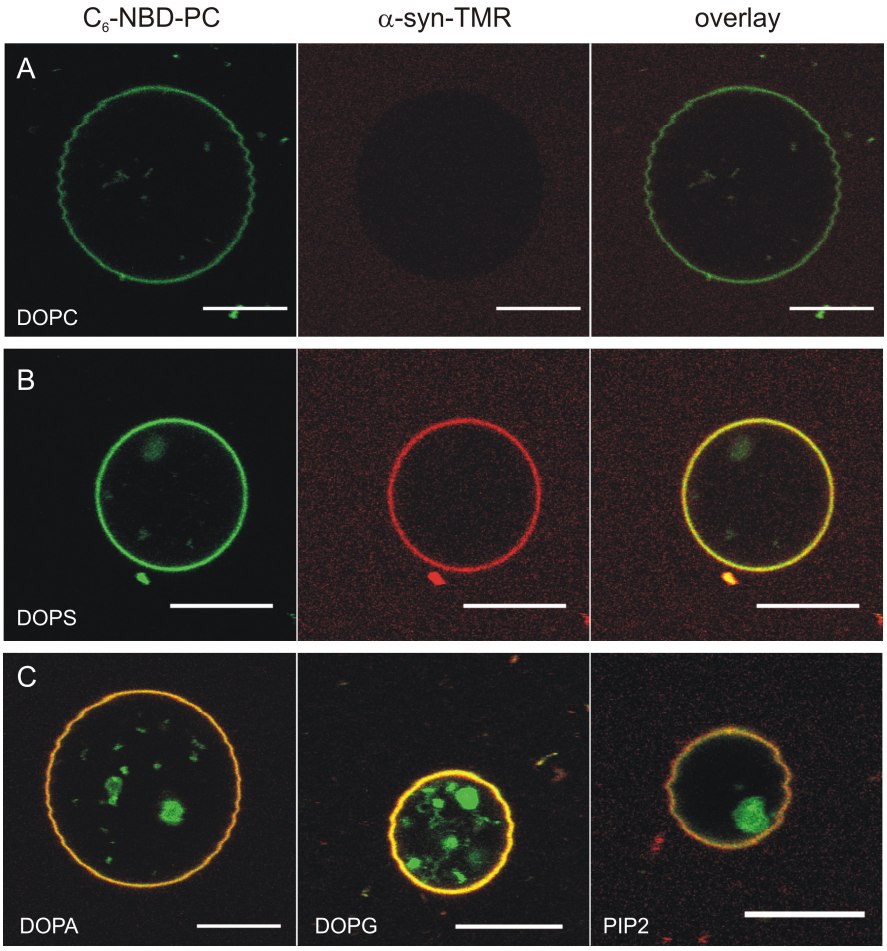

Fig. 26: Binding of α-synuclein requires negatively charged lipids. Laser scanning microcopy images showing equatorial sections of GUV incubated with α-synuclein (0.1 µM S129C-TMR; red fluorescence). All GUV were labeled with 1 mol% C_6-NBD-PC (green fluorescence). DOPC: DOPC only; DOPS: DOPC/DOPS = 70/30; DOPA: DOPC/DOPA = 70/30; DOPG: DOPC/DOPG = 70/30; PIP2: DOPC/PI(4,5)P_2 = 70/30. (A and B) Left image – fluorescence of C_6-NBD-PC; Center image – fluorescence of α-synuclein; Right image – overlay of left and center images. (C) The images of DOPA, DOPG and PIP2 superimpose green and red channels. Colocalization appears as yellow color. All images were taken at 25 °C. Some GUV contain smaller vesicles or lipid debris. White bars correspond to 10 µm.

The fluorescence of C_6-NBD-PC is shown in green (Fig. 26 A and B; left column) while the fluorescence of TMR-labeled α-synuclein is shown in red (Fig. 26 A and B; middle column). Yellow colored regions indicate the colocalization of fluorescent lipid analogue and α-synuclein (Fig. 26 A and B; right column and Fig. 26 C). It can be clearly seen that α-synuclein S129C-TMR does not interact with GUV consisting only of DOPC (Fig. 26 A). However, binding was observed for vesicles which contain anionic phospholipids, whereas the type of the negatively charged headgroup did not matter (Fig. 26 B and C). The homogeneous distribution of bound α-synuclein indicates that also the anionic phospholipids are distributed homogeneously and no lipid or α-synuclein clustering occurred at least on the

microscopic scale. Although the protein did bind to GUV with anionic lipids, it did not penetrate the membrane in the time course of the experiment as indicated by the absence of TMR-fluorescence at small membrane vesicles and patches inside the GUV.
Membrane binding of the protein is not induced by the S129C amino acid exchange or the covalently bound dye. Control experiments showed that free dye did not bind to the vesicles (not shown). Also an excess of unlabeled α-synuclein effectively competed for the binding sites at the membrane. Experiments in which DOPC/DOPS vesicles (70/30) were incubated with 0.5 µM labeled α-synuclein (S129C-TMR) and with different concentrations of the unlabeled wildtype protein (lacking S129C) additionally showed that the S129C-mutation and the attached TMR-dye did not change the membrane affinity of α-synuclein as the amount of fluorescence which was detectable at the membrane was reduced to approx. 50 % when equal amounts of labeled and unlabeled α-synuclein were present (see 4.3.6 and Fig. 32).

4.3.3 α-Synuclein binds to saturated and unsaturated negatively charged phospholipids

To assess whether binding of α-synuclein requires that acyl chains of negatively charged phospholipids have to be unsaturated, the binding to GUV prepared from DOPC and anionic phospholipids with saturated (DSPS, DPPA, DPPG) acyl chains was studied. Except for DPPA, GUV contained 70 mol% of DOPC and 30 mol% of the anionic phospholipid. DPPA was incorporated only to 15 mol%, because preparation of GUV with 30 mol% of DPPA failed. Again to each mixture 1 mol% of C_6-NBD-PC was added to visualize lipid domain formation. Similar to GUV with unsaturated anionic phospholipids, C_6-NBD-PC was homogeneously distributed and did not show lateral domain separation within the optical resolution in GUV prepared from DOPC/DSPS or DOPC/DPPA (Fig. 27 A).

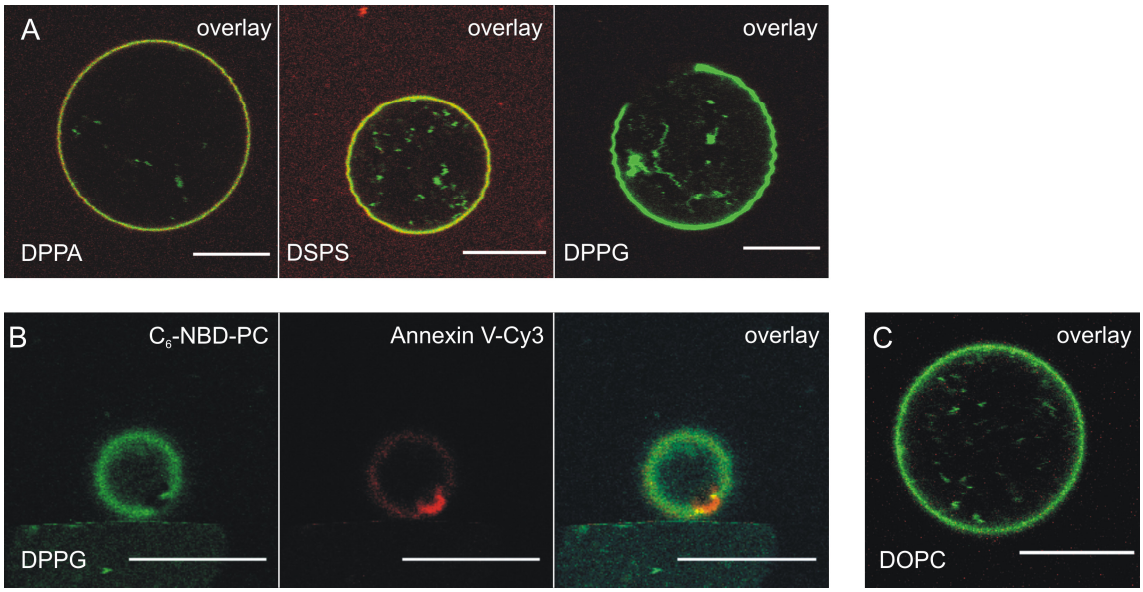

Fig. 27: α-Synuclein does not bind to raft-like domains. GUV were labeled with 1 mol% C_6-NBD-PC (green) which partitions into the ld-phase. Domains lacking C_6-NBD-PC appear as dark regions. (A) Laser scanning microcopy images showing equatorial sections of GUV incubated with α-synuclein (0.1 µM S129C-TMR; red fluorescence). All images show the overlay of NBD- and TMR-fluorescence. DPPA: DOPC/DPPA = 85/15; DSPS: DOPC/DSPS = 70/30; DPPG: DOPC/DPPG = 70/30 (B and C) Laser scanning microcopy images showing equatorial sections of GUV incubated with Annexin V-Cy3 (red fluorescence). Images in (B) separately show NBD- (green), Cy3-fluorescence (red) and the overlay. In (C) only the overlay is shown. (B) DPPG: DOPC/DPPG = 70/30 (C) DOPC: DOPC only. All images were taken at 25 °C. White bars correspond to 10 µm.

Binding of α-synuclein was observed for DOPC vesicles which contained the saturated anionic phospholipids DSPS or DPPA (Fig. 27 A). The interaction with DSPS and DPPA demonstrates that saturated acyl chains of anionic phospholipids do not interfere with binding of α-synuclein. In contrast, no binding was observed for DOPC/DPPG GUV where DPPG was segregated into ordered domains (Fig. 27 A). This strongly suggests that anionic phospholipids do not have to consist of unsaturated acyl chains, but must reside in ld domains for binding of α-synuclein (see also 4.3.4 and 5.2.3). This is supported by the observation that no binding of α-synuclein was observed for DPPC/DSPS, DPPC/DPPA and DPPC/DPPG (all 70/30) at 25°C (images not shown). Because the temperatures for the gel-liquid transition of these four phospholipids are at neutral pH well above 25 °C, membranes are in the gel phase under that condition. To assess the presence and lateral distribution of anionic phospholipids, in particular of phosphatidylserine, binding of Annexin V-Cy3 was studied. It is well established that membrane binding of this protein requires the presence of anionic phospholipids. Annexin V-Cy3 was bound homogeneously to DSPS and DPPA containing DOPC GUV indicating also that anionic lipids were homogeneously distributed. By contrast,

DOPC/DPPG GUV formed dark C_6-NBD-PC depleted domains to which Annexin V-Cy3 was found to bind, while no binding to pure DOPC GUV was observable (Fig. 27 B and C). That such domains were not seen in pure DOPC GUV suggests that DPPG segregates and forms ordered domains excluding C_6-NBD-PC.

4.3.4 α-synuclein binds to liquid disordered domains

The results on negatively charged GUV with ordered membranes (DPPC/DPPG, DPPC/DSPS and DPPC/DPPA) might not be in agreement with previous reports on association of α-synuclein with lo domains. As gel-like lipid phases are likely not to be present in biological membranes, GUV from a lipid mixture composed of DOPC/SSM/Chol (33/33/33) were prepared. Those vesicles form lo and ld domains [49]. As already described, domains were visualized by C_6-NBD-PC which is known to localize preferentially in the ld domain. In the absence of anionic lipids, α-synuclein binds neither to the ld nor to the lo domain (Fig. 28 A).

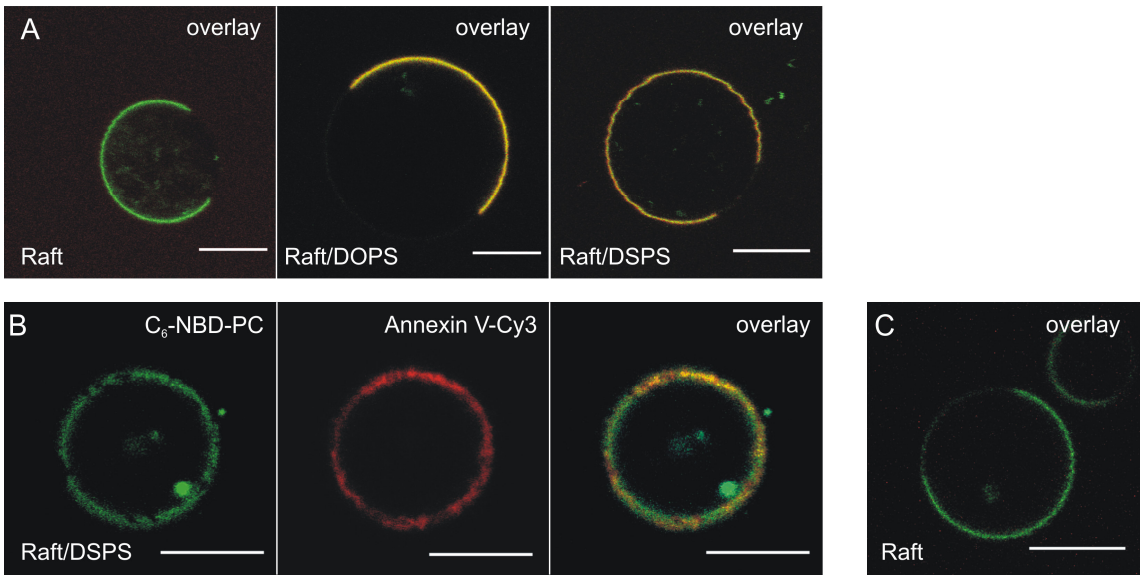

Fig. 28: α-Synuclein binds only to ld domains. GUV were labeled with 1 mol% C_6-NBD-PC (green) which partitions into the ld-phase. Domains lacking C_6-NBD-PC appear as dark regions. (A) Laser scanning microcopy images showing equatorial sections of GUV incubated with α-synuclein (0.1 µM S129C-TMR; red fluorescence). All images show the overlay of NBD- and TMR-fluorescence. Raft: DOPC/SSM/Chol = 33/33/33; Raft/DOPS: DOPC/SSM/Chol/DOPS = 25/25/25/25; Raft/DSPS: DOPC/SSM/Chol/DSPS = 25/25/25/25 (B and C) Laser scanning microcopy images showing equatorial sections of GUV incubated with Annexin V-Cy3 (red fluorescence). Images in (B) separately show NBD- (green), Cy3-fluorescence (red) and the overlay. In (C) only the overlay is shown. (B) Raft/DSPS: DOPC/SSM/Chol/DSPS = 25/25/25/25 (C) Raft: DOPC/SSM/Chol = 33/33/33 All images were taken at 25 °C. White bars correspond to 10 µm.

However, α-synuclein was bound to the ld phase if the monounsaturated anionic phospholipid DOPS was incorporated into GUV (DOPC/SSM/Chol/DOPS = 25/25/25/25) (Fig. 28 A). The absence of binding to the lo domain could either be due to the absence of DOPS from this domain or to inhibition of binding to negatively charged lipids when organized in the lo domain. Therefore, to generate vesicles for which the lo domain harbors phosphatidylserine, GUV containing 25 mol% DOPC, 25 mol% SSM, 25 mol% cholesterol and 25 mol% of the saturated anionic phospholipids DSPS were prepared. Lateral lipid domains were formed as shown by the inhomogeneous distribution of C_6-NBD-PC (Fig. 28 A). While Annexin V-Cy3 bound to such vesicles irrespective of the domain (Fig. 28 B), proving the domain independent incorporation of DSPS, binding of α-synuclein was observed only at the ld domain but not at the lo domain, again suggesting that an interaction of α-synuclein with membranes requires anionic lipids in a ld environment. Again, no binding of Annexin V-Cy3 to vesicles lacking PS was observed (Fig. 28 C).

In summary, the qualitative binding experiments of α-synuclein to GUV yielded insights about the factors determining the recruitment of the protein to the membrane. While membrane binding of α-synuclein relied on the presence of negatively charged phospholipids in the membrane, the nature of their headgroup did not matter. GUV showing lipid domains on the µm-scale allowed to explore the influence of the saturation grade of the anionic lipids on membrane binding of α-synuclein. While binding of the protein was observed irrespectively of the saturation grade of the negatively charged lipids their recruitment into different lipid domains had a strong influence. So, binding of α-synuclein to membranes was only observed if the negatively charged lipids were incorporated in ld domains. Lipids in lo domains or gel phases were not able to mediate the interaction with the membrane.

4.3.5 Mechanism of interaction between α-synuclein and lipid membranes

The dependence of the interaction between α-synuclein and the GUV on the presence of anionic phospholipids suggests that the binding is based on electrostatic attraction involving the anionic headgroups and the positively charged lysine residues from the N-terminal part of α-synuclein. Incubating DOPC/DOPS GUV with rising amounts of TMR-labeled α-synuclein showed a saturation of the binding for higher α-synuclein concentrations (Fig. 29 A).

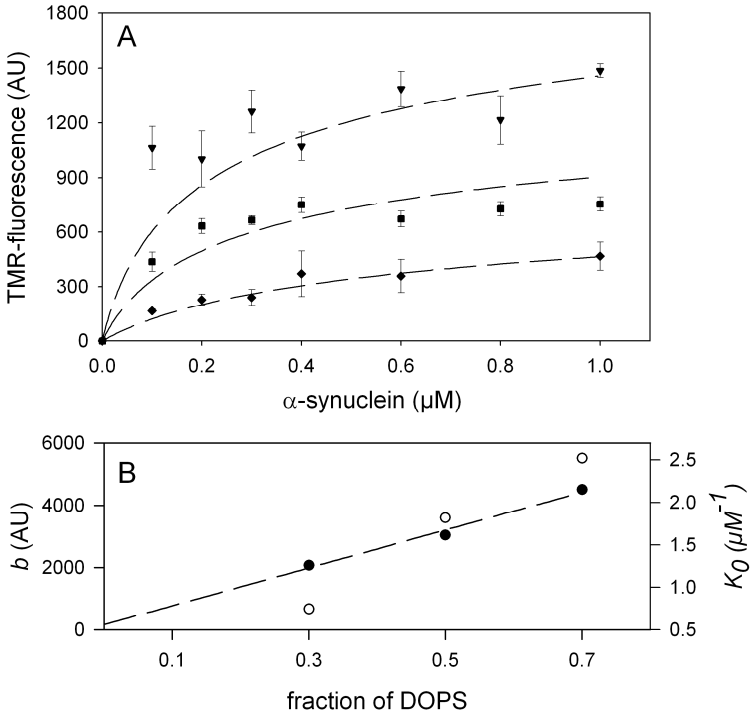

Fig. 29: Analysis of α-synuclein binding to negatively charged DOPC/DOPS GUV. (A) TMR-intensities at GUV membranes (♦) DOPC/DOPS = 70/30; (■) DOPC/DOPS = 50/50; (▼) DOPC/DOPS = 30/70. Mean values measured from six different GUV. Bars correspond to the SEM. The data was fitted according to the scaled particle theory [225]. (B) The determined values for the amount of available binding sites (●) *b* and the binding constant (○) K_0. Note that *b* is proportional to the fraction of DOPS. Measurements were done at 25 °C.

To characterize the binding in a quantitative manner, the data were fitted to isotherms according to the scaled particle theory proposed by Chatelier and Minton (1996) [225]. In contrast to the mass action law this isotherm takes into account that the binding of α-synuclein takes place at the finite space of the membrane surface. As expected, the number of available α-synuclein binding sites (*b*) is proportional to the amount of incorporated DOPS (Fig. 29 B). This confirms that essentially DOPS contributes to the binding sites for α-synuclein. The dependence of the binding constant (K_0) on the rising fraction of DOPS in DOPC/DOPS GUV strongly suggests cooperative effects of α-synuclein binding to negatively charged membranes (Fig. 29 B) which is in agreement with a previous report [232]. To assess whether binding is reversible, equal amounts (0.5 μM) of TMR-labeled α-synuclein and unlabeled α-synuclein were allowed to bind to DOPC/DOPS (70/30) GUV. As expected, membrane associated fluorescence decreased to the same amount irrespective of whether the GUV were preincubated with TMR-labeled or unlabeled α-synuclein or both α-synuclein variants were premixed before incubation (Fig. 30). This verifies that binding of α-synuclein corresponds to an association-dissociation equilibrium.

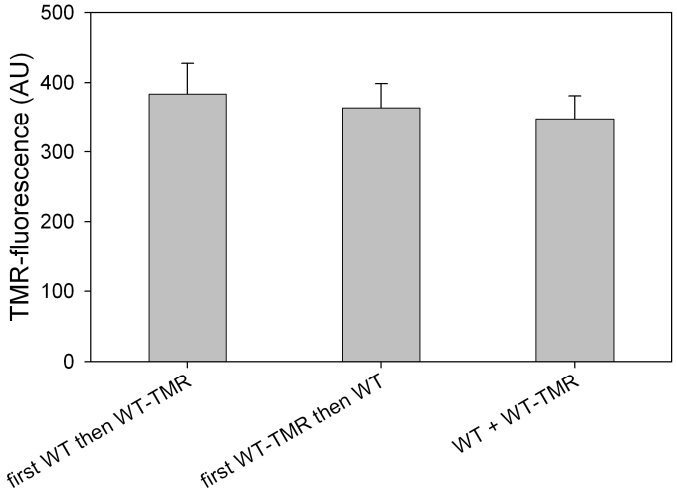

Fig. 30: Reversible binding of α-synuclein to DOPC/DOPS GUV. The same fluorescence intensity was observed when 0.5 µM TMR-labeled α-synuclein were added to DOPC/DOPS (7/3) GUV which had been preincubated for 5 min with 0.5 µM unlabeled α-synuclein ("first WT then WT-TMR"). The same intensity was observed if the order of incubation was reversed ("first WT-TMR then WT") or both proteins were added at the same time ("WT + WT-TMR"). Mean values measured from six different GUV. Bars correspond to the SEM. Measurements were done at 25 °C.

The N-terminal part of α-synuclein which forms an amphipathic helix mediating the membrane interactions is rich in positively charged lysine residues. Therefore it is likely that binding to membranes containing anionic lipids is mediated by electrostatic interactions. To support this hypothesis the ionic concentration (NaCl) of the microscopy buffer was varied during the binding assay. α-Synuclein was bound to DOPC/DOPS containing GUV at low ionic concentration (see 3.2.4.8). Subsequently, protein vesicle complexes were resuspended in buffer of low and high NaCl concentrations. As at 0.1 µM α-synuclein the binding sites at the vesicles are not saturated (Fig. 29 A), shielding the charges by salt should reduce binding of α-synuclein to the membrane. Indeed, at high ionic strength (105 mM NaCl) the amount of wildtype α-synuclein bound to the membrane declined to about 50 % with respect to low ionic strength (0 mM NaCl; Fig. 31). This is consistent with a binding mechanism mainly relying on ionic interactions.

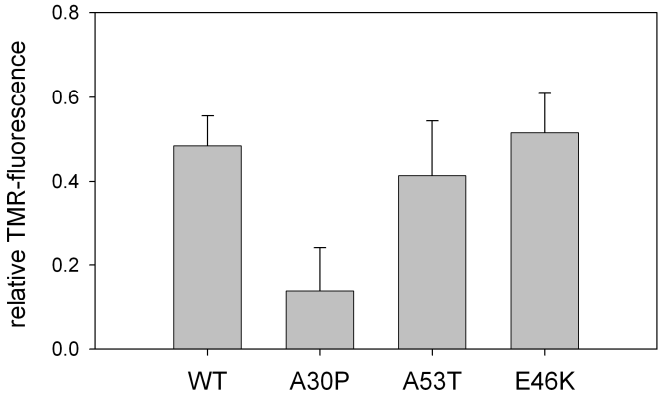

Fig. 31: α-Synuclein affinity is reduced at high ionic concentrations. TMR-intensity of 0.1 µM α-synuclein variants (as indicated and S129C-TMR) at GUV membranes (DOPC/DOPS = 70/30) in the presence of 105 mM NaCl. Data was normalized for each variant respective to the amount of TMR-fluorescence at 0 mM NaCl. Mean values from three independent measurements. Bars correspond to the SEM. Measurements were done at 25 °C.

4.3.6 Binding of the pathogenous mutants to GUV

Several mutations in the α-synuclein gene have been identified which seem to be related with the development of early onset of Parkinson's disease. To characterize the influence of these mutations on membrane interaction, the binding of the mutant α-synuclein proteins A30P, A53T, and E46K to GUV made from 70 mol% DOPC and 30 mol% DOPS was investigated. Important features of the binding pattern of wildtype α-synuclein were conserved as all investigated mutants bound to ld domains of vesicles harboring anionic phospholipids. No interaction with vesicles lacking DOPS was observed (images not shown).

As an altered affinity towards phospholipid membranes harboring anionic lipids caused by the mutations could impair the function of α-synuclein, the relative binding strength of the pathogenous α-synuclein variants compared to the wildtype protein was measured. This was done using a competition approach. DOPC/DOPS vesicles were incubated with 0.5 µM TMR-labeled wildtype α-synuclein (S129C-TMR) and with different concentrations of the unlabeled protein variants (A30P, A53T, E46K and WT). The decrease of the TMR-fluorescence at the membrane caused by the competition of the TMR-labeled α-synuclein wildtype against the unlabeled variants was measured. For equal concentrations of TMR-labeled and unlabeled wildtype α-synuclein a reduction of fluorescence of about 50 % was found (Fig. 32), demonstrating the similar affinities of these proteins for the lipid

membrane. A high excess of unlabeled α-synuclein was able to displace most of the TMR-labeled protein from the membrane.

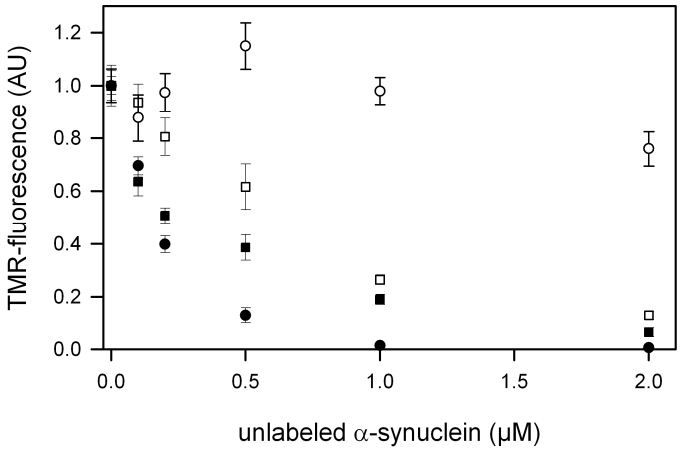

Fig. 32: Mutations of α-synuclein affect membrane binding. TMR-intensity of 0.5 μM wildtype α-synuclein (S129C-TMR) at GUV membranes (DOPC/DOPS = 70/30) in the presence of different concentrations of unlabeled α-synuclein variants ((□) WT; (○) A30P; (■) A53T; (●) E46K). Mean values measured from six different GUV. Bars correspond to the SEM. Measurements were done at 25 °C.

The binding affinity of the A53T variant was comparable to the wildtype. The affinity of the A30P mutant was strongly reduced, as this variant was not able to compete for the binding sites. In contrast, the E46K mutant showed an enhanced binding with respect to the wildtype (Fig. 32). The higher affinity of the E46K mutant clearly shows that membrane binding is very sensitive to charge changes in the N-terminal part of α-synuclein. The competition approach nicely confirms previous results found by Choi *et al.* (2004) [177]. The investigated mutants have in common that high ionic strength reduces the membrane binding as observed for the wildtype. A53T and E46K showed also a reduction of about 50 % of binding at high ionic strength (105 mM NaCl). Due to the impaired membrane interactions membrane binding of A30P was almost abolished completely under those conditions (Fig. 31).

In summary, quantitative analysis of the binding of α-synuclein to lipid membranes showed that the membrane binding of the protein exclusively was due to interactions with PS, where one molecule of α-synuclein bound to several lipids. Shielding ionic interactions showed that membrane binding was to a large extent mediated by ionic interactions. This is also reflected by the different membrane affinities of the pathogenous protein variants, as the impairment of the formation of the N-terminal α-helix strongly reduces (A30P) while the introduction of additional positive charges (E46K) increases membrane binding.

5 Discussion

5.1 Fluorescence lifetime analysis of NBD-labeled lipid analogues allows the visualization of lipid domains in model and cellular membranes

In the first part of the work a novel method for the detection of lipid domains in phospholipid membranes is demonstrated. A single dye approach which relies on the environment dependent fluorescence lifetime behavior of NBD-labeled lipid analogues has been established. In a first step the influence of different lipid species on these lifetimes has been measured in model GUV systems showing a homogeneous lipid distribution. Knowing these specific fluorescence lifetimes of the NBD-analogues it was possible to characterize the different lipid domains observed in lipid mixtures with a heterogeneous lipid distribution. Even the existence of submicrocopic domains could be detected in the model system, as the characteristic fluorescence lifetimes are conserved and bring such domains to light by their presence in the fluorescence decay. The application of this approach to more biological GPMV reveals that the domain specific lifetime behavior is still valid despite an inverted distribution coefficient. However, distinct lipid domains in the plasma membrane of living cells could not be detected. Yet, the approach can be used to draw conclusions about membrane properties. It is also useful to visualize and characterize physical properties of membrane structures serving as binding sites for peripheral and integral membrane proteins as demonstrated for α-synuclein.

5.1.1 Fluorescence lifetimes of NBD-lipid analogues in a homogeneous environment

In GUV with a homogeneous environment such as pure DOPC (or DOPC/DOPS = 98/2) GUV two lifetimes for the NBD-lipid analogues were observed, a short (τ_1) and a long one (τ_2) around 3 ns and 7 ns, respectively. This bi-exponential decay in homogeneous DOPC bilayers is in agreement with previous experimental observations [233,234,235] and molecular dynamics simulations [236]. While Mukherjee *et al.* (2004) measured values in the order of 5 ns [235], Chattopadhyay and Mukherjee (1993) reported values between 1 ns and 3 ns depending on the excitation wavelength [234]. A simple explanation of the bi-exponential decay arises from the red edge excitation shift of NBD in membranes, as in FLIM imaging the excitation wavelength of the NBD-fluorescence is at 468 nm, that is 3 nm above the excitation maximum. Because of that photons emitted early with a small Stokes-shift are preselected and

give rise to the observed decay component additional to the mean decay component of the main fraction of the fluorophores [234]. As the shift is quite small, τ_1 should contribute only a small fraction to the overall decay what is observed in most of the experiments. Also NBD-groups exposed to an aqueous environment show lifetimes of about 1 ns and could therefore be responsible for τ_1 [233,237]. In addition Loura and Ramalho (2007) suggest that the short lifetime component reflects rotational motion involving the NBD fluorophore [236]. In summary, it is likely that many factors contribute to the observed short lifetime component, causing variations in the short lifetime (τ_1) in the range of 1 - 3 ns in the GUV experiments. Therefore the short lifetime component was omitted from further studies. Loura and Ramalho (2007) also propose that the long lifetime component (τ_2) characterizes motions of the whole lipid molecule [236]. This leads to the assumption that τ_2 should be sensitive to physical properties of the lipid bilayer such as lipid packing. Indeed, very similar lifetimes for the different NBD-analogues were found, suggesting that the NBD-moiety senses a similar lipid environment. This is in good agreement with the measured distances of the NBD-group from the center of the bilayer (d_z) of about 20.3 to 20.7 Å for C_6-NBD-PC, C_{12}-NBD-PC and N-NBD-PE or 18.8 Å for C_6-NBD-PC showing that in each case the fluorophore is localized in the vicinity of the glycerol backbone and the phosphate groups [235]. A similar localization is suggested by experiments made by Huster *et al.* (2001) [238] or simulations carried out by Loura and Ramalho (2007) [236]. Their work also provides clues why C_6-NBD-PC and C_{12}-NBD-PC show different lifetime behaviour (Tab. 7) despite their similar localization ($d_z = 20.7$ Å) in the membrane. While for C_6-NBD-PC mostly intramolecular interactions with the glycerol backbone prevail, for C_{12}-NBD-PC the nitrogen atom at which the NBD-moiety is linked to the acyl-chain is exclusively H-bonded to surrounding DPPC lipids [236]. These intermolecular interactions can lead to a higher susceptibility of the fluorophore to disturbances and therefore may cause the observed decrease in the mean lifetime. This is also reflected by the work of Huster *et al.* who found that the NBD-group of C_{12}-NBD-PC in comparison with C_6-NBD-PC is more accessible from the aqueous phase [238].

As biological membranes apart from the above mentioned PC consist of various different lipid species, the influence of the charged phosphatidylserine which is abundant on the inner leaflet of the plasma membrane on the lifetime behavior of C_6-NBD-PC was exemplarily investigated. The observed concentration dependent tendency of the long fluorescence lifetime component τ_2 towards shorter values for larger DOPS fractions in DOPC/DOPS mixtures can be explained by different mechanisms. Firstly, in the presence of PS bearing an

overall negative charge and a quite large headgroup, an altered organisation of the water-membrane interface compared to pure DOPC bilayers is likely [239]. Secondly, the amino- and carboxyl-moieties which are absent in the PC headgroup, could be able to directly establish interactions via H-bonds with the NBD-fluorophore again changing its properties. Additionally, repulsive forces between the overall negatively charged PS headgroups and the nitro-group of NBD could play a role. Besides the shorter lifetime values of τ_2 the relative contribution of τ_1 increases in a PS concentration dependent manner, while the mean value of that component does not change. Depending on the underlying mechanism (see above) this suggests that the probe is embedded in a less ordered and/or more polar environment, but also altered spectral characteristics could cause such an effect. In contrast to PS the addition of cholesterol to DOPC membranes has the opposite effect, as it is accompanied by an increase of the values of τ_2 from approx. 7 ns for pure DOPC GUV to approx. 8 ns for vesicles containing 30 mol% cholesterol. The longer lifetime of the NBD-group reflects the higher degree of order induced by the cholesterol and is presumably due to a slower rate of non-radiative emission of the excited state. These results clearly demonstrate that the lifetime of NBD-labeled lipid analogues is sensitive to the surrounding lipid environment. Therefore these probes are adapted for the characterization of physical parameters of lipid membranes.

5.1.2 Fluorescence lifetimes of C_6-NBD-PC in vesicles forming microscopic lipid domains

Next the phase dependent fluorescence lifetime behavior of C_6-NBD-PC was investigated in GUV showing lateral lipid separation in the µm-scale. Enrichment of C_6-NBD-PC in ld domains of model lipid membranes as demonstrated by Shaw *et al.* (2006) allowed a straight forward identification of the respective membrane domains in these GUV [38]. For GUV prepared of DOPC/SSM/Chol (1/1/1) τ_2 of C_6-NBD-PC was strongly affected by the lipid environment of the fluorophore. In ld domains, the lifetime $\tau_{2(ld)}$ was about 7 ns, similar to that found for pure DOPC GUV. In contrast, in lo domains, enriched in cholesterol and saturated lipids, this lifetime component was remarkably shifted to about 11 ns to 12 ns ($\tau_{2(lo)}$). The same lifetime values were found for GUV preparations of DOPC/DPPC/Chol (1/1/1), clearly demonstrating that the distinct headgroup of sphingomyelin with the altered possibility to form H-bonds is not the cause of the longer lifetimes. While the membrane interior is quite unstructured, the phosphate region of the phospholipids, in which the NBD-moiety is located,

is especially ordered allowing the probe to sensitively sense its environment [235]. The increase in the degree of order when going from a ld to a lo phase could cause the large shift of τ_2 towards longer fluorescence lifetimes. The longer lifetimes in the lo domain could also be explained by recent findings, suggesting a relocation of the probe from the phosphate region in ld domains to the more hydrophobic membrane interior in lo domains [240]. Notably, only minor amounts if at all of the longer lifetime $\tau_{2(lo)}$ of about 12 ns in the ld domain and no contributions of the shorter $\tau_{2(ld)}$ in the lo domain were detected (Fig. 18 B). This shows that the lo and ld domains are well separated and do not harbor ld or lo domains of submicroscopic size, respectively. This also clearly demonstrates the identical nature of facing domains in both leaflets confirming previous studies on inter-bilayer coupling [45,46]. Hence, the lateral organisation of lipid domains is identical in either monolayer.

At high and low cholesterol concentration neither microscopic nor submicroscopic domains could be detected in GUV which is consistent with previous results [50]. At low cholesterol concentrations only lifetimes comparable to those of the ld domain ($\tau_{2(ld)}$) of domain-forming GUV were found (Tab. 11 and Tab. 12). For high cholesterol concentrations lifetimes similar to those of lo domains were measured. While detection of small submicroscopical lo domains surrounded by a large ld domain might be hampered by the fact that the partition of C_6-NBD-PC into ld domains is favored, this is not the case for the opposite event. Hence, the absence of a short lifetime component equivalent to $\tau_{2(ld)}$ at high cholesterol concentration strongly suggests that no ld domains even on the submicroscopic scale have been formed.

Due to the domain specific partition and fluorescence lifetimes of C_6-NBD-PC, domains on the µm-scale could also be identified for POPC/PSM/Chol GUV and GPMV prepared from HeLa-cells at 10 °C. Here the differences in fluorescence intensity allowed the separate analysis of the lifetime distribution in the lo and the ld domain (Fig. 21). In GUV prepared from a POPC/PSM/Chol mixture (1/1/1) C_6-NBD-PC at 10 °C showed only a weak preference for the ld domain and showed no domains in the microscopic range at 25 °C. C_6-NBD-PC shows no domain specific enrichment or only a small preference for the lo domain in GPMV. However, in each case the fluorescence lifetimes of the domains deviated only a little from $\tau_{2(ld)}$ and $\tau_{2(lo)}$ found for DOPC/SSM/Chol mixtures at 25 °C. This clearly demonstrates that the fluorescence lifetime component τ_2 of C_6-NBD-PC depends only on the phospholipid environment, but not on the distribution of the probe into the various lipid domains.

5.1.3 FLIM is suitable to detect transient small lipid domains

In contrast to steady state fluorescence techniques based on differential distribution of fluorescence probes in different membrane domains, fluorescence lifetime still allows a detection of membrane inhomogeneities in the case that these are below the resolution of fluorescence microscopy, as the technique is not based on changes in the fluorescence intensities but directly measures physical parameters of the probe. Thus the detection of two different domains in one "pixel" is still possible, as the fluorescence lifetime decay will show both characteristic components typical of the lipid environment surrounding the respective probe, thus revealing their presence. A prerequisite to study domains of submicroscopical dimension is that the temporal resolution does not interfere with the size and the dynamics of those domains. Due to the high time resolution FLIM should be a suitable method to detect even very small lipid domains. To resolve two distinct lipid environments by FLIM, lipid analogues must not interchange between the environments during emission, otherwise the two different lifetimes would average out. Thus, domains should be stable at least for about three times the fluorescence lifetime of the analogue, e.g. for about 30 ns in case of a C_6-NBD-PC. In this time period, an analogue would diffuse about 2 nm assuming a lateral lipid diffusion of about 10^{-7} cm²/s. Thus, lipid domains as small as approx. 10 nm² should be detectable by FLIM. This corresponds to about 16 lipid molecules with a surface area of about 0.6 nm² per lipid. Taking into account that a lateral diffusion coefficient of 10^{-7} cm²/s is an upper estimate, domains resolvable by FLIM could be even smaller. Typical values for lateral diffusion of lipid analogues in plasma membranes are between 1 x 10^{-9} cm²/s and 5 x 10^{-9} cm²/s as measured for fibroblasts [241] and red blood-cells [242], respectively. Hence, FLIM should be capable to capture even very small lipid domains as long as they are stable for at least 30 ns. However, these estimates also show the limitations of FLIM in that FLIM is not sensitive to domain sizes and lifetimes beyond 12 nm and 30 ns, respectively.

5.1.4 Fluorescence lifetimes in POPC/PSM/Chol GUV forming submicroscopic lipid domains

To assess whether lifetime measurements of C_6-NBD-PC can resolve small lipid domains not detectable by fluorescence microscopy, GUV from various mixtures of POPC/PSM/Chol with a constant content of PSM (20 mol%) were prepared. Indeed, consistent with previous

observations, those GUV did not form visible domains at 25 °C [49,70,71,243,244]. However, at cholesterol concentrations between 20 and 60 mol%, two different lifetime components (additional to τ_1) similar to $\tau_{2(ld)}$ and $\tau_{2(lo)}$ were found, as observed for DOPC/SSM/Chol GUV (see 4.2.3). This indicates that domains with submicroscopic dimensions are formed. Previous studies have already suggested that in such POPC/PSM/Chol mixtures with a cholesterol content above approx. 35 mol% domains of submicroscopic sizes between 20 nm and 100 nm could be formed [70,71]. The authors surmised that at cholesterol concentrations below 35 mol% domains could be present which could not be detected by their approach based on FRET between fluorescent lipid analogues. The FLIM data show that below 35 mol% of cholesterol domains are indeed present. This is in agreement with a very recent NMR study showing that in POPC/PSM/Chol mixtures with less than 35 mol% cholesterol domains in the order of about 40 nm² to 70 nm² are formed [72].

5.1.5 Fluorescence lifetimes of C_6-NBD-PC in GPMV

GPMV prepared from HeLa-cells show lipid domains on the µm-scale. As recently shown by mathematical modeling, the presence of membrane proteins and their interaction with lipids significantly reduces the ability of lipids to phase separate already at a rather low area fraction (5 - 10 %) covered by proteins [24]. Baumgart *et al.* (2007) suggested that the coupling of the membrane to the actin cytoskeleton may prevent formation of domains on the µm-scale in the intact plasma membrane which have been observed for giant blebs of the plasma membrane lacking the cortical actin assembly [25]. Hancock (2006) discussed a model of formation of domains in membranes emphasizing the role of different classes of laterally diffusing membrane proteins [22]. He suggested that the two classes of proteins of which either can capture and stabilize lo domains and those which are excluded from lo domains represent the two ends of a continuous spectrum of membrane proteins which can give rise to a distribution of intermediate size and stability of domains.

The comparison of the distribution coefficient of C_6-NBD-PC in GUV prepared from different lipid mixtures and GPMV clearly showed that the preferential enrichment of C_6-NBD-PC is not only dependent on the lipid phase but also on the direct lipid environment. In GUV in which a large difference of physical properties exists (DOPC/SSM/Chol; e.g. µm-domains at 25 °C) C_6-NBD-PC is mainly enriched in the ld domain, while for GUV in which the difference of enthalpy between the lipid domains is smaller (POPC/PSM/Chol; e.g. no

domains at 25 °C) the preference for the ld domain is much weaker. In GPMV which consist of various lipid species originating from the plasma membrane the differences should be much smaller, as a transition between different membrane states should be easily achievable. Actually, for such vesicles no domain specific enrichment of C_6-NBD-PC was observed. Although the domain dependent distribution changes drastically, distinct lifetimes for ld and lo domains are still preserved.

For GPMV forming large domains lifetimes could be separately extracted for lo and ld domains. Although the lifetimes of both domains could be clearly distinguished from each other, the difference was much lower in comparison with that found for lo and ld domains of GUV. This is also evident from the fact that the envelope of the two lifetime distributions of domain forming GPMV gives rise to a continuous lifetime distribution but not to a bimodal distribution as found for GUV. Surprisingly, the envelope was almost identical with the lifetime distribution of GPMV which did not form any visible lipid domains. This may indicate that in those GPMV the large domains disintegrated into smaller ones below microscopic resolution while essential physical properties, e.g. lipid packing, are preserved. Keeping the limitations of GPMV in mind [25], a similar situation may apply to intact plasma membranes corroborating the findings that a spectrum of lipid domains differing in their physical properties exists in those membranes [22,23]. Probably appropriate deconvolution might allow the resolution of different types/classes of lipid domains.

5.1.6 Fluorescence lifetimes of C_6-NBD-analogues in cellular membranes

A bimodal distribution of fluorescence lifetime of C_6-NBD-PC or C_6-NBD-PS for HeLa- and HepG2-cells was observed. FLIM based image analysis revealed that the shorter component (τ_i) corresponds to intracellular membranes while the longer lifetime (τ_p) is related to the plasma membrane. Support to this conclusion is given by the higher amplitude of the short component in the case of C_6-NBD-PS. It is known that this analogue readily redistributes among intracellular membranes upon its rapid transport from the exoplasmic to the cytoplasmic leaflet of the plasma membrane by the aminophospholipid translocase activity in mammalian cells, e.g. for HepG2- [228] and HeLa-cells [230]. Also, the plasma membrane associated lifetime of C_6-NBD-PS is slightly shorter than that of C_6-NBD-PC. This might as well be explained by the fact that a higher fraction of the analogue is localized in the

cytoplasmic leaflet. A conclusion from previous biochemical and biophysical studies is that the inner leaflet has reduced lipid packing with respect to the exoplasmic leaflet [241,242].

A similar dependence of lifetime on membrane localization has been shown for the perylene imide chromophore in Jurkat-cells [31]. The fluorescence decay of this probe was shorter in intracellular membranes with respect to the plasma membrane. Very likely, this difference of lifetimes between intracellular membranes and the plasma membrane is related to the higher presence of cholesterol in the plasma membrane (see 4.2.5).

This is in good agreement with results of cholesterol depletion experiments on HeLa-cells (data kindly provided by Anna P. Plazzo). Upon depletion of cholesterol by MßCD, a shift of the lifetime distribution of τ_p to lower values was observed (Fig. 33). MßCD extracted about 20 % of total cholesterol from these cells (20.4 % ± 1.2; n=2) as measured after labeling of the cells with ^{3}H-cholesterol. In Figure 33 the lifetime histogram (only longer component τ_p) of C_6-NBD-PC in the plasma membrane is shown.

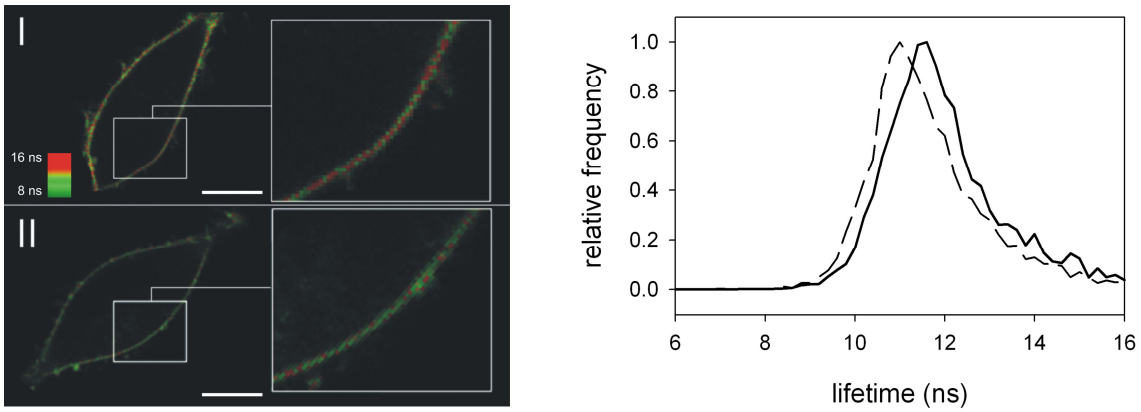

Fig. 33: Fluorescence lifetime of C_6-NBD-PC in the plasma membrane of HeLa-cells. Left: The average lifetime (images) in the plasma membrane of HeLa-cells at 25 °C before (I) and after (II) depletion of cholesterol by treatment of cells with MßCD is shown as pseudocolor image (see scale in (I)). White bars correspond to 10 µm. Right: Histograms of τ_p of C_6-NBD-PC in HeLa-cells at 25 °C before (solid line) and after (dashed line) depletion of cholesterol by treatment of cells with MßCD. Histograms were normalized by setting the maximum to 1. Images were taken and analyzed by Anna P. Plazzo.

In general, the distribution of lifetimes of the plasma membrane of HepG2- and Jurkat-cells was rather broad centered at about 11 ns for C_6-NBD-PC. This lifetime corresponds to that one observed for the lo domains of GUV. The distribution did not reveal resolvable peaks corresponding to different lifetimes as found for lo and ld domains of GUV. However, several studies suggest that in resting cells rather small lipid (raft-like) domains with only transient stability and nanometer dimensions exist (for reviews see Lagerholm and Weinreb (2005)

[245], Hancock (2006) [22], Shaw (2006) [246] and Jacobson *et al.* (2007) [23]). Sophisticated biophysical techniques and mathematical modeling of generated experimental data have indeed shown that such domains are between 5 nm and 20 nm in diameter [11,34]. Employing time-resolved FRET Sharma *et al.* (2004) concluded that about four GPI-anchored proteins are localized in small clusters with approx. 40 lipids [11]]. Single particle tracking experiments indicated that single GPI-anchored proteins are organized in very small domains (<10 nm) with a short lifetime being in the order of 0.1 ms [34]. This short transient stability is in agreement with electron paramagnetic resonance measurements revealing that spin-labeled lipids reside within a typical time of about 100 µs in rafts [247]. Based on these characteristic properties of lipid domains and the estimates on the resolution of FLIM measurements (see 5.1.3), the approach should be suitable to detect even nanometer sized domains with very short stability. However, no distinguishable lifetime components in the plasma membrane of cells as found for domain forming GUV could be resolved. This may support recent scepticism about the existence and relevance of raft domains in biological membranes [246]. On the other hand, alternative explanations which are in agreement with recent studies may account for these results. Firstly, one should keep in mind that the cholesterol content of the plasma membrane typically is very high. Based on that one would expect that the plasma membrane would rather consist of a continuous lo phase with embedded possible small ld domains [248,249]. This could explain a lifetime distribution of C_6-NBD-analogues in the plasma membrane centered at typical values found for lo domains of GUV. Secondly, one can suppose that the data are compatible with the existence of a large variety of different types of lipid domains or clusters differing in their composition as well as in their properties such as size and stability. This gives rise to an overlapping distribution of lifetimes rather than to well resolvable ones. Indeed, the NBD lifetime distribution of the NBD analogues in the plasma membrane is much broader compared to that one in the lo domain of GUV. Previous reports have already discussed the presence of a variety of domains varying in size and composition [22,23]. Jacobson *et al.* (2007) pointed out that the plasma membrane should be viewed as a lipid-protein composite, rather than a dilute solution of proteins in a lipid bilayer. Even a very simple model membrane system which normally only separates into a distinct ld and lo domains shows a more complex phase behavior if membrane asymmetry is generated [62]. In biological systems apart from pure lipid-lipid interactions plasma membrane organization and dynamics are determined additionally by protein-lipid and protein-protein interactions, giving rise to an even more complex network of

regulation. The existence of such a complex network of different lipid domains is in good agreement with the alterations in the lifetime behavior of C_6-NBD-PC upon cholesterol depletion or cell activation. The experiments on GUV have shown that C_6-NBD-PC should only be excluded from strongly ordered lipid domains but should be able to enter such lo domains which normally exist in the plasma membrane of cells (see 5.1.5). Having this in mind, a straightforward explanation of the observed lifetime changes observed in cells upon cholesterol depletion, activation or sphingomyelinase treatment of Jurkat-cells is possible. The depletion of cholesterol in HeLa-cells which leads to the disruption of "Raft" domains, caused shorter fluorescence lifetimes of C_6-NBD-PC. This is obvious, as the disruption of the ordered "Raft" domains exposes a higher fraction of the probe to a more disordered lipid environment. However, the induction of strongly ordered domain compartments by cell activation or ceramide enrichment also caused a decrease of fluorescence lifetimes which is contradictory at the first glance. Keeping in mind that C_6-NBD-PC is excluded from strongly ordered lo domains, the induction of those types of domains in cells again leads to an enrichment of the probe in the surrounding disordered environment that may cause the observed decrease in fluorescence lifetimes.

5.2 α-Synuclein selectively binds to anionic phospholipids embedded in ld domains

In the second part of the present study the binding of α-synuclein to GUV was investigated. This allowed a direct characterization of the lipid and domain specificity of membrane interaction of α-synuclein by fluorescence microscopy. For this purpose a fluorescent label was covalently attached at the C-terminus of the protein to avoid any interference with the lysine-rich N-terminus mediating membrane binding. Experiments with DOPC GUV containing different types of anionic lipids agree with previous findings that anionic phospholipid headgroups are important for membrane binding of α-synuclein. While the saturation degree of the acyl chains of these phospholipids is of marginal relevance if at all, it is essential for α-synuclein binding that they are embedded in a ld environment indicating the relevance of lipid packing for binding. Although important features of wildtype α-synuclein binding to membranes were preserved, mutations of the protein affected membrane binding quantitatively showing that apart from an altered overall charge also other single amino acid exchanges can modulate membrane association.

5.2.1 Membrane binding of α-synuclein requires anionic head groups

In a first step it was investigated whether α-synuclein interacts with specific structures at the lipid headgroups or merely the anionic charge is of importance. Strong binding of α-synuclein to GUV containing DOPC and either DOPS, DOPA, DOPG or PI (4,5)P_2 confirmed previous reports [144]. The dependence of the binding constant on the fraction of incorporated DOPS clearly showed the cooperative action of negatively charged lipids forming the α-synuclein binding sites. The results implicate the importance of electrostatic interaction for membrane binding of α-synuclein. This is supported by the significant decrease of binding of α-synuclein to GUV upon increasing the ionic concentration (Fig. 31). Similar observations have been made for SUV, LUV and MLV [142,144,153,232]. Lysine residues of the 11-mer repeat sequences forming α-helices are responsible for interaction with negatively charged surface of membranes. Plotting the N-terminal part as an α-helical wheel reveals a clustering of basic residues at polar/nonpolar interfaces. The hydrophobic side chains of the lysine residues are known to support the interaction of the hydrophobic surface of such amphipathic helices with membranes [144,250]. In particular, the relative contribution of hydrophobic interactions to binding of α-synuclein with membranes may be enhanced when electrostatic attraction between protein and negatively charged headgroups is strongly shielded at high ionic strength (this work and refs. [142,144]). This point is assessed in ongoing studies investigating the depth of penetration of the N-terminal α-helix of α-synuclein in LUV at different conditions. However, for all α-synuclein variants no binding to pure DOPC membranes was detected, indicating that hydrophobic interactions alone are not sufficient to mediate binding.

5.2.2 α-Synuclein binds to negatively charged phospholipids with saturated fatty acid chains

As clearly shown by the interaction of α-synuclein with DOPC GUV containing the saturated lipid species DSPS or DPPA, the interaction of α-synuclein with negatively charged phospholipids does not require that those lipids consist of unsaturated fatty acyl chains. This is in contrast to previous results indicating that binding to phospholipid membranes requires the presence of negatively charged lipids, preferentially PS with acyl chains being a combination of oleic and polyunsaturated (20:4 or 22:6) fatty acyl chains [147]. However, one has to keep in mind that in the GUV DSPS and DPPA were embedded in a DOPC

environment which is of lowered lipid packing. Indeed, no binding to DPPC membranes containing DSPS or DPPA being in the gel phase was observed. Thus, the next issue to refer to was whether apart from the negative charge of the headgroup, a lipid phase of lower lipid packing is of importance for the interactions between α-synuclein and the vesicles as well.

5.2.3 α-Synuclein binds to negatively charged ld domains but not to raft-like domains

Binding of α-synuclein neither to the ld nor to the lo domain of GUV composed of a lipid mixture of DOPC/SSM/Chol could be detected, again proving that the presence of anionic lipids is a strict prerequisite for binding in the GUV system. When DOPS was added, binding of α-synuclein to the ld domain – where the unsaturated DOPS should preferentially enrich – but not to the lo domain was observed. Even in the presence of the saturated DSPS no association of the protein with the lo domain was detected, although the binding of Annexin V-Cy3 demonstrated the presence of DSPS in those domains (see 4.3.4 and Fig. 28). This suggests that binding of α-synuclein to membranes also depends on lower lipid packing, as it is typical for ld domains, or even on lipid packing defects. A role of lipid packing in binding to membranes is supported by the results on binding of α-synuclein to phosphatidylglycerol. α-Synuclein binds efficiently to GUV composed of DOPC and DOPG. However, no binding was detected for GUV made from DOPC/DPPG. In the latter case DPPG segregates and forms an ordered, very likely, gel-phase domain as indicated by the absence of C_6-NBD-PC from this domain. The phase transition temperature of DPPG is about 40°C [251]. In contrast to α-synuclein, Annexin V-Cy3 was found to associate with DPPG domains what indicates that the negatively charged head group is accessible for peripheric proteins (see 4.3.3 and Fig. 27). Presumably the tight lipid packing of DPPG prevents binding of α-synuclein.

In conclusion, it is likely that both the negative surface charge and lipid packing are essential determinants of membrane binding of α-synuclein. Indeed, CD measurements done by Nuscher *et al.* (2004) suggested that binding and helix formation of the N-terminus depends on defects of the membrane [149]. It is already known that insertion of peptides and proteins into lipid bilayers is facilitated by lipid packing defects. Notable is that, hydrophobic interactions may become more efficient by packing defects of the lipid bilayer, for example, due to high bending. Previous studies have suggested that bilayer bending plays an important role in binding of α-synuclein becoming enhanced in membranes of high curvature such as

micelles or small unilamellar vesicles [144]. These findings would also hint towards the proposed function of the protein as an incorporation of the amphipathic helix in the cytoplasmic leaflet of vesicles would relief bending stress and therefore may contribute to vesicle stability and prevent premature vesicle fusion.

5.2.4 Implications of lipid specific binding of α-synuclein – Physiological relevance

Synaptic vesicles, with which most presumably the biological function of α-synuclein is associated, consist of about 12 % PS [252] of total phospholipid, while PA and PI make up to only 0 - 2 % [253,254]. Previous data are indicative of an enrichment of PS on the cytosolic leaflet [253], very likely due to the presence of an aminophospholipid translocase belonging to the P-type ATPases [252,255,256]. This translocase is thought to be capable of flipping PS and PE from the lumenal leaflet to the cytoplasmic leaflet to generate an asymmetric distribution of these lipids in the two leaflets of the synaptic vesicle. Thus, the concentration of PS in the cytosolic leaflet corresponds to about 24 %, being comparable to the concentration mainly used in the experiments. Furthermore, analysis of fatty acid composition of phospholipids revealed that the majority of fatty acids in synaptic vesicles are unsaturated (approx. 90 %; mainly polyunsaturated species [252]) giving rise to a reduced lipid packing. Hence, the cytosolic leaflet of synaptic vesicles resembles a good target for α-synuclein due to the enrichment of negatively charged PS and the reduced lipid packing.

These results may not exclude a role of raft-like lipid domains in binding of α-synuclein, eventually serving as binding sites at the plasma membrane [128,257]. In comparison with GUV, raft domains have been found to be much smaller in biological membranes with diameters being in the order of about 5 nm [11] which corresponds to a surface area of about 20 nm². This is in the order of the area covered by the membrane binding N-terminus of α-synuclein on the assumption that a 100-residue helix would correspond to 15 nm² [232]. Thus, α-synuclein may sense both negatively charged lipids in ld domains and discontinuities in lipid organization at the border of lo and ld domains which may give rise to fluctuations of lipid packing favoring the interaction of α-synuclein with membranes. Notable is that, formation of pathogenic amyloid fibrils of various human diseases has been shown to be associated with a lipid component which is specifically rich in sphingomyelin and cholesterol, both lipids are typical for lipid rafts [257,258,259]. Thus, the relevance of raft-like domains

for formation of amyloid-like fibrillar structures of α-synuclein remains an important issue for understanding mechanisms of Parkinson's disease.

5.2.5 Mutation of α-synuclein affects membrane binding

The competition approach allows to investigate the influence of different single mutations of α-synuclein which have been associated with PD (for a review see Moore *et al.* (2005) [260]) in a quantitative manner. The strong dependence of the membrane binding of α-synuclein on electrostatic interactions easily explains the enhanced affinity of the E46K variant to DOPC/DOPS GUV with respect to wildtype, as in overall two additional positive charges are introduced by this amino acid exchange. A previous study using multilamellar vesicles found the same enhancement [177]. In contrast, the mutation A30P caused a lower binding affinity of α-synuclein to those GUV. The reduced binding of this mutant is in agreement with previous observations [128,142,145,177]. Fortin *et al.* (2004) found that the mutation A30P interferes with α-synuclein recruitment at synapses [128]. The lower affinity of the A30P mutant can be rationalized by structural studies carried out by Ulmer and Bax (2005) [98]. These authors found that the proline residue of this mutant interrupts the α-helical structure of the N-terminus which mediates membrane binding. Thereby, the canonical succession of polar and hydrophobic residues is perturbed which points to the relevance of this specific arrangement for membrane binding. The perturbed arrangement of hydrophobic residues may also interfere with an enhanced relative contribution of hydrophobic interactions to binding at high ionic strength (see 4.3.5 and Fig. 31) explaining why those conditions have a stronger impact for A30P with respect to wildtype. The membrane affinity of the A53T mutant was not changed, being in agreement with previous results [177] and the observation that this mutation does not affect the conformation of membrane bound α-synuclein [98]. These results on mutants clearly show that apart from the presence of positively charged and hydrophobic amino acid residues the conformation of α-synuclein is an important factor for its membrane association.

So, the precise role of membranes in the genesis of fibrils remains to be clarified. While several studies have shown that interaction of α-synuclein with membranes promote fibril formation [141,261,262], other studies reported that membrane interaction may inhibit formation of fibrillar α-synuclein depending on the protein to lipid ratio [188,189]. In addition, mutations of α-synuclein may be pathogenous in different ways. For example,

reduced binding may interfere with a protective function of α-synuclein binding to membranes. Kamp and Beyer (2006) have suggested that α-synuclein may anneal packing defects which may prevent premature fusion of synaptic vesicles [146]. Further studies are warranted to identify the role of interaction of α-synuclein with membranes in pathogenesis and, in particular, in formation of α-synuclein fibrils.

6 Summary and Outlook

Their ability to form lipid domains in the µm-scale, allowing a straightforward identification by fluorescence microscopy, and the possibility to adjust the lipid mixture to one's liking, renders GUV an ideal tool to study phenomena associated with genesis, characteristics and function of lipid domains. In this study a new method based on fluorescence lifetime measurements was demonstrated to distinguish different lipid domains with a single membrane probe. C_6-NBD-PC shows a domain dependent fluorescence lifetime behavior, which allows the detection of ld and lo domains also below the diffraction limit of the fluorescence microscope. While the presence of such domains in a defined lipid system has been demonstrated and their physical properties have been characterized quite well, the exact nature of such lipid heterogeneities in the plasma membrane is still elusive. Therefore the application of the FLIM-approach to investigate such biological systems may provide valuable insights into the composition and structure of the plasma membrane of living cells. As the fluorescence lifetime behavior of C_6-NBD-PC is also sensitive to the presence of PS or cholesterol, this approach could be an invaluable tool to study an altered membrane composition in cellular models with regard to diseases associated with an impaired lipid metabolism. Furthermore, this technique could help to understand certain metabolic processes like the intracellular transport of cholesterol or other lipid plasma membrane components.

An application of fluorescence microscopy to domain forming GUV is covered by the second part of the work in which the domain specific membrane interactions of α-synuclein were studied by using GUV. Apart from corroborating previous findings concerning the dependence of the membrane interactions on the presence of anionic lipids, it was possible to shed light on the controversially discussed point, whether the anionic lipids have to have unsaturated acyl chains in order to support membrane binding of α-synuclein. It could be demonstrated that not the degree of saturation of the negatively charged lipids but mainly the phase state of the membrane harboring these lipids is crucial, as α-synuclein only binds to these lipids if they are liquid disordered membrane domains. Apart from these purely qualitative findings it was also possible to study the interactions of α-synuclein (or its pathogenous variants) with GUV in a quantitative way, as it is possible to directly measure the amount of α-synuclein bound to the lipid membrane. Yet it has to be admitted that if it is possible to detect membrane binding by intrinsic methods (FRET, Trp-blue shift) LUV based experiments in the cuvette may yield better experimental statistics. However, the strength of

the huge GUV lies in the directly observable lipid domain structure. As the interaction of α-synuclein with lipid membranes seems to alter the aggregation propensity of the protein, further studies are indicated to investigate whether domains specific interactions exist between the oligomeric or fibrillar species. In combination with reconstitution of fluorescently labeled proteins or peptides in lipid membranes the described methods can also be applied to study the domain specific distribution of such compounds.

Addendum

Bibliography

[1] Mansy, S. S.; Schrum, J. P.; Krishnamurthy, M.; Tobe, S.; Treco, D. A. and Szostak, J. W. (2008): Template-directed synthesis of a genetic polymer in a model protocell, Nature 454 [7200], pp. 122-5.

[2] Meldrum, E.; Parker, P. J. and Carozzi, A. (1991): The PtdIns-PLC superfamily and signal transduction, Biochim Biophys Acta 1092 [1], pp. 49-71.

[3] Marsh, D. (2008): Protein modulation of lipids, and vice-versa, in membranes, Biochim Biophys Acta 1778 [7-8], pp. 1545-75.

[4] Allen, J. A.; Halverson-Tamboli, R. A. and Rasenick, M. M. (2007): Lipid raft microdomains and neurotransmitter signalling, Nat Rev Neurosci 8 [2], pp. 128-40.

[5] Benarroch, E. E. (2007): Lipid rafts, protein scaffolds, and neurologic disease, Neurology 69 [16], pp. 1635-9.

[6] Hanzal-Bayer, M. F. and Hancock, J. F. (2007): Lipid rafts and membrane traffic, FEBS Lett 581 [11], pp. 2098-104.

[7] Lajoie, P. and Nabi, I. R. (2007): Regulation of raft-dependent endocytosis, J Cell Mol Med 11 [4], pp. 644-53.

[8] Rajendran, L. and Simons, K. (2005): Lipid rafts and membrane dynamics, J Cell Sci 118 [Pt 6], pp. 1099-102.

[9] Salaun, C.; James, D. J. and Chamberlain, L. H. (2004): Lipid rafts and the regulation of exocytosis, Traffic 5 [4], pp. 255-64.

[10] Varma, R. and Mayor, S. (1998): GPI-anchored proteins are organized in submicron domains at the cell surface, Nature 394 [6695], pp. 798-801.

[11] Sharma, P.; Varma, R.; Sarasij, R. C.; Ira; Gousset, K.; Krishnamoorthy, G.; Rao, M. and Mayor, S. (2004): Nanoscale organization of multiple GPI-anchored proteins in living cell membranes, Cell 116 [4], pp. 577-89.

[12] Sengupta, P.; Holowka, D. and Baird, B. (2007): Fluorescence resonance energy transfer between lipid probes detects nanoscopic heterogeneity in the plasma membrane of live cells, Biophys J 92 [10], pp. 3564-74.

[13] Petit, V. A. and Edidin, M. (1974): Lateral phase separation of lipids in plasma membranes: effect of temperature on the mobility of membrane antigens, Science 184 [142], pp. 1183-5.

[14] Tillack, T. W.; Allietta, M.; Moran, R. E. and Young, W. W., Jr. (1983): Localization of globoside and Forssman glycolipids on erythrocyte membranes, Biochim Biophys Acta 733 [1], pp. 15-24.

[15] van Meer, G.; Stelzer, E. H.; Wijnaendts-van-Resandt, R. W. and Simons, K. (1987): Sorting of sphingolipids in epithelial (Madin-Darby canine kidney) cells, J Cell Biol 105 [4], pp. 1623-35.

[16] Brown, D. A. and Rose, J. K. (1992): Sorting of GPI-anchored proteins to glycolipid-enriched membrane subdomains during transport to the apical cell surface, Cell 68 [3], pp. 533-44.

[17] Simons, K. and Ikonen, E. (1997): Functional rafts in cell membranes, Nature 387 [6633], pp. 569-72.

[18] Heerklotz, H. (2002): Triton promotes domain formation in lipid raft mixtures, Biophys J 83 [5], pp. 2693-701.

[19] Munro, S. (2003): Lipid rafts: elusive or illusive? Cell 115 [4], pp. 377-88.

[20] Lichtenberg, D.; Goni, F. M. and Heerklotz, H. (2005): Detergent-resistant membranes should not be identified with membrane rafts, Trends Biochem Sci 30 [8], pp. 430-6.

[21] Poveda, J. A.; Fernandez, A. M.; Encinar, J. A. and Gonzalez-Ros, J. M. (2008): Protein-promoted membrane domains, Biochim Biophys Acta 1778 [7-8], pp. 1583-90.

[22] Hancock, J. F. (2006): Lipid rafts: contentious only from simplistic standpoints, Nat Rev Mol Cell Biol 7 [6], pp. 456-62.

[23] Jacobson, K.; Mouritsen, O. G. and Anderson, R. G. (2007): Lipid rafts: at a crossroad between cell biology and physics, Nat Cell Biol 9 [1], pp. 7-14.

[24] Yethiraj, A. and Weisshaar, J. C. (2007): Why are lipid rafts not observed in vivo? Biophys J 93 [9], pp. 3113-9.

[25] Baumgart, T.; Hammond, A. T.; Sengupta, P.; Hess, S. T.; Holowka, D. A.; Baird, B. A. and Webb, W. W. (2007): Large-scale fluid/fluid phase separation of proteins and lipids in giant plasma membrane vesicles, Proc Natl Acad Sci U S A 104 [9], pp. 3165-70.

[26] Bagatolli, L. A. (2006): To see or not to see: lateral organization of biological membranes and fluorescence microscopy, Biochim Biophys Acta 1758 [10], pp. 1541-56.

[27] Gaus, K.; Chklovskaia, E.; Fazekas de St Groth, B.; Jessup, W. and Harder, T. (2005): Condensation of the plasma membrane at the site of T lymphocyte activation, J Cell Biol 171 [1], pp. 121-31.

[28] Gousset, K.; Wolkers, W. F.; Tsvetkova, N. M.; Oliver, A. E.; Field, C. L.; Walker, N. J.; Crowe, J. H. and Tablin, F. (2002): Evidence for a physiological role for membrane rafts in human platelets, J Cell Physiol 190 [1], pp. 117-28.

[29] Grassme, H.; Jekle, A.; Riehle, A.; Schwarz, H.; Berger, J.; Sandhoff, K.; Kolesnick, R. and Gulbins, E. (2001): CD95 signaling via ceramide-rich membrane rafts, J Biol Chem 276 [23], pp. 20589-96.

[30] Gri, G.; Molon, B.; Manes, S.; Pozzan, T. and Viola, A. (2004): The inner side of T cell lipid rafts, Immunol Lett 94 [3], pp. 247-52.

[31] Margineanu, A.; Hotta, J.; Vallee, R. A.; Van der Auweraer, M.; Ameloot, M.; Stefan, A.; Beljonne, D.; Engelborghs, Y.; Herrmann, A.; Mullen, K.; De Schryver, F. C. and Hofkens, J. (2007): Visualization of membrane rafts using a perylene monoimide derivative and fluorescence lifetime imaging, Biophys J 93 [8], pp. 2877-91.

[32] Singer, S. J. and Nicolson, G. L. (1972): The fluid mosaic model of the structure of cell membranes, Science 175 [23], pp. 720-31.

[33] Dietrich, C.; Yang, B.; Fujiwara, T.; Kusumi, A. and Jacobson, K. (2002): Relationship of lipid rafts to transient confinement zones detected by single particle tracking, Biophys J 82 [1 Pt 1], pp. 274-84.

[34] Kusumi, A.; Koyama-Honda, I. and Suzuki, K. (2004): Molecular dynamics and interactions for creation of stimulation-induced stabilized rafts from small unstable steady-state rafts, Traffic 5 [4], pp. 213-30.

[35] Orr, G.; Hu, D.; Ozcelik, S.; Opresko, L. K.; Wiley, H. S. and Colson, S. D. (2005): Cholesterol Dictates the Freedom of EGF Receptors and HER2 in the Plane of the Membrane, Biophys J 89 [2], pp. 1362-73.

[36] Kusumi, A. and Suzuki, K. (2005): Toward understanding the dynamics of membrane-raft-based molecular interactions, Biochim Biophys Acta 1746 [3], pp. 234-51.

[37] Perkovic, S. and McConnell, H.M. (1997): Cloverleaf Monolayer Domains, J. Phys. Chem. B 101, pp. 381-388.

[38] Shaw, J. E.; Epand, R. F.; Epand, R. M.; Li, Z.; Bittman, R. and Yip, C. M. (2006): Correlated fluorescence-atomic force microscopy of membrane domains: structure of fluorescence probes determines lipid localization, Biophys J 90 [6], pp. 2170-8.

[39] Kiessling, V.; Crane, J. M. and Tamm, L. K. (2006): Transbilayer effects of raft-like lipid domains in asymmetric planar bilayers measured by single molecule tracking, Biophys J 91 [9], pp. 3313-26.

[40] Coste, V.; Puff, N.; Lockau, D.; Quinn, P. J. and Angelova, M. I. (2006): Raft-like domain formation in large unilamellar vesicles probed by the fluorescent phospholipid analogue, C12NBD-PC, Biochim Biophys Acta 1758 [4], pp. 460-7.

[41] Farge, E. and Devaux, P. F. (1992): Shape changes of giant liposomes induced by an asymmetric transmembrane distribution of phospholipids, Biophys J 61 [2], pp. 347-57.

[42] Papadopulos, A.; Vehring, S.; Lopez-Montero, I.; Kutschenko, L.; Stöckl, M.; Devaux, P. F.; Kozlov, M.; Pomorski, T. and Herrmann, A. (2007): Flippase activity detected with unlabeled lipids by shape changes of giant unilamellar vesicles, J Biol Chem 282 [21], pp. 15559-68.

[43] Staneva, G.; Angelova, M. I. and Koumanov, K. (2004): Phospholipase A2 promotes raft budding and fission from giant liposomes, Chem Phys Lipids 129 [1], pp. 53-62.

[44] Ambroggio, E.; Separovic, F.; John, B.; Fidelio, G. D. and Bagatolli, L. A. (2005): Direct visualization of membrane leakage induced by the antibiotic peptides: Maculatin, Citropin and Aurein, Biophys J 89, pp. 1874-81.

[45] Korlach, J.; Schwille, P.; Webb, W. W. and Feigenson, G. W. (1999): Characterization of lipid bilayer phases by confocal microscopy and fluorescence correlation spectroscopy, Proc Natl Acad Sci U S A 96 [15], pp. 8461-6.

[46] Dietrich, C.; Bagatolli, L. A.; Volovyk, Z. N.; Thompson, N. L.; Levi, M.; Jacobson, K. and Gratton, E. (2001): Lipid rafts reconstituted in model membranes, Biophys J 80 [3], pp. 1417-28.

[47] Baumgart, T.; Hunt, G.; Farkas, E. R.; Webb, W. W. and Feigenson, G. W. (2007): Fluorescence probe partitioning between Lo/Ld phases in lipid membranes, Biochim Biophys Acta 1768 [9], pp. 2182-94.

[48] Owen, D. M.; Lanigan, P. M.; Dunsby, C.; Munro, I.; Grant, D.; Neil, M. A.; French, P. M. and Magee, A. I. (2006): Fluorescence lifetime imaging provides enhanced contrast when imaging the phase-sensitive dye di-4-ANEPPDHQ in model membranes and live cells, Biophys J 90 [11], pp. L80-2.

[49] Veatch, S. L. and Keller, S. L. (2003): Separation of liquid phases in giant vesicles of ternary mixtures of phospholipids and cholesterol, Biophys J 85 [5], pp. 3074-83.

[50] Veatch, S. L. and Keller, S. L. (2005): Seeing spots: complex phase behavior in simple membranes, Biochim Biophys Acta 1746 [3], pp. 172-85.

[51] Vidal, A. and McIntosh, T. J. (2005): Transbilayer Peptide Sorting between Raft and Nonraft Bilayers: Comparisons of Detergent Extraction and Confocal Microscopy, Biophys J 89 [2], pp. 1102-8.

[52] Bacia, K.; Schuette, C. G.; Kahya, N.; Jahn, R. and Schwille, P. (2004): SNAREs prefer liquid-disordered over "raft" (liquid-ordered) domains when reconstituted into giant unilamellar vesicles, J Biol Chem 279 [36], pp. 37951-5.

[53] Nicolini, C.; Baranski, J.; Schlummer, S.; Palomo, J.; Lumbierres-Burgues, M.; Kahms, M.; Kuhlmann, J.; Sanchez, S.; Gratton, E.; Waldmann, H. and Winter, R. (2006): Visualizing association of N-ras in lipid microdomains: influence of domain structure and interfacial adsorption, J Am Chem Soc 128 [1], pp. 192-201.

[54] Janiak, M. J.; Small, D. M. and Shipley, G. G. (1979): Temperature and compositional dependence of the structure of hydrated dimyristoyl lecithin, J Biol Chem 254 [13], pp. 6068-78.

[55] Koster, K. L.; Lei, Y. P.; Anderson, M.; Martin, S. and Bryant, G. (2000): Effects of vitrified and nonvitrified sugars on phosphatidylcholine fluid-to-gel phase transitions, Biophys J 78 [4], pp. 1932-46.

[56] Terova, B.; Heczko, R. and Slotte, J. P. (2005): On the importance of the phosphocholine methyl groups for sphingomyelin/cholesterol interactions in membranes: a study with ceramide phosphoethanolamine, Biophys J 88 [4], pp. 2661-9.

[57] Ramstedt, B. and Slotte, J. P. (1999): Interaction of cholesterol with sphingomyelins and acyl-chain-matched phosphatidylcholines: a comparative study of the effect of the chain length, Biophys J 76 [2], pp. 908-15.

[58] Gennis, R.B. (2006): Biomembranes: Molecular Structure and Function, Springer, New York, ISBN: 0-387-94824-4.

[59] Korlach, J.; Baumgart, T.; Webb, W. W. and Feigenson, G. W. (2005): Detection of motional heterogeneities in lipid bilayer membranes by dual probe fluorescence correlation spectroscopy, Biochim Biophys Acta 1668 [2], pp. 158-63.

[60] Kahya, N.; Scherfeld, D.; Bacia, K. and Schwille, P. (2004): Lipid domain formation and dynamics in giant unilamellar vesicles explored by fluorescence correlation spectroscopy, J Struct Biol 147 [1], pp. 77-89.

[61] Douglass, A. D. and Vale, R. D. (2005): Single-molecule microscopy reveals plasma membrane microdomains created by protein-protein networks that exclude or trap signaling molecules in T cells, Cell 121 [6], pp. 937-50.

[62] Collins, M. D. and Keller, S. L. (2008): Tuning lipid mixtures to induce or suppress domain formation across leaflets of unsupported asymmetric bilayers, Proc Natl Acad Sci U S A 105 [1], pp. 124-8.

[63] Devaux, P. F. and Morris, R. (2004): Transmembrane asymmetry and lateral domains in biological membranes, Traffic 5 [4], pp. 241-6.

[64] de Almeida, R. F.; Borst, J.; Fedorov, A.; Prieto, M. and Visser, A. J. (2007): Complexity of lipid domains and rafts in giant unilamellar vesicles revealed by combining imaging and microscopic and macroscopic time-resolved fluorescence, Biophys J 93 [2], pp. 539-53.

[65] Heberle, F. A.; Buboltz, J. T.; Stringer, D. and Feigenson, G. W. (2005): Fluorescence methods to detect phase boundaries in lipid bilayer mixtures, Biochim Biophys Acta 1746 [3], pp. 186-92.

[66] Silvius, J. R. and Nabi, I. R. (2006): Fluorescence-quenching and resonance energy transfer studies of lipid microdomains in model and biological membranes, Mol Membr Biol 23 [1], pp. 5-16.

[67] Loura, L. M.; Fedorov, A. and Prieto, M. (2000): Partition of membrane probes in a gel/fluid two-component lipid system: a fluorescence resonance energy transfer study, Biochim Biophys Acta 1467 [1], pp. 101-12.

[68] Loura, L. M.; Fedorov, A. and Prieto, M. (2000): Membrane Probe Distribution Heterogeneity: A Resonance Energy Transfer Study, J. Phys. Chem. B 104, pp. 6920-31.

[69] Loura, L. M.; Fedorov, A. and Prieto, M. (2001): Fluid-fluid membrane microheterogeneity: a fluorescence resonance energy transfer study, Biophys J 80 [2], pp. 776-88.

[70] Silvius, J. R. (2003): Fluorescence energy transfer reveals microdomain formation at physiological temperatures in lipid mixtures modeling the outer leaflet of the plasma membrane, Biophys J 85 [2], pp. 1034-45.

[71] de Almeida, R. F.; Loura, L. M.; Fedorov, A. and Prieto, M. (2005): Lipid rafts have different sizes depending on membrane composition: a time-resolved fluorescence resonance energy transfer study, J Mol Biol 346 [4], pp. 1109-20.

[72] Bunge, A.; Müller, P.; Stöckl, M.; Herrmann, A. and Huster, D. (2008): Characterization of the ternary mixture of sphingomyelin, POPC, and cholesterol: support for an inhomogeneous lipid distribution at high temperatures, Biophys J 94 [7], pp. 2680-90.

[73] Eisenblatter, J. and Winter, R. (2006): Pressure effects on the structure and phase behavior of DMPC-gramicidin lipid bilayers: a synchrotron SAXS and 2H-NMR spectroscopy study, Biophys J 90 [3], pp. 956-66.

[74] Kraft, M. L.; Weber, P. K.; Longo, M. L.; Hutcheon, I. D. and Boxer, S. G. (2006): Phase separation of lipid membranes analyzed with high-resolution secondary ion mass spectrometry, Science 313 [5795], pp. 1948-51.

[75] de Rijk, M. C.; Launer, L. J.; Berger, K.; Breteler, M. M.; Dartigues, J. F.; Baldereschi, M.; Fratiglioni, L.; Lobo, A.; Martinez-Lage, J.; Trenkwalder, C. and Hofman, A. (2000): Prevalence of Parkinson's disease in Europe: A collaborative study of population-based cohorts. Neurologic Diseases in the Elderly Research Group, Neurology 54 [11 Suppl 5], pp. S21-3.

[76] Parkinson, J. (2002): An essay on the shaking palsy. 1817, J Neuropsychiatry Clin Neurosci 14 [2], pp. 223-36; discussion 222.

[77] Farrer, M. J. (2006): Genetics of Parkinson disease: paradigm shifts and future prospects, Nat Rev Genet 7 [4], pp. 306-18.

[78] Ohama, E. and Ikuta, F. (1976): Parkinson's disease: distribution of Lewy bodies and monoamine neuron system, Acta Neuropathol 34 [4], pp. 311-9.

[79] Langston, J. W.; Ballard, P.; Tetrud, J. W. and Irwin, I. (1983): Chronic Parkinsonism in humans due to a product of meperidine-analog synthesis, Science 219 [4587], pp. 979-80.

[80] Ascherio, A.; Chen, H.; Weisskopf, M. G.; O'Reilly, E.; McCullough, M. L.; Calle, E. E.; Schwarzschild, M. A. and Thun, M. J. (2006): Pesticide exposure and risk for Parkinson's disease, Ann Neurol 60 [2], pp. 197-203.

[81] Ossowska, K.; Smialowska, M.; Kuter, K.; Wieronska, J.; Zieba, B.; Wardas, J.; Nowak, P.; Dabrowska, J.; Bortel, A.; Biedka, I.; Schulze, G. and Rommelspacher, H. (2006): Degeneration of dopaminergic mesocortical neurons and activation of compensatory processes induced by a long-term paraquat administration in rats: implications for Parkinson's disease, Neuroscience 141 [4], pp. 2155-65.

[82] Betarbet, R.; Sherer, T. B.; MacKenzie, G.; Garcia-Osuna, M.; Panov, A. V. and Greenamyre, J. T. (2000): Chronic systemic pesticide exposure reproduces features of Parkinson's disease, Nat Neurosci 3 [12], pp. 1301-6.

[83] Thomas, B. and Beal, M. F. (2007): Parkinson's disease, Hum Mol Genet 16 Spec No. 2, pp. R183-94.

[84] Mizuno, Y.; Hattori, N.; Kubo, S.; Sato, S.; Nishioka, K.; Hatano, T.; Tomiyama, H.; Funayama, M.; Machida, Y. and Mochizuki, H. (2008): Progress in the pathogenesis and genetics of Parkinson's disease, Philos Trans R Soc Lond B Biol Sci 363 [1500], pp. 2215-27.

[85] Krüger, R.; Kuhn, W.; Müller, T.; Woitalla, D.; Graeber, M.; Kosel, S.; Przuntek, H.; Epplen, J. T.; Schols, L. and Riess, O. (1998): Ala30Pro mutation in the gene encoding alpha-synuclein in Parkinson's disease, Nat Genet 18 [2], pp. 106-8.

[86] Polymeropoulos, M. H.; Lavedan, C.; Leroy, E.; Ide, S. E.; Dehejia, A.; Dutra, A.; Pike, B.; Root, H.; Rubenstein, J.; Boyer, R.; Stenroos, E. S.; Chandrasekharappa, S.; Athanassiadou, A.; Papapetropoulos, T.; Johnson, W. G.; Lazzarini, A. M.; Duvoisin, R. C.; Di Iorio, G.; Golbe, L. I. and Nussbaum, R. L. (1997): Mutation in the alpha-synuclein gene identified in families with Parkinson's disease, Science 276 [5321], pp. 2045-7.

[87] Zarranz, J. J.; Alegre, J.; Gomez-Esteban, J. C.; Lezcano, E.; Ros, R.; Ampuero, I.; Vidal, L.; Hoenicka, J.; Rodriguez, O.; Atares, B.; Llorens, V.; Gomez Tortosa, E.; del Ser, T.; Munoz, D. G. and de Yebenes, J. G. (2004): The new mutation, E46K, of alpha-synuclein causes Parkinson and Lewy body dementia, Ann Neurol 55 [2], pp. 164-73.

[88] Myhre, R.; Toft, M.; Kachergus, J.; Hulihan, M. M.; Aasly, J. O.; Klungland, H. and Farrer, M. J. (2008): Multiple alpha-synuclein gene polymorphisms are associated with Parkinson's disease in a Norwegian population, Acta Neurol Scand, pp. doi:10.1111/j.1600-0404.2008.01019.x.

[89] Ueda, K.; Saitoh, T. and Mori, H. (1994): Tissue-dependent alternative splicing of mRNA for NACP, the precursor of non-A beta component of Alzheimer's disease amyloid, Biochem Biophys Res Commun 205 [2], pp. 1366-72.

[90] Beyer, K.; Domingo-Sabat, M.; Lao, J. I.; Carrato, C.; Ferrer, I. and Ariza, A. (2008): Identification and characterization of a new alpha-synuclein isoform and its role in Lewy body diseases, Neurogenetics 9 [1], pp. 15-23.

[91] Clayton, D. F. and George, J. M. (1998): The synucleins: a family of proteins involved in synaptic function, plasticity, neurodegeneration and disease, Trends Neurosci 21 [6], pp. 249-54.

[92] Sung, Y. H. and Eliezer, D. (2007): Residual structure, backbone dynamics, and interactions within the synuclein family, J Mol Biol 372 [3], pp. 689-707.

[93] George, J. M.; Jin, H.; Woods, W. S. and Clayton, D. F. (1995): Characterization of a novel protein regulated during the critical period for song learning in the zebra finch, Neuron 15 [2], pp. 361-72.

[94] Eliezer, D.; Kutluay, E.; Bussell, R., Jr. and Browne, G. (2001): Conformational properties of alpha-synuclein in its free and lipid-associated states, J Mol Biol 307 [4], pp. 1061-73.

[95] Bussell, R., Jr. and Eliezer, D. (2003): A structural and functional role for 11-mer repeats in alpha-synuclein and other exchangeable lipid binding proteins, J Mol Biol 329 [4], pp. 763-78.

[96] Jao, C. C.; Der-Sarkissian, A.; Chen, J. and Langen, R. (2004): Structure of membrane-bound alpha-synuclein studied by site-directed spin labeling, Proc Natl Acad Sci U S A 101 [22], pp. 8331-6.

[97] Ulmer, T. S.; Bax, A.; Cole, N. B. and Nussbaum, R. L. (2005): Structure and dynamics of micelle-bound human alpha-synuclein, J Biol Chem 280 [10], pp. 9595-603.

[98] Ulmer, T. S. and Bax, A. (2005): Comparison of structure and dynamics of micelle-bound human alpha-synuclein and Parkinson disease variants, J Biol Chem 280 [52], pp. 43179-87.

[99] Chandra, S.; Chen, X.; Rizo, J.; Jahn, R. and Sudhof, T. C. (2003): A broken alpha -helix in folded alpha -Synuclein, J Biol Chem 278 [17], pp. 15313-8.

[100] Bortolus, M.; Tombolato, F.; Tessari, I.; Bisaglia, M.; Mammi, S.; Bubacco, L.; Ferrarini, A. and Maniero, A. L. (2008): Broken helix in vesicle and micelle-bound alpha-synuclein: insights from site-directed spin labeling-EPR experiments and MD simulations, J Am Chem Soc 130 [21], pp. 6690-1.

[101] Drescher, M.; Veldhuis, G.; van Rooijen, B. D.; Milikisyants, S.; Subramaniam, V. and Huber, M. (2008): Antiparallel arrangement of the helices of vesicle-bound alpha-synuclein, J Am Chem Soc 130 [25], pp. 7796-7.

[102] Mihajlovic, M. and Lazaridis, T. (2008): Membrane-bound structure and energetics of alpha-synuclein, Proteins 70 [3], pp. 761-78.

[103] Ueda, K.; Fukushima, H.; Masliah, E.; Xia, Y.; Iwai, A.; Yoshimoto, M.; Otero, D. A.; Kondo, J.; Ihara, Y. and Saitoh, T. (1993): Molecular cloning of cDNA encoding an unrecognized component of amyloid in Alzheimer disease, Proc Natl Acad Sci U S A 90 [23], pp. 11282-6.

[104] Giasson, B. I.; Murray, I. V.; Trojanowski, J. Q. and Lee, V. M. (2001): A hydrophobic stretch of 12 amino acid residues in the middle of alpha-synuclein is essential for filament assembly, J Biol Chem 276 [4], pp. 2380-6.

[105] Periquet, M.; Fulga, T.; Myllykangas, L.; Schlossmacher, M. G. and Feany, M. B. (2007): Aggregated alpha-synuclein mediates dopaminergic neurotoxicity in vivo, J Neurosci 27 [12], pp. 3338-46.

[106] Koo, H. J.; Lee, H. J. and Im, H. (2008): Sequence determinants regulating fibrillation of human alpha-synuclein, Biochem Biophys Res Commun 368 [3], pp. 772-8.

[107] Zibaee, S.; Jakes, R.; Fraser, G.; Serpell, L. C.; Crowther, R. A. and Goedert, M. (2007): Sequence Determinants for Amyloid Fibrillogenesis of Human alpha-Synuclein, J Mol Biol 374 [2], pp. 454-64.

[108] Heise, H.; Celej, M. S.; Becker, S.; Riedel, D.; Pelah, A.; Kumar, A.; Jovin, T. M. and Baldus, M. (2008): Solid-state NMR reveals structural differences between fibrils of wild-type and disease-related A53T mutant alpha-synuclein, J Mol Biol 380 [3], pp. 444-50.

[109] Heise, H.; Hoyer, W.; Becker, S.; Andronesi, O. C.; Riedel, D. and Baldus, M. (2005): Molecular-level secondary structure, polymorphism, and dynamics of full-length alpha-synuclein fibrils studied by solid-state NMR, Proc Natl Acad Sci U S A 102 [44], pp. 15871-6.

[110] Chen, M.; Margittai, M.; Chen, J. and Langen, R. (2007): Investigation of alpha-synuclein fibril structure by site-directed spin labeling, J Biol Chem 282 [34], pp. 24970-9.

[111] Del Mar, C.; Greenbaum, E. A.; Mayne, L.; Englander, S. W. and Woods, V. L., Jr. (2005): Structure and properties of {alpha}-synuclein and other amyloids determined at the amino acid level, Proc Natl Acad Sci U S A 102 [43], pp. 15477-82.

[112] Der-Sarkissian, A.; Jao, C. C.; Chen, J. and Langen, R. (2003): Structural organization of alpha-synuclein fibrils studied by site-directed spin labeling, J Biol Chem 278 [39], pp. 37530-5.

[113] Qin, Z.; Hu, D.; Han, S.; Hong, D. P. and Fink, A. L. (2007): Role of different regions of alpha-synuclein in the assembly of fibrils, Biochemistry 46 [46], pp. 13322-30.

[114] Vilar, M.; Chou, H. T.; Luhrs, T.; Maji, S. K.; Riek-Loher, D.; Verel, R.; Manning, G.; Stahlberg, H. and Riek, R. (2008): The fold of alpha-synuclein fibrils, Proc Natl Acad Sci U S A 105 [25], pp. 8637-42.

[115] Lee, J. C.; Langen, R.; Hummel, P. A.; Gray, H. B. and Winkler, J. R. (2004): Alpha-synuclein structures from fluorescence energy-transfer kinetics: implications for the role of the protein in Parkinson's disease, Proc Natl Acad Sci U S A 101 [47], pp. 16466-71.

[116] Lee, J. C.; Lai, B. T.; Kozak, J. J.; Gray, H. B. and Winkler, J. R. (2007): Alpha-synuclein tertiary contact dynamics, J Phys Chem B 111 [8], pp. 2107-12.

[117] Bertoncini, C. W.; Fernandez, C. O.; Griesinger, C.; Jovin, T. M. and Zweckstetter, M. (2005): Familial mutants of alpha -synuclein with increased neurotoxicity have a destabilized conformation, J Biol Chem 280 [35], pp. 30649-52.

[118] Bertoncini, C. W.; Jung, Y. S.; Fernandez, C. O.; Hoyer, W.; Griesinger, C.; Jovin, T. M. and Zweckstetter, M. (2005): Release of long-range tertiary interactions potentiates aggregation of natively unstructured alpha-synuclein, Proc Natl Acad Sci U S A 102 [5], pp. 1430-5.

[119] Fernandez, C. O.; Hoyer, W.; Zweckstetter, M.; Jares-Erijman, E. A.; Subramaniam, V.; Griesinger, C. and Jovin, T. M. (2004): NMR of alpha-synuclein-polyamine complexes elucidates the mechanism and kinetics of induced aggregation, Embo J 23 [10], pp. 2039-46.

[120] Crowther, R. A.; Jakes, R.; Spillantini, M. G. and Goedert, M. (1998): Synthetic filaments assembled from C-terminally truncated alpha-synuclein, FEBS Lett 436 [3], pp. 309-12.

[121] Serpell, L. C.; Berriman, J.; Jakes, R.; Goedert, M. and Crowther, R. A. (2000): Fiber diffraction of synthetic alpha-synuclein filaments shows amyloid-like cross-beta conformation, Proc Natl Acad Sci U S A 97 [9], pp. 4897-902.

[122] Murray, I. V.; Giasson, B. I.; Quinn, S. M.; Koppaka, V.; Axelsen, P. H.; Ischiropoulos, H.; Trojanowski, J. Q. and Lee, V. M. (2003): Role of alpha-synuclein carboxy-terminus on fibril formation in vitro, Biochemistry 42 [28], pp. 8530-40.

[123] Liu, C. W.; Giasson, B. I.; Lewis, K. A.; Lee, V. M.; Demartino, G. N. and Thomas, P. J. (2005): A precipitating role for truncated alpha-synuclein and the proteasome in alpha-synuclein aggregation: implications for pathogenesis of Parkinson disease, J Biol Chem 280 [24], pp. 22670-8.

[124] Iwai, A.; Masliah, E.; Yoshimoto, M.; Ge, N.; Flanagan, L.; de Silva, H. A.; Kittel, A. and Saitoh, T. (1995): The precursor protein of non-A beta component of Alzheimer's disease amyloid is a presynaptic protein of the central nervous system, Neuron 14 [2], pp. 467-75.

[125] Maroteaux, L.; Campanelli, J. T. and Scheller, R. H. (1988): Synuclein: a neuron-specific protein localized to the nucleus and presynaptic nerve terminal, J Neurosci 8 [8], pp. 2804-15.

[126] Jakes, R.; Spillantini, M. G. and Goedert, M. (1994): Identification of two distinct synucleins from human brain, FEBS Lett 345 [1], pp. 27-32.

[127] Murphy, D. D.; Rueter, S. M.; Trojanowski, J. Q. and Lee, V. M. (2000): Synucleins are developmentally expressed, and alpha-synuclein regulates the size of the presynaptic vesicular pool in primary hippocampal neurons, J Neurosci 20 [9], pp. 3214-20.

[128] Fortin, D. L.; Troyer, M. D.; Nakamura, K.; Kubo, S.; Anthony, M. D. and Edwards, R. H. (2004): Lipid rafts mediate the synaptic localization of alpha-synuclein, J Neurosci 24 [30], pp. 6715-23.

[129] Totterdell, S. and Meredith, G. E. (2005): Localization of Alpha-synuclein to identified fibers and synapses in the normal mouse brain, Neuroscience 135 [3], pp. 907-13.

[130] Outeiro, T. F. and Lindquist, S. (2003): Yeast cells provide insight into alpha-synuclein biology and pathobiology, Science 302 [5651], pp. 1772-5.

[131] Cooper, A. A.; Gitler, A. D.; Cashikar, A.; Haynes, C. M.; Hill, K. J.; Bhullar, B.; Liu, K.; Xu, K.; Strathearn, K. E.; Liu, F.; Cao, S.; Caldwell, K. A.; Caldwell, G. A.; Marsischky, G.; Kolodner, R. D.; Labaer, J.; Rochet, J. C.; Bonini, N. M. and Lindquist, S. (2006): Alpha-synuclein blocks ER-Golgi traffic and Rab1 rescues neuron loss in Parkinson's models, Science 313 [5785], pp. 324-8.

[132] Sharon, R.; Bar-Joseph, I.; Mirick, G. E.; Serhan, C. N. and Selkoe, D. J. (2003): Altered fatty acid composition of dopaminergic neurons expressing alpha-synuclein and human brains with alpha-synucleinopathies, J Biol Chem 278 [50], pp. 49874-81.

[133] Castagnet, P. I.; Golovko, M. Y.; Barcelo-Coblijn, G. C.; Nussbaum, R. L. and Murphy, E. J. (2005): Fatty acid incorporation is decreased in astrocytes cultured from alpha-synuclein gene-ablated mice, J Neurochem 94 [3], pp. 839-49.

[134] Golovko, M. Y.; Faergeman, N. J.; Cole, N. B.; Castagnet, P. I.; Nussbaum, R. L. and Murphy, E. J. (2005): Alpha-synuclein gene deletion decreases brain palmitate uptake and alters the palmitate metabolism in the absence of alpha-synuclein palmitate binding, Biochemistry 44 [23], pp. 8251-9.

[135] Bonini, N. M. and Giasson, B. I. (2005): Snaring the function of alpha-synuclein, Cell 123 [3], pp. 359-61.

[136] Chandra, S.; Gallardo, G.; Fernandez-Chacon, R.; Schluter, O. M. and Sudhof, T. C. (2005): Alpha-synuclein cooperates with CSPalpha in preventing neurodegeneration, Cell 123 [3], pp. 383-96.

[137] Larsen, K. E.; Schmitz, Y.; Troyer, M. D.; Mosharov, E.; Dietrich, P.; Quazi, A. Z.; Savalle, M.; Nemani, V.; Chaudhry, F. A.; Edwards, R. H.; Stefanis, L. and Sulzer, D. (2006): Alpha-synuclein overexpression in PC12 and chromaffin cells impairs catecholamine release by interfering with a late step in exocytosis, J Neurosci 26 [46], pp. 11915-22.

[138] Gitler, A. D. and Shorter, J. (2007): Prime time for alpha-synuclein, J Neurosci 27 [10], pp. 2433-4.

[139] Gureviciene, I.; Gurevicius, K. and Tanila, H. (2007): Role of alpha-synuclein in synaptic glutamate release, Neurobiol Dis 28 [1], pp. 83-9.

[140] Jensen, P. H.; Nielsen, M. S.; Jakes, R.; Dotti, C. G. and Goedert, M. (1998): Binding of alpha-synuclein to brain vesicles is abolished by familial Parkinson's disease mutation, J Biol Chem 273 [41], pp. 26292-4.

[141] Lee, H. J.; Choi, C. and Lee, S. J. (2002): Membrane-bound alpha-synuclein has a high aggregation propensity and the ability to seed the aggregation of the cytosolic form, J Biol Chem 277 [1], pp. 671-8.

[142] Kim, Y. S.; Laurine, E.; Woods, W. and Lee, S. J. (2006): A novel mechanism of interaction between alpha-synuclein and biological membranes, J Mol Biol 360 [2], pp. 386-97.

[143] Soper, J. H.; Roy, S.; Stieber, A.; Lee, E.; Wilson, R. B.; Trojanowski, J. Q.; Burd, C. G. and Lee, V. M. (2008): {alpha}-Synuclein-induced Aggregation of Cytoplasmic Vesicles in Saccharomyces cerevisiae, Mol Biol Cell 19 [3], pp. 1093-103.

[144] Davidson, W. S.; Jonas, A.; Clayton, D. F. and George, J. M. (1998): Stabilization of alpha-synuclein secondary structure upon binding to synthetic membranes, J Biol Chem 273 [16], pp. 9443-9.

[145] Perrin, R. J.; Woods, W. S.; Clayton, D. F. and George, J. M. (2000): Interaction of human alpha-Synuclein and Parkinson's disease variants with phospholipids. Structural analysis using site-directed mutagenesis, J Biol Chem 275 [44], pp. 34393-8.

[146] Kamp, F. and Beyer, K. (2006): Binding of alpha-synuclein affects the lipid packing in bilayers of small vesicles, J Biol Chem 281 [14], pp. 9251-9.

[147] Kubo, S.; Nemani, V. M.; Chalkley, R. J.; Anthony, M. D.; Hattori, N.; Mizuno, Y.; Edwards, R. H. and Fortin, D. L. (2005): A Combinatorial Code for the Interaction of {alpha}-Synuclein with Membranes, J Biol Chem 280 [36], pp. 31664-72.

[148] Madine, J.; Doig, A. J. and Middleton, D. A. (2006): A study of the regional effects of alpha-synuclein on the organization and stability of phospholipid bilayers, Biochemistry 45 [18], pp. 5783-92.

[149] Nuscher, B.; Kamp, F.; Mehnert, T.; Odoy, S.; Haass, C.; Kahle, P. J. and Beyer, K. (2004): Alpha-synuclein has a high affinity for packing defects in a bilayer membrane: a thermodynamics study, J Biol Chem 279 [21], pp. 21966-75.

[150] Ferreon, A. C. and Deniz, A. A. (2007): Alpha-synuclein multistate folding thermodynamics: implications for protein misfolding and aggregation, Biochemistry 46 [15], pp. 4499-509.

[151] Uversky, V. N. (2007): Neuropathology, biochemistry, and biophysics of alpha-synuclein aggregation, J Neurochem 103 [1], pp. 17-37.

[152] Beyer, K. (2007): Mechanistic aspects of Parkinson's disease: alpha-synuclein and the biomembrane, Cell Biochem Biophys 47 [2], pp. 285-99.

[153] Jo, E.; McLaurin, J.; Yip, C. M.; St George-Hyslop, P. and Fraser, P. E. (2000): alpha-Synuclein membrane interactions and lipid specificity, J Biol Chem 275 [44], pp. 34328-34.

[154] Giannakis, E.; Pacifico, J.; Smith, D. P.; Hung, L. W.; Masters, C. L.; Cappai, R.; Wade, J. D. and Barnham, K. J. (2008): Dimeric structures of alpha-synuclein bind preferentially to lipid membranes, Biochim Biophys Acta 1778 [4], pp. 1112-9.

[155] Zhu, M.; Qin, Z. J.; Hu, D.; Munishkina, L. A. and Fink, A. L. (2006): Alpha-synuclein can function as an antioxidant preventing oxidation of unsaturated lipid in vesicles, Biochemistry 45 [26], pp. 8135-42.

[156] Jenco, J. M.; Rawlingson, A.; Daniels, B. and Morris, A. J. (1998): Regulation of phospholipase D2: selective inhibition of mammalian phospholipase D isoenzymes by alpha- and beta-synucleins, Biochemistry 37 [14], pp. 4901-9.

[157] Dev, K. K.; Hofele, K.; Barbieri, S.; Buchman, V. L. and van der Putten, H. (2003): Part II: alpha-synuclein and its molecular pathophysiological role in neurodegenerative disease, Neuropharmacology 45 [1], pp. 14-44.

[158] Jin, J.; Li, G. J.; Davis, J.; Zhu, D.; Wang, Y.; Pan, C. and Zhang, J. (2007): Identification of novel proteins associated with both alpha-synuclein and DJ-1, Mol Cell Proteomics 6 [5], pp. 845-59.

[159] Brown, D. R. (2007): Interactions between metals and alpha-synuclein--function or artefact? Febs J 274 [15], pp. 3766-74.

[160] Wright, J. A. and Brown, D. R. (2008): Alpha-synuclein and its role in metal binding: relevance to Parkinson's disease, J Neurosci Res 86 [3], pp. 496-503.

[161] Forster, E. and Lewy, F.H. (1912): Paralysis agitans, M., Lewandowsky, Ed, Pathologische Anatomie. Handbuch der Neurologie, Springer Verlag, Berlin.

[162] Uversky, V. N.; Lee, H. J.; Li, J.; Fink, A. L. and Lee, S. J. (2001): Stabilization of partially folded conformation during alpha-synuclein oligomerization in both purified and cytosolic preparations, J Biol Chem 276 [47], pp. 43495-8.

[163] Uversky, V. N.; Li, J. and Fink, A. L. (2001): Evidence for a partially folded intermediate in alpha-synuclein fibril formation, J Biol Chem 276 [14], pp. 10737-44.

[164] Kaylor, J.; Bodner, N.; Edridge, S.; Yamin, G.; Hong, D. P. and Fink, A. L. (2005): Characterization of oligomeric intermediates in alpha-synuclein fibrillation: FRET studies of Y125W/Y133F/Y136F alpha-synuclein, J Mol Biol 353 [2], pp. 357-72.

[165] Dusa, A.; Kaylor, J.; Edridge, S.; Bodner, N.; Hong, D. P. and Fink, A. L. (2006): Characterization of oligomers during alpha-synuclein aggregation using intrinsic tryptophan fluorescence, Biochemistry 45 [8], pp. 2752-60.

[166] Kamiyoshihara, T.; Kojima, M.; Ueda, K.; Tashiro, M. and Shimotakahara, S. (2007): Observation of multiple intermediates in alpha-synuclein fibril formation by singular value decomposition analysis, Biochem Biophys Res Commun 355 [2], pp. 398-403.

[167] Apetri, M. M.; Maiti, N. C.; Zagorski, M. G.; Carey, P. R. and Anderson, V. E. (2006): Secondary structure of alpha-synuclein oligomers: characterization by raman and atomic force microscopy, J Mol Biol 355 [1], pp. 63-71.

[168] Ehrnhoefer, D. E.; Bieschke, J.; Boeddrich, A.; Herbst, M.; Masino, L.; Lurz, R.; Engemann, S.; Pastore, A. and Wanker, E. E. (2008): EGCG redirects amyloidogenic polypeptides into unstructured, off-pathway oligomers, Nat Struct Mol Biol 15 [6], pp. 558-66.

[169] Hegde, M. L. and Rao, K. S. (2007): DNA induces folding in alpha-synuclein: understanding the mechanism using chaperone property of osmolytes, Arch Biochem Biophys 464 [1], pp. 57-69.

[170] Uversky, V. N. and Fink, A. L. (2004): Conformational constraints for amyloid fibrillation: the importance of being unfolded, Biochim Biophys Acta 1698 [2], pp. 131-53.

[171] Gerard, M.; Debyser, Z.; Desender, L.; Kahle, P. J.; Baert, J.; Baekelandt, V. and Engelborghs, Y. (2006): The aggregation of alpha-synuclein is stimulated by FK506 binding proteins as shown by fluorescence correlation spectroscopy, Faseb J 20 [3], pp. 524-6.

[172] Gerard, M.; Debyser, Z.; Desender, L.; Baert, J.; Brandt, I.; Baekelandt, V. and Engelborghs, Y. (2008): FK506 binding protein 12 differentially accelerates fibril formation of wild type alpha-synuclein and its clinical mutants A30P or A53T, J Neurochem 106 [1], pp. 121-33.

[173] Outeiro, T. F.; Putcha, P.; Tetzlaff, J. E.; Spoelgen, R.; Koker, M.; Carvalho, F.; Hyman, B. T. and McLean, P. J. (2008): Formation of toxic oligomeric alpha-synuclein species in living cells, PLoS ONE 3 [4], p. e1867.

[174] Danzer, K. M.; Haasen, D.; Karow, A. R.; Moussaud, S.; Habeck, M.; Giese, A.; Kretzschmar, H.; Hengerer, B. and Kostka, M. (2007): Different species of alpha-synuclein oligomers induce calcium influx and seeding, J Neurosci 27 [34], pp. 9220-32.

[175] Li, J.; Uversky, V. N. and Fink, A. L. (2001): Effect of familial Parkinson's disease point mutations A30P and A53T on the structural properties, aggregation, and fibrillation of human alpha-synuclein, Biochemistry 40 [38], pp. 11604-13.

[176] Pandey, N.; Schmidt, R. E. and Galvin, J. E. (2006): The alpha-synuclein mutation E46K promotes aggregation in cultured cells, Exp Neurol 197 [2], pp. 515-20.

[177] Choi, W.; Zibaee, S.; Jakes, R.; Serpell, L. C.; Davletov, B.; Crowther, R. A. and Goedert, M. (2004): Mutation E46K increases phospholipid binding and assembly into filaments of human alpha-synuclein, FEBS Lett 576 [3], pp. 363-8.

[178] Fredenburg, R. A.; Rospigliosi, C.; Meray, R. K.; Kessler, J. C.; Lashuel, H. A.; Eliezer, D. and Lansbury, P. T., Jr. (2007): The impact of the E46K mutation on the properties of alpha-synuclein in its monomeric and oligomeric states, Biochemistry 46 [24], pp. 7107-18.

[179] Smith, D.P.; Tew, D.J.; Hill, A.F.; Bottomley, S.P.; Masters, C.L.; Barnham, K.J. and Cappai, R. (2008): Formation of a High Affinity Lipid-Binding Intermediate during the Early Aggregation Phase of alpha-Synuclein, Biochemistry 47, pp. 1425-1434.

[180] Uversky, V. N.; Li, J. and Fink, A. L. (2001): Metal-triggered structural transformations, aggregation, and fibrillation of human alpha-synuclein. A possible molecular NK between Parkinson's disease and heavy metal exposure, J Biol Chem 276 [47], pp. 44284-96.

[181] Bharathi; Indi, S. S. and Rao, K. S. (2007): Copper- and iron-induced differential fibril formation in alpha-synuclein: TEM study, Neurosci Lett 424 [2], pp. 78-82.

[182] Kostka, M.; Hogen, T.; Danzer, K. M.; Levin, J.; Habeck, M.; Wirth, A.; Wagner, R.; Glabe, C. G.; Finger, S.; Heinzelmann, U.; Garidel, P.; Duan, W.; Ross, C. A.; Kretzschmar, H. and Giese, A. (2008): Single particle characterization of iron-induced pore-forming alpha-synuclein oligomers, J Biol Chem 283 [16], pp. 10992-1003.

[183] Glaser, C. B.; Yamin, G.; Uversky, V. N. and Fink, A. L. (2005): Methionine oxidation, alpha-synuclein and Parkinson's disease, Biochim Biophys Acta 1703 [2], pp. 157-69.

[184] Krishnan, S.; Chi, E. Y.; Wood, S. J.; Kendrick, B. S.; Li, C.; Garzon-Rodriguez, W.; Wypych, J.; Randolph, T. W.; Narhi, L. O.; Biere, A. L.; Citron, M. and Carpenter, J. F. (2003): Oxidative dimer formation is the critical rate-limiting step for Parkinson's disease alpha-synuclein fibrillogenesis, Biochemistry 42 [3], pp. 829-37.

[185] Rott, R.; Szargel, R.; Haskin, J.; Shani, V.; Shainskaya, A.; Manov, I.; Liani, E.; Avraham, E. and Engelender, S. (2008): Monoubiquitylation of {alpha}-Synuclein by Seven in Absentia Homolog (SIAH) Promotes Its Aggregation in Dopaminergic Cells, J Biol Chem 283 [6], pp. 3316-28.

[186] Engelender, S. (2008): Ubiquitination of alpha-synuclein and autophagy in Parkinson's disease, Autophagy 4 [3], pp. 372-4.

[187] Lee, J. T.; Wheeler, T. C.; Li, L. and Chin, L. S. (2008): Ubiquitination of alpha-synuclein by Siah-1 promotes alpha-synuclein aggregation and apoptotic cell death, Hum Mol Genet 17 [6], pp. 906-17.

[188] Zhu, M. and Fink, A. L. (2003): Lipid binding inhibits alpha-synuclein fibril formation, J Biol Chem 278 [19], pp. 16873-7.

[189] Zhu, M.; Li, J. and Fink, A. L. (2003): The association of alpha-synuclein with membranes affects bilayer structure, stability, and fibril formation, J Biol Chem 278 [41], pp. 40186-97.

[190] Bar-On, P.; Crews, L.; Koob, A. O.; Mizuno, H.; Adame, A.; Spencer, B. and Masliah, E. (2008): Statins reduce neuronal alpha-synuclein aggregation in in vitro models of Parkinson's disease, J Neurochem 105 [5], pp. 1656-67.

[191] Jo, E.; Darabie, A. A.; Han, K.; Tandon, A.; Fraser, P. E. and McLaurin, J. (2004): alpha-Synuclein-synaptosomal membrane interactions: implications for fibrillogenesis, Eur J Biochem 271 [15], pp. 3180-9.

[192] Lashuel, H. A.; Hartley, D.; Petre, B. M.; Walz, T. and Lansbury, P. T., Jr. (2002): Neurodegenerative disease: amyloid pores from pathogenic mutations, Nature 418 [6895], p. 291.

[193] Lashuel, H. A.; Petre, B. M.; Wall, J.; Simon, M.; Nowak, R. J.; Walz, T. and Lansbury, P. T., Jr. (2002): Alpha-synuclein, especially the Parkinson's disease-associated mutants, forms pore-like annular and tubular protofibrils, J Mol Biol 322 [5], pp. 1089-102.

[194] Ding, T. T.; Lee, S. J.; Rochet, J. C. and Lansbury, P. T., Jr. (2002): Annular alpha-synuclein protofibrils are produced when spherical protofibrils are incubated in solution or bound to brain-derived membranes, Biochemistry 41 [32], pp. 10209-17.

[195] Tsigelny, I. F.; Bar-On, P.; Sharikov, Y.; Crews, L.; Hashimoto, M.; Miller, M. A.; Keller, S. H.; Platoshyn, O.; Yuan, J. X. and Masliah, E. (2007): Dynamics of alpha-synuclein aggregation and inhibition of pore-like oligomer development by beta-synuclein, Febs J 274 [7], pp. 1862-77.

[196] Volles, M. J. and Lansbury, P. T., Jr. (2002): Vesicle permeabilization by protofibrillar alpha-synuclein is sensitive to Parkinson's disease-linked mutations and occurs by a pore-like mechanism, Biochemistry 41 [14], pp. 4595-602.

[197] Volles, M. J.; Lee, S. J.; Rochet, J. C.; Shtilerman, M. D.; Ding, T. T.; Kessler, J. C. and Lansbury, P. T., Jr. (2001): Vesicle permeabilization by protofibrillar alpha-synuclein: implications for the pathogenesis and treatment of Parkinson's disease, Biochemistry 40 [26], pp. 7812-9.

[198] Zakharov, S. D.; Hulleman, J. D.; Dutseva, E. A.; Antonenko, Y. N.; Rochet, J. C. and Cramer, W. A. (2007): Helical alpha-synuclein forms highly conductive ion channels, Biochemistry 46 [50], pp. 14369-79.

[199] Furukawa, K.; Matsuzaki-Kobayashi, M.; Hasegawa, T.; Kikuchi, A.; Sugeno, N.; Itoyama, Y.; Wang, Y.; Yao, P. J.; Bushlin, I. and Takeda, A. (2006): Plasma membrane ion permeability induced by mutant alpha-synuclein contributes to the degeneration of neural cells, J Neurochem 97 [4], pp. 1071-7.

[200] Mosharov, E. V.; Staal, R. G.; Bove, J.; Prou, D.; Hananiya, A.; Markov, D.; Poulsen, N.; Larsen, K. E.; Moore, C. M.; Troyer, M. D.; Edwards, R. H.; Przedborski, S. and Sulzer, D. (2006): Alpha-synuclein overexpression increases cytosolic catecholamine concentration, J Neurosci 26 [36], pp. 9304-11.

[201] Follmer, C.; Romao, L.; Einsiedler, C. M.; Porto, T. C.; Lara, F. A.; Moncores, M.; Weissmüller, G.; Lashuel, H. A.; Lansbury, P.; Neto, V. M.; Silva, J. L. and Foguel, D. (2007): Dopamine affects the stability, hydration, and packing of protofibrils and fibrils of the wild type and variants of alpha-synuclein, Biochemistry 46 [2], pp. 472-82.

[202] Devi, L.; Raghavendran, V.; Prabhu, B. M.; Avadhani, N. G. and Anandatheerthavarada, H. K. (2008): Mitochondrial import and accumulation of alpha-synuclein impair complex I in human dopaminergic neuronal cultures and Parkinson disease brain, J Biol Chem 283 [14], pp. 9089-100.

[203] Smith, W. W.; Jiang, H.; Pei, Z.; Tanaka, Y.; Morita, H.; Sawa, A.; Dawson, V. L.; Dawson, T. M. and Ross, C. A. (2005): Endoplasmic reticulum stress and mitochondrial cell death pathways mediate A53T mutant alpha-synuclein-induced toxicity, Hum Mol Genet 14 [24], pp. 3801-11.

[204] Gosavi, N.; Lee, H. J.; Lee, J. S.; Patel, S. and Lee, S. J. (2002): Golgi fragmentation occurs in the cells with prefibrillar alpha-synuclein aggregates and precedes the formation of fibrillar inclusion, J Biol Chem 277 [50], pp. 48984-92.

[205] Chen, L.; Jin, J.; Davis, J.; Zhou, Y.; Wang, Y.; Liu, J.; Lockhart, P. J. and Zhang, J. (2007): Oligomeric alpha-synuclein inhibits tubulin polymerization, Biochem Biophys Res Commun 356 [3], pp. 548-53.

[206] Kim, M.; Jung, W.; Lee, I. H.; Bhak, G.; Paik, S. R. and Hahn, J. S. (2008): Impairment of microtubule system increases alpha-synuclein aggregation and toxicity, Biochem Biophys Res Commun 365 [4], pp. 628-35.

[207] Gitler, A. D.; Bevis, B. J.; Shorter, J.; Strathearn, K. E.; Hamamichi, S.; Su, L. J.; Caldwell, K. A.; Caldwell, G. A.; Rochet, J. C.; McCaffery, J. M.; Barlowe, C. and Lindquist, S. (2008): The Parkinson's disease protein alpha-synuclein disrupts cellular Rab homeostasis, Proc Natl Acad Sci U S A 105 [1], pp. 145-50.

[208] Willingham, S.; Outeiro, T. F.; DeVit, M. J.; Lindquist, S. L. and Muchowski, P. J. (2003): Yeast genes that enhance the toxicity of a mutant huntingtin fragment or alpha-synuclein, Science 302 [5651], pp. 1769-72.

[209] Snyder, H.; Mensah, K.; Theisler, C.; Lee, J.; Matouschek, A. and Wolozin, B. (2003): Aggregated and monomeric alpha-synuclein bind to the S6' proteasomal protein and inhibit proteasomal function, J Biol Chem 278 [14], pp. 11753-9.

[210] Lindersson, E.; Beedholm, R.; Hojrup, P.; Moos, T.; Gai, W.; Hendil, K. B. and Jensen, P. H. (2004): Proteasomal inhibition by alpha-synuclein filaments and oligomers, J Biol Chem 279 [13], pp. 12924-34.

[211] Zhang, N. Y.; Tang, Z. and Liu, C. W. (2008): {alpha}-Synuclein Protofibrils Inhibit 26 S Proteasome-mediated Protein Degradation: UNDERSTANDING THE CYTOTOXICITY OF PROTEIN PROTOFIBRILS IN NEURODEGENERATIVE DISEASE PATHOGENESIS, J Biol Chem 283 [29], pp. 20288-98.

[212] Stefanis, L.; Larsen, K. E.; Rideout, H. J.; Sulzer, D. and Greene, L. A. (2001): Expression of A53T mutant but not wild-type alpha-synuclein in PC12 cells induces alterations of the ubiquitin-dependent degradation system, loss of dopamine release, and autophagic cell death, J Neurosci 21 [24], pp. 9549-60.

[213] Tanaka, Y.; Engelender, S.; Igarashi, S.; Rao, R. K.; Wanner, T.; Tanzi, R. E.; Sawa, A.; V, L. Dawson; Dawson, T. M. and Ross, C. A. (2001): Inducible expression of mutant alpha-synuclein decreases proteasome activity and increases sensitivity to mitochondria-dependent apoptosis, Hum Mol Genet 10 [9], pp. 919-26.

[214] Lee, F. J.; Liu, F.; Pristupa, Z. B. and Niznik, H. B. (2001): Direct binding and functional coupling of alpha-synuclein to the dopamine transporters accelerate dopamine-induced apoptosis, Faseb J 15 [6], pp. 916-26.

[215] Cookson, M. R. and van der Brug, M. (2008): Cell systems and the toxic mechanism(s) of alpha-synuclein, Exp Neurol 209 [1], pp. 5-11.

[216] Angelova, M. I. and Dimitrov, D.S (1986): Liposome electroformation, Faraday Discuss. Chem. Soc. 81, pp. 303-311.

[217] Angelova, M. I.; Soleau, S.; Meleard, P.; Faucon, J.F. and Bothorel, P. (1992): Preparation of giant vesicles by external AC electric fields. Kinetics and applications, Progress in Colloid & Polymer Science 89, pp. 127-131.

[218] Dimitrov, D.S and Angelova, M. I. (1987): Lipid swelling and liposome formation on solid surfaces in external electric fields., Progress in Colloid & Polymer Science 73, pp. 48-56.

[219] Ayuyan, A. G. and Cohen, F. S. (2006): Lipid peroxides promote large rafts: effects of excitation of probes in fluorescence microscopy and electrochemical reactions during vesicle formation, Biophys J 91 [6], pp. 2172-83.

[220] Scott, R. E. (1976): Plasma membrane vesiculation: a new technique for isolation of plasma membranes, Science 194 [4266], pp. 743-5.

[221] Scott, R. E. and Maercklein, P. B. (1979): Plasma membrane vesiculation in 3T3 and SV3T3 cells. II. Factors affecting the process of vesiculation, J Cell Sci 35, pp. 245-52.

[222] Holowka, D. and Baird, B. (1983): Structural studies on the membrane-bound immunoglobulin E-receptor complex. 1. Characterization of large plasma membrane vesicles from rat basophilic leukemia cells and insertion of amphipathic fluorescent probes, Biochemistry 22 [14], pp. 3466-74.

[223] Sambrook, J. and Russell, D.W (2001): Molecular cloning: a laboratory manual, 3. ed. ed., Sambrook, J. and Russell, D.W, Eds, Cold Spring Harbor Laboratory Press, Cold Spring Harbor, ISBN: 0-87969-576-5.

[224] Laemmli, U. K. (1970): Cleavage of structural proteins during the assembly of the head of bacteriophage T4, Nature 227 [5259], pp. 680-5.

[225] Chatelier, R. C. and Minton, A. P. (1996): Adsorption of globular proteins on locally planar surfaces: models for the effect of excluded surface area and aggregation of adsorbed protein on adsorption equilibria, Biophys J 71 [5], pp. 2367-74.

[226] Stöckl, M.; Plazzo, A.P.; Korte, T. and Herrmann, A. (2008): Detection of lipid domains in model and cell membranes by fluorescence lifetime imaging microscopy of fluorescent lipid analogues, J. Biol. Chem., p. doi:10.1074/jbc.M801418200.

[227] Wüstner, D.; Mukherjee, S.; Maxfield, F. R.; Müller, P. and Herrmann, A. (2001): Vesicular and nonvesicular transport of phosphatidylcholine in polarized HepG2 cells, Traffic 2 [4], pp. 277-96.

[228] Müller, P.; Pomorski, T.; Porwoli, S.; Tauber, R. and Herrmann, A. (1996): Transverse movement of spin-labeled phospholipids in the plasma membrane of a hepatocytic cell line (HepG2): implications for biliary lipid secretion, Hepatology 24 [6], pp. 1497-503.

[229] Tannert, A.; Wüstner, D.; Bechstein, J.; Müller, P.; Devaux, P. F. and Herrmann, A. (2003): Aminophospholipids have no access to the luminal side of the biliary canaliculus: implications for thr specific lipid composition of the bile fluid, J Biol Chem 278 [42], pp. 40631-9.

[230] Alder-Baerens, N.; Müller, P.; Pohl, A.; Korte, T.; Hamon, Y.; Chimini, G.; Pomorski, T. and Herrmann, A. (2005): Headgroup-specific exposure of phospholipids in ABCA1-expressing cells, J Biol Chem 280 [28], pp. 26321-9.

[231] Stöckl, M.; Fischer, P.; Wanker, E. and Herrmann, A. (2008): Alpha-synuclein selectively binds to anionic phospholipids embedded in liquid-disordered domains, J Mol Biol 375 [5], pp. 1394-404.

[232] Rhoades, E.; Ramlall, T. F.; Webb, W. W. and Eliezer, D. (2006): Quantification of alpha-synuclein binding to lipid vesicles using fluorescence correlation spectroscopy, Biophys J 90 [12], pp. 4692-700.

[233] Arvinte, T.; Cudd, A. and Hildenbrand, K. (1986): Fluorescence studies of the incorporation of N-(7-nitrobenz-2-oxa-1,3-diazol-4-yl)-labeled phosphatidylethanolamines into liposomes, Biochimica et Biophysica Acta 860, pp. 215-28.

[234] Chattopadhyay, A. and Mukherjee, S. (1993): Fluorophore environments in membrane-bound probes: a red edge excitation shift study, Biochemistry 32 [14], pp. 3804-11.

[235] Mukherjee, S.; Raghuraman, H.; Dasgupta, S. and Chattopadhyay, A. (2004): Organization and dynamics of N-(7-nitrobenz-2-oxa-1,3-diazol-4-yl)-labeled lipids: a fluorescence approach, Chem Phys Lipids 127 [1], pp. 91-101.

[236] Loura, L. M. and Ramalho, J. P. (2007): Location and dynamics of acyl chain NBD-labeled phosphatidylcholine (NBD-PC) in DPPC bilayers. A molecular dynamics and time-resolved fluorescence anisotropy study, Biochim Biophys Acta 1768 [3], pp. 467-78.

[237] Lin, S. and Struve, W. S. (1991): Time-resolved fluorescence of nitrobenzoxadiazole-aminohexanoic acid: effect of intermolecular hydrogen-bonding on non-radiative decay, Photochem Photobiol 54 [3], pp. 361-5.

[238] Huster, D.; Müller, P.; Arnold, K. and Herrmann, A. (2001): Dynamics of membrane penetration of the fluorescent 7-nitrobenz-2-oxa-1,3-diazol-4-yl (NBD) group attached to an acyl chain of phosphatidylcholine, Biophys J 80 [2], pp. 822-31.

[239] Polyansky, A. A.; Volynsky, P. E.; Nolde, D. E.; Arseniev, A. S. and Efremov, R. G. (2005): Role of lipid charge in organization of water/lipid bilayer interface: insights via computer simulations, J Phys Chem B 109 [31], pp. 15052-9.

[240] Raghuraman, H.; Shrivastava, S. and Chattopadhyay, A. (2007): Monitoring the looping up of acyl chain labeled NBD lipids in membranes as a function of membrane phase state, Biochim Biophys Acta 1768 [5], pp. 1258-67.

[241] el Hage Chahine, J. M.; Cribier, S. and Devaux, P. F. (1993): Phospholipid transmembrane domains and lateral diffusion in fibroblasts, Proc Natl Acad Sci U S A 90 [2], pp. 447-51.

[242] Morrot, G.; Cribier, S.; Devaux, P. F.; Geldwerth, D.; Davoust, J.; Bureau, J. F.; Fellmann, P.; Herve, P. and Frilley, B. (1986): Asymmetric lateral mobility of phospholipids in the human erythrocyte membrane, Proc Natl Acad Sci U S A 83 [18], pp. 6863-7.

[243] de Almeida, R. F.; Fedorov, A. and Prieto, M. (2003): Sphingomyelin/phosphatidylcholine/cholesterol phase diagram: boundaries and composition of lipid rafts, Biophys J 85 [4], pp. 2406-16.

[244] Veatch, S. L. and Keller, S. L. (2003): A closer look at the canonical 'Raft Mixture' in model membrane studies, Biophys J 84 [1], pp. 725-6.

[245] Lagerholm, B. C.; Weinreb, G. E.; Jacobson, K. and Thompson, N. L. (2005): Detecting microdomains in intact cell membranes, Annu Rev Phys Chem 56, pp. 309-36.

[246] Shaw, A. S. (2006): Lipid rafts: now you see them, now you don't, Nat Immunol 7 [11], pp. 1139-42.

[247] Kawasaki, K.; Yin, J. J.; Subczynski, W. K.; Hyde, J. S. and Kusumi, A. (2001): Pulse EPR detection of lipid exchange between protein-rich raft and bulk domains in the membrane: methodology development and its application to studies of influenza viral membrane, Biophys J 80 [2], pp. 738-48.

[248] Mukherjee, S. and Maxfield, F. R. (2004): Membrane domains, Annu Rev Cell Dev Biol 20, pp. 839-66.

[249] Almeida, P. F.; Pokorny, A. and Hinderliter, A. (2005): Thermodynamics of membrane domains, Biochim Biophys Acta 1720 [1-2], pp. 1-13.

[250] Segrest, J. P.; De Loof, H.; Dohlman, J. G.; Brouillette, C. G. and Anantharamaiah, G. M. (1990): Amphipathic helix motif: classes and properties, Proteins 8 [2], pp. 103-17.

[251] Wohlgemuth, R.; Waespe-Sarcevic, N. and Seelig, J. (1980): Bilayers of phosphatidylglycerol. A deuterium and phosphorus nuclear magnetic resonance study of the head-group region, Biochemistry 19 [14], pp. 3315-21.

[252] Takamori, S.; Holt, M.; Stenius, K.; Lemke, E. A.; Gronborg, M.; Riedel, D.; Urlaub, H.; Schenck, S.; Brugger, B.; Ringler, P.; Muller, S. A.; Rammner, B.; Grater, F.; Hub, J. S.; De Groot, B. L.; Mieskes, G.; Moriyama, Y.; Klingauf, J.; Grubmuller, H.; Heuser, J.; Wieland, F. and Jahn, R. (2006): Molecular anatomy of a trafficking organelle, Cell 127 [4], pp. 831-46.

[253] Deutsch, J. W. and Kelly, R. B. (1981): Lipids of synaptic vesicles: relevance to the mechanism of membrane fusion, Biochemistry 20 [2], pp. 378-85.

[254] Michaelson, D. M.; Barkai, G. and Barenholz, Y. (1983): Asymmetry of lipid organization in cholinergic synaptic vesicle membranes, Biochem J 211 [1], pp. 155-62.

[255] Hicks, B. W. and Parsons, S. M. (1992): Characterization of the P-type and V-type ATPases of cholinergic synaptic vesicles and coupling of nucleotide hydrolysis to acetylcholine transport, J Neurochem 58 [4], pp. 1211-20.

[256] Tang, X.; Halleck, M. S.; Schlegel, R. A. and Williamson, P. (1996): A subfamily of P-type ATPases with aminophospholipid transporting activity, Science 272 [5267], pp. 1495-7.

[257] Gellermann, G. P.; Appel, T. R.; Tannert, A.; Radestock, A.; Hortschansky, P.; Schroeckh, V.; Leisner, C.; Lutkepohl, T.; Shtrasburg, S.; Rocken, C.; Pras, M.; Linke, R. P.; Diekmann, S. and Fandrich, M. (2005): Raft lipids as common components of human extracellular amyloid fibrils, Proc Natl Acad Sci U S A 102 [18], pp. 6297-302.

[258] Bucciantini, M.; Giannoni, E.; Chiti, F.; Baroni, F.; Formigli, L.; Zurdo, J.; Taddei, N.; Ramponi, G.; Dobson, C. M. and Stefani, M. (2002): Inherent toxicity of aggregates implies a common mechanism for protein misfolding diseases, Nature 416 [6880], pp. 507-11.

[259] Moore, D. J.; West, A. B.; Dawson, V. L. and Dawson, T. M. (2005): Molecular pathophysiology of Parkinson's disease, Annu Rev Neurosci 28, pp. 57-87.

[260] Cole, N. B.; Murphy, D. D.; Grider, T.; Rueter, S.; Brasaemle, D. and Nussbaum, R. L. (2002): Lipid droplet binding and oligomerization properties of the Parkinson's disease protein alpha-synuclein, J Biol Chem 277 [8], pp. 6344-52.

[261] Zhao, H.; Tuominen, E. K. and Kinnunen, P. K. (2004): Formation of amyloid fibers triggered by phosphatidylserine-containing membranes, Biochemistry 43 [32], pp. 10302-7.

Acknowledgements

The present work has been carried out at the Humboldt-Universität zu Berlin in the workgroup “Molekulare Biophysik” under the supervision of Prof. Dr. Andreas Herrmann. I would like to thank all the people who helped me to successfully accomplish this work.

At first I want to thank Prof. Dr. Andreas Herrmann for providing me with the exciting topic and for the introduction into the world of lipid research. He is also responsible for the welcoming atmosphere of the lab untiringly caring for his various projects while at the same time allowing free space to pursue own ideas independently.

I’m also very grateful to Prof. Dr. Thomas Pomorski and Dr. Peter Müller who organize the tedium-routine of the lab providing the basis for successful research. Moreover, their expertise was always helpful to get over difficulties.

I especially want to thank Dr. Thomas Korte who introduced me into the complex field of microscopy and always took the time to discuss and resolve the occurring problems. Also for all the time he invests to keep the electronic equipment running – making smooth progress possible in the first place – I’m very thankful.

I’m also obliged to Sabine Schiller and Gudrun Habermann who care for the daily chores and keep the lab running.

Many thanks also go to Anna-Pia Plazzo and Dr. Thomas Korte who were involved in the experiments on living cells and giant vesicles. I’m also very grateful to Patricia Fischer who contributed a lot to the preparation of the α-synuclein variants.

In general I’d like to thank all the members of the workgroups “Molekulare Biophysik” and “Zellbiophysik” for creating a welcoming and encouraging environment.

I’m grateful to Jörg Nikolaus for reviewing parts of this work and Franziska Hopfinger for carefully proofreading the scripture.

I’m especially grateful to my family who, although being far away, always provided the support and backup necessary to pursue my goals.

Last but not least, I would like to thank my companion in life Tanja for her everlasting support especially in the hard times and her endurance and tough nerves during the final stage of writing up.

Publications

Talks

"Visualization of Lateral Phospholipid Distribution Using Fluorescence Lifetime Microscopy" Workshop of the Laser Microscopy Facility of the "Medizinische Hochschule Hannover" (Hannover, Germany). 03.02.2006

"Visualization of Interactions between α-Synuclein and Phospholipid Membranes" 50th Annual Meeting of the Biophysical Society (Salt Lake City, UT, USA). 18.02.2006-22.02.2006

"Visualization of Interactions of α-Synuclein with Phospholipid Membranes" at "Neurodegenerative Diseases: Molecular Mechanisms in a Functional Genomics Framework" (Berlin, Germany) 06.09.2006-09.09.2006

"α-Synuclein selectively binds to anionic phospholipids in liquid-disordered domains" Annual meeting of the *EST Network "Biomem"* (Berlin, Germany) 13.09.2007-15.09.2007

"Determinants of membrane binding of the β-amyloid sheet forming protein α-synuclein" at the symposium "Folding and Stability of beta-sheets" (Golm, Germany) 16.11-17.11.2007

Posters

"Visualization of lateral phospholipid distribution using fluorescence lifetime microscopy" International Workshop on "Dynamics of artificial and biological membranes" (Gomadingen, Germany) 20.03.2006-22.03.2006

Stoeckl, M.T., Plazzo, A.P. & Herrmann, A. (2007) "Lipid domains detected by fluorescence microscopy based FLIM analysis - A single dye approach." 51st Annual Meeting of the Biophysical Society (Baltimore, MD, USA). 03.03.2007-07.03.2007

Stoeckl, M.T., Fischer, P. & Herrmann, A. (2008) "α-Synuclein Selectively Binds To Anionic Phospholipids In Liquid-disordered Domains" 52nd Annual Meeting of the Biophysical Society (Long Beach, CA, USA). 02.02.2008-06.02.2008 *Biophys. J.* 94: 2053

Manuscripts

Papadopulos, A., Vehring, S., Lopez-Montero, I., Kutschenko, L., Stöckl, M., Devaux, P. F., Kozlov, M., Pomorski, T. & Herrmann, A. (2007). Flippase activity detected with unlabeled lipids by shape changes of giant unilamellar vesicles. *J Biol Chem* **282**, 15559-15568.

Stöckl, M., Fischer, P., Wanker, E. & Herrmann, A. (2008). Alpha-synuclein selectively binds to anionic phospholipids embedded in liquid-disordered domains. *J Mol Biol* **375**, 1394-1404.

Stöckl, M., Plazzo, A. P., Korte, T. & Herrmann, A. (2008). Detection of lipid domains in model and cell membranes by fluorescence lifetime imaging microscopy of fluorescent lipid analogues. *J. Biol. Chem.* doi:10.1074/jbc.M801418200

Bunge, A., Müller, P., Stöckl, M., Herrmann, A. & Huster, D. (2008). Characterization of the ternary mixture of sphingomyelin, POPC, and cholesterol: support for an inhomogeneous lipid distribution at high temperatures. *Biophys J* **94**, 2680-2690.

Tünnemann, G., Ter-Avetisyan, G., Martin, R. M., Stöckl, M., Herrmann, A. & Cardoso, M. C. (2008). Live-cell analysis of cell penetration ability and toxicity of oligo-arginines. *Journal of Peptide Science* **14**, 469-476.

Stöckl, M., Nikolaus, J. & Herrmann, A. (2008). "Visualization of lipid domain specific protein sorting in giant unilamellar vesicles." *Methods in Molecular Biology: Liposomes.* The Humana Press Inc. (Totowa, NJ, USA) (submitted)

Eidesstattliche Erklärung

Hiermit erkläre ich, die vorliegende Arbeit selbständig ohne fremde Hilfe verfasst und nur die angegebene Literatur verwendet zu haben. Ein Teil der beschriebenen Ergebnisse wurde in Zusammenarbeit mit anderen Mitarbeitern der Arbeitsgruppe Molekulare Biophysik erzielt. Diese sind entsprechend gekennzeichnet.

Ich besitze keinen entsprechenden Doktorgrad und habe mich anderwärts nicht um einen Doktorgrad beworben.

Die dem Promotionsverfahren zugrunde liegende Promotionsordnung ist mir bekannt.

Martin Stöckl